Technische Universität München
Fakultät für Mathematik
Lehrstuhl für Mathematische Modelle biologischer Systeme

Computing the Adaptive Cycle

Hannah Schrenk

Vollständiger Abdruck der von der Fakultät für Mathematik der Technischen Universität München zur Erlangung des akademischen Grades eines

Doktors der Naturwissenschaften (Dr. rer. nat.)

genehmigten Dissertation.

Vorsitzender:	Prof. Dr. Stefan Weltge
Prüfende der Dissertation:	1. Priv.-Doz. Dr. Wolfgang Graf zu Castell-Rüdenhausen
	2. Prof. Dr. Christina Kuttler
	3. Prof. Dr. Marc-Thorsten Hütt

Die Dissertation wurde am 02.12.2020 bei der Technischen Universität München eingereicht und durch die Fakultät für Mathematik am 10.03.2021 angenommen.

Acknowledgements

First of all, I wish to thank my supervisor Wolfgang for giving me the opportunity to spend four wonderful years at the Helmholtz Zentrum München. His curiosity and strong belief in research ahead of the times, as well as his enthusiasm and his ability to spread it have always inspired me.
Special thanks apply to Karin and Christina. I could not have wished for a more pleasant, positive, and encouraging thesis committee.
I want to thank Marion, a fantastic colleague and mentor, who has always had an open ear for me and was up to every fun.
Big thanks to Carlos, who is so enjoyable to work with (and who saved me last minute). I hope that our ways will often cross in future.
I want to thank Sandra, who accompanied and facilitated my first years at the center with her kind and warm nature.
Thanks to all my former and current colleagues at ICT and cooperation partners abroad. I have greatly benefited from their knowledge and experience.
Thank you to all of my great friends for the unforgettable times we share and for being there whenever I need them.
I want to thank my family, especially my wonderful parents and siblings, who fully and unconditionally support me and whose faith in me has and will always motivate me.
Above all, I wish to thank my beloved fiancé Leo for being by my side in good and bad times, for making me feel at home wherever we are, and for knowing an answer to all of my questions.

Abstract

In this thesis, we present a method to quantify complex systems' development in the sense of Gunderson and Holling's adaptive cycle metaphor. The metaphor describes systems' evolution as alternation of predictable and stochastic periods, defined by the three systemic variables of potential, connectedness, and resilience. There have been various attempts to capture the metaphor in quantitative terms, however, all of them system-specific. We introduce a universally applicable method to estimate a system's position within the adaptive cycle, requiring time-series of components' abundance data only. By means of Schreiber's transfer entropy, this data is transferred into networks of information transfer, serving as a basis to compute the three systemic variables. Our definitions of potential and connectedness are inspired by Ulanowicz's notions of capacity and ascendancy. In order to measure resilience, we define a variant of the established graph theoretical measure of connectivity. Various case studies, ranging from economic, over ecological, to micro-biological systems, validate our method and demonstrate its broad field of application. By means of an agent-based model, we identify the interplay of adaptation and perturbation as possible driver of the adaptive cycle.

Zusammenfassung

In dieser Dissertation stellen wir eine Methode vor, mittels derer sich der Entwicklungsprozess komplexer Systeme im Sinne von Gunderson und Hollings Adaptive Cycle Metaphor quantifizieren lässt. Die Metapher beschreibt den Entwicklungsprozess als Wechsel zwischen stabilen und chaotischen Phasen, welche durch die drei systemische Variablen Potenzial, Connectedness, und Resilienz definiert sind. Unsere Methode ermöglicht es, die Position eines allgemeinen komplexen Systems im adaptiven Zyklus zu schätzen. Dabei benötigt sie lediglich Zeitreihen von Abundanzdaten der Systemkomponenten. Diese Daten werden mittels Schreibers Transfer-Entropie in Informations-Netzwerke umgewandelt, auf deren Basis die drei systemischen Variablen berechnet werden. Unsere Definitionen von Potenzial und Connectedness sind aus Ulanowicz's Ascendancy Theory entlehnt. Resilienz messen wir in Form einer Variante des etablierten graphentheoretischen Maßes der Konnektivität. Anhand verschiedener Fallbeispiele aus den Bereichen der Ökonomie, Ökologie und Mikrobiologie validieren wir unsere Methode und demonstrieren ihr breites Anwendungsgebiet. Abschließend identifizieren wir anhand eines Agenten-basierten Modells das Zusammenspiel von Adaptation und Perturbation als möglichen Treiber des adaptiven Zyklus.

Data availability statement

All data and materials used in this thesis are either freely accessible and correspondingly referenced or provided by the author on reasonable request.

Introduction

There is nothing permanent except change.

— Heraclitus (544 BC - 483 BC)

Our world is defined by change. Changes over millions of years, like the Earth's development throughout the geological eras, changes over decades, like the industrial revolution, changes over years, like economic crises, changes over days, like the movements on stock markets, or changes over minutes, like local drops of temperature. Some changes, like the shift of continental plates, can span the whole Earth, others, like human cell development, span just a few micrometers. Changes do not only differ in their extent but in the way they are evaluated as well. While changes like medical advancement or technical progress are supported and actively driven, there are others which people fear and try to prevent, among them the global climate change as most recent example. In order to handle the changes of today and prepare for the changes of tomorrow, we need to understand them. The main challenge lies in the fact that they usually result from a multitude of interacting factors. Economic crises can be traced back to the interplay of most diverse financial, political, and social events. Ecological succession is not only driven by the most dominant plant species. On the contrary, it is not uncommon that initially inconspicuous species turn out to be key players in change. Besides, abiotic factors like climatic and soil conditions can have a huge impact as well. Hence, understanding change means understanding the dynamics and mechanisms of the underlying complex system.

In this thesis, we develop a method to quantify the process of change in complex systems. The theoretical foundations for our method were established at the end of the 20th century, when a group of ecologists and economists around L.H. Gunderson and C.S. Holling formed with the aim to develop a uniform theory of change [39]. They had realized that, independent of temporal and local scale, ecological, economic, and socio-ecological systems share a certain pattern of change. This pattern is subject of the *adaptive cycle metaphor*, a schematic description of complex systems' development. According to the metaphor, system development is defined by three variables: the system's *potential* for future changes, the *connectedness* among its components and internal processes, and its *resilience* to unpredicted perturbations. Four repeating phases of system development can be distinguished. During the long phases of *exploitation* and *conservation*, stability and predictability prevail. The subsequent rapid phases of *release* and *reorganization* are characterized by unpredictability and chance. The alternation between growth and renewal allows the system to adapt to changing environmental conditions.

The adaptive cycle metaphor does not provide a computational framework for system development. It is meant to be a conceptual description, a "*tool for thought*" [1]. Naturally,

various attempts to quantitatively capture the adaptive cycle followed. Applications range from urban systems [62], over public governance of land use [17], to coastal-marine systems [22], and phytoplankton communities [10]. However, in all of these examples, system-specific variables are used to measure potential, connectedness, and resilience. Hence, these approaches cannot be readily transferred to other systems. In this thesis, we develop a method to determine a complex system's position within the adaptive cycle. The method is independent of the underlying system, aiming to be universally applicable and thereby satisfying the abstract nature of the metaphor itself.

Our method follows a two-step approach. In the first step, we derive an interaction-based network representation of the system, which then, in the second step, provides the basis for quantifying potential, connectedness, and resilience independently of the concrete instantiation of the system.

Some notes on the first step: with complexity emerging from interactions among system components, interactions constitute the lowest common denominator of complex systems. Basing our method on interactions therefore ensures its general applicability. Naturally, interactions occur in different forms, be it predator-prey relationships in ecological systems, nutrient fluxes in microbiological systems, services in social systems, or cash flows in economic systems. In reality, these interactions are often difficult to quantify. Assuming that any effective interaction among system components leads to a transfer of information among them, interactions can be quantified via Schreiber's measure of *transfer entropy* [67], resulting in networks of information transfer. We estimate transfer entropy on basis of time series of components' abundance data reflecting the outcome of interactions. Depending on the system, this data can be of various types. In ecological systems, the abundance of a component could be measured by the number of individuals or the total biomass of a species, in economic systems, a company's abundance could be quantified by its capital.

Our definitions of potential and connectedness are inspired by the information theoretical notions of ascendancy and capacity, which were introduced by Ulanowicz in the course of his ascendancy theory [76]. But while he applied them to systems being represented as networks of *physical* flows, we apply them to networks of information transfer. The main challenge of the operationalization lies in the definition of resilience. All previous proposals are either depending on the specific observed system (see e.g. [23, 28, 63, 73]) or, originating from dynamic systems or viability theory, requiring deep knowledge of the underlying systems' dynamics (see [57] for an overview). Ulanowicz provided a measure of resilience in the course of his ascendancy theory. However, according to this definition, resilience is completely determined by the values of capacity and ascendancy, making it redundant in our case. Within the last years, the notion of resilience has been increasingly studied from network perspective (see e.g. [29, 43]). Considering complex systems as networks, this is our starting point as well. Our definition is inspired by the well-established measure of connectivity of

undirected graphs [25], the smallest non-trivial eigenvalue of the graph's Laplacian matrix, quantifying its vulnerability to perturbations. Transferring this notion to directed graphs and applying it to systems' networks of information transfer yields a suitable measure of the resilience of a system.

Our method is mainly based on three assumptions. In the first step, we implicitly assume that networks of information transfer reflect complex systems' interaction dynamics. This assumption is an aspect of the established practice to consider (living) complex systems as computing systems [53]. We introduce this practice and illustrate its application with a model of a simplified human intestinal microbiota. In the second step, we assume that our definitions of potential, connectedness, and resilience capture Gunderson and Holling's understanding of these notions. We support our choices by means of an agent-based model imitating a system on its course through the adaptive cycle. Finally, we assume that the adaptive behavior of a system is indeed reflected in its interaction dynamics. We justify this assumption by extracting the typical cyclic pattern from the purely interaction-based Tangled Nature Model [24].

Due to its high generality and the fact that it requires only the most basic information about a system, our method opens a wide field of application. The application examples in this thesis range from (simulated and real-world) ecological, over microbiological, to economic systems, demonstrating the method's capabilities in comparing, exploring, and understanding system development.

The various case studies show that the developmental pattern described in the adaptive cycle metaphor naturally occurs in complex systems. This raises the question of general drivers behind this phenomenon. We hypothesize that constant small perturbations in combination with cascading adaptive moves of the system's components result in the typical cyclic behavior. We support this hypothesis by means of numerical and theoretical examinations of an agent-based model.

The thesis starts with a review of the adaptive cycle metaphor in Section 1. The cycle's phases and defining variables are described and illustrated by means of an ecological example. Section 2 provides the mathematical framework for our method in form of an introduction to information theory. We derive the notions and laws that we will refer to throughout the thesis. After introducing the basic notions in Section 2.1, we put them in the wider context of total information composition in Section 2.2. Subsequently, we extend the definitions to continuous variables in Section 2.3, since we are mainly considering those in practice.
Section 3 is the centerpiece of the thesis. In this section, we explain our approach, present our method, and study basic properties of the systemic variables. In Section 3.1, we start with a description of the first step of our method, the estimation of networks of information transfer. In the following, we derive our definitions of potential and connectedness in Section 3.2, referring back to Ulanowicz's ascendancy theory (Section 3.2.1). The check of continuity

in Section 3.2.2 allows the application of these measures to continuously developing networks. The derivation of our definition of resilience (Section 3.3) requires more preliminary work. We present basic graph theoretical notions in 3.3.1 as basis for the introduction of directed Laplacian matrices in Section 3.3.2. Having defined resilience, we prove its relation to the graph's topology in Section 3.3.3, thereby justifying our choice. The study of the three systemic variables on simple Gilbert graphs in Section 3.4 gives a first impression of their behavior. In Section 3.5, we give an overview of the method, illustrated by a little toy example. Finally, we briefly present the R package QtAC, which allows a straightforward application of our method, in Section 3.6.

The application examples in Section 4 contribute to the validation of our method. We examine the distributed computation of a human intestinal microbiota in Section 4.1. Our definitions of potential, connectedness, and resilience are tested in Section 4.2. A study of the tangled nature model in Section 4.3 supports our interaction-based approach.

Section 5 comprises three case studies. We compare the development of different countries during the Euro crisis in Section 5.1. The exploration of two ecological systems is subject of Section 5.2. The first example treats the succession of a plant community on the volcanic island of Surtsey (Section 5.2.1). In the second example, a prairie-forest ecotone exposed to human intervention is considered (Section 5.2.2).

In Section 6, we address the question for the drivers of the adaptive cycle. We hypothesize that the typical pattern of change described in the adaptive cycle metaphor can result from the interplay of two processes, adaptation and perturbation. We test these hypotheses by means of an agent-based model, which is described in Section 6.1. Both simulation results (Section 6.2) and a mathematical examination of the model (Section 6.3) support our hypotheses.

The thesis ends with a conclusion, including a brief outlook to future research.

Contents

1 The Adaptive Cycle Metaphor **1**

2 Information Theoretic Framework **7**

2.1 Basic notions . . . 7

2.2 Total information composition . . . 11

2.3 Differential entropy . . . 13

3 Quantification of the Adaptive Cycle **15**

3.1 Estimation of networks of information transfer . . . 16

3.2 Definition of potential and connectedness . . . 18

3.2.1 Ulanowicz's ascendancy theory . . . 19

3.2.2 Continuity of the measures . . . 22

3.3 Definition of resilience . . . 25

3.3.1 Graph theoretical preliminaries . . . 26

3.3.2 Directed Laplacian matrices and their eigenvalues . . . 27

3.3.3 The Laplacian spectrum related to the graph's topology . . . 30

3.4 Potential, connectedness, and resilience of random graphs . . . 34

3.5 Overview of the method . . . 41

3.6 R package QtAC . . . 43

4 Validation of the Method **45**

4.1 Justification of the information theoretic approach . . . 46

4.2 Interplay of the systemic variables . . . 61

4.3 Capturing cyclic development in an interaction-based model . . . 67

5 Cases of Application **71**

5.1 Comparing economic systems during the Euro crisis . . . 71

5.2 Exploring systems . . . 75

5.2.1 Systemic analysis of a developing plant community on the island of Surtsey . . . 75

5.2.2 A prairie-forest ecotone under human intervention . . . 82

6 Drivers of the Adaptive Cycle **89**

6.1 Description of the model . . . 90

6.2 Simulation of the model . . . 92

6.3 Mathematical exploration of the model . . . 95

Supplementary **113**
A Manual of the R package QtAC 113
B Exemplary series of networks generated on basis of the principle of overexploitation 121
C Parameters of the Tangled Nature Model simulation 125
D Species and metadata of the Kansas case study 127
E System components in the Europe case study 129
F Information networks of the vascular plant system on Surtsey 131

1 The Adaptive Cycle Metaphor

The adaptive cycle metaphor is a heuristic model of change, schematically describing the development of general complex systems. *Complex system* is a very broad term and we do not intend to define it more precisely than as a set of interacting agents. In particular, we do not make any restrictions on the agents' and the interactions' nature.
This review contains excerpts of [83]. It is based on the descriptions in [39].

The metaphor is based on the assumption that the future behavior of a complex system is shaped by the development of three comprehensive properties, potential, connectedness, and resilience. According to Gunderson and Holling, a system's *potential* encompasses the capacity the system has at its disposal to react to future changes. It thereby determines the range of options possible. The *connectedness* between internal variables and processes captures the level of inner organization and regulation, in contrast to a high sensitivity to external variation. It can be understood as a measure of flexibility or rigidity. *Resilience* is defined as "*the magnitude of disturbance that can be absorbed before the system changes the variables and processes that control behavior*" [39, p.28].

Referring solely to the definitions given by Gunderson and Holling, it is difficult to properly separate the three properties. They all affect the system's relation to its surrounding, however, there are subtle differences, given as follows.

- Potential measures the magnitude of external variation a system can survive. Survival can involve deep internal structural changes.
- Connectedness quantifies the internal controllability of a system, i.e. the degree to which it controls its own development. It contrasts the degree to which external variation forces the system into internal changes.
- Resilience measures the magnitude of internal structural change which can be reversed by the system.

The application of these definitions to specific systems is still not obvious since some notions leave scope for interpretation. When does a system "survive"? If all of its components are still alive? And when is a change a "structural change"? Answers to these questions are always case specific and subjective.

Let us briefly illustrate the three systemic variables in the context of a specific system, a community of plant species being exposed to an unexpected drought. A high number and a good state of health of the individual plants contribute to the system's chance of survival and thereby to its potential. Assume smaller plants at ground level keep the soil moisture for larger plants, which, in return, provide shelter for the smaller plants. Symbioses like this lead to a higher connectedness since they increase the plants' mutual regulation and decrease their sensitivity to weather conditions. Imagine the drought is so severe that the

large species get extinct. In this case, the small species, depending on the large species' shade, will probably disappear as well. Even some time after the drought, the system won't be able to return to its former state. Hence, its resilience was not high enough to absorb the effects of the drought without changing its defining structure.

We will now describe the predicted development of the three systemic variables in the course of the adaptive cycle. Envisioning an environment of largely unexplored resources, a system will first tend to make use of these resources without any need for higher efficiency. In ecology, this is the opportunity for r-strategists [64]. These generalists are characterized by a high dispersal ability [31], large growth rates, and few demands on their habitat. Following this terminology, the exploitation phase is also called the *r-phase* of system development. Connectedness is still low, potential first needs to be build-up, while resilience is typically high.

Starting to make use of the resources, the system will increase its inner level of organization. Expertise is generated and through the action of the system, new opportunities (i.e. *niches* [60]) are generated, contributing to an optimization in resource utilization. Subsets of components begin to develop closer relationships and resources are accumulated. Potential and connectedness slowly increase. However, while increasing levels of optimization make better use of resources, the dependency among processes and components grows and the increased level of internal organization and specialization has to be sustained. Organization is not free of cost and therefore requires a share of the resources being captured. These factors typically lead to a decrease in resilience. At some point, the system enters the conservation or *K-phase*. Indeed, in ecological terms, K-strategists dominate this period. These specialists have a slower growth rate and lower dispersal ability but are strongly competitive. The K-phase is characterized by high efficiency and thus extreme rigidity.

The probability of encountering an external event the system cannot immediately cope with increases. "*In the cases of extreme and growing rigidity, all systems become accidents waiting to happen*" [39, p.45]. Sooner or later, a presumably small trigger then leads to a breakdown of the current organization in the following Ω-*phase*. Resources being captured by the system will be released, connections are broken. Connectedness and potential strongly decline while resilience increases.

Eventually, processes of mobilization initiate the beginning of a new cycle in form of the α-*phase*. Various opportunities will be exploited, some of them leading to new developments, while others quickly disappear. A system is exposed to a high level of stochasticity. During this period, the system is being driven by changing environmental conditions, rather than being capable of shaping the environment towards its own favor. New components might enter the system, while others get lost. At the shift from α- to r-phase, the *collapse of organization* [39, p.38] and the sequestration of remaining capital by components slowly settling in lead to a decrease in potential. Note that, in our case studies, the α-phase

is mainly characterized by its lack of a clear pattern in the variables' development. In particular, we do not generally see a collapse of organization.

Visualizing the development of the variables in the space spanned by potential, connectedness, and resilience generates the typical "lying-eight" depicted in Figure 1. The alternation between periods of predictability and stability (front loop) and shorter periods of "creative destruction" [39, p.73] and renewal (back loop) enables complex systems to adapt to a changing environment. Gunderson and Holling consider a balanced interplay between these two antagonistic tendencies as key to complex systems' sustainability.

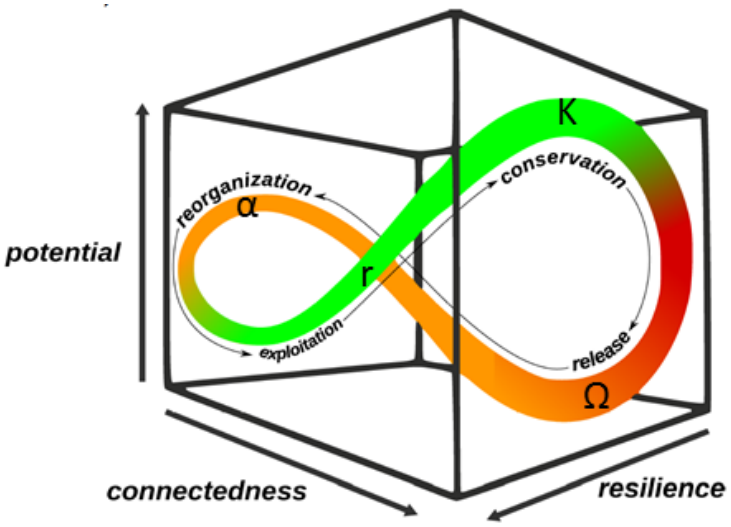

Figure 1: Visualization of Holling's and Gunderson's adaptive cycle metaphor (as appeared in [83]).

The metaphor's high degree of generality makes it a valuable framework to classify the development of a broad range of complex systems. However, it has its limits as well. There are systems living totally passively with external variability, like open-water communities, and systems anticipating and manipulating variability that do not run through the whole adaptive cycle but remain in single phases [39]. The case studies underlying the idea of the adaptive cycle metaphor were all of a third kind: systems (partially) controlling variability and thereby minimizing its influence on the internal structure, like temperate, terrestrial ecosystems [39]. We will give an example of a system following this strategy to illustrate the adaptive cycle metaphor.

In the 1960s, the island of Surtsey was formed during a volcanic eruption south of Iceland. Since then, the flora and fauna on the island has been closely monitored, providing a unique possibility to follow every developmental stage of a natural ecosystem. In [55], Magnússon et al. provide an overview of the succession waves on Surtsey (see Figure 2 for a schematic

representation). Further details can be found in [65]. We will now interpret the succession development in the context of the adaptive cycle metaphor.

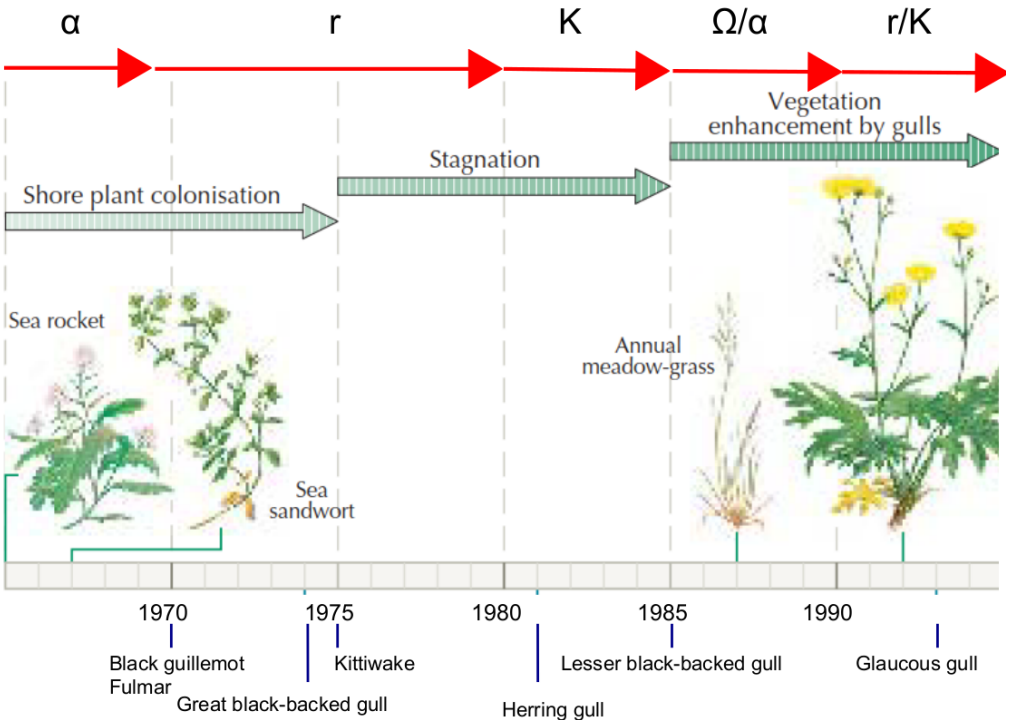

Figure 2: The adaptive cycle of the ecosystem on Surtsey. Edited version of Figure 20 in [55].

During the first decade, both lava and sand soil on Surtsey are largely nutrient-poor and barren. Only a few mosses, lichen species, and shore plants are found growing on Surtsey. Their seeds have been brought to the island by wind. *Honckenya peploides*, or sea sandwort, is the most successful among the pioneer plants and starts forming patches. At the end of the decade, the first birds are breeding on the island and ten of the twelve observed vascular plant species have become established.
Considering the ecosystem on Surtsey as complex system, we interpret the first years after the island's formation as α-phase. Typically for this phase, the system is driven by its environmental conditions, captured by a low connectedness, and various opportunities are exploited in form of new species trying to settle down. Potential is still low, whereas resilience is high since the system could easily return to this state after most types of perturbation. As soon as the first pioneer plants have established, the system's r-phase starts. It is characterized by the slow growth and spreading of r-strategists, in this case undemanding pioneer plants.

During the next decade, the succession more or less stagnates. Several new species are

observed on the island, however, only a few of them have become established at the end of the decade. Among the successful new colonizers is *Leymus arenarius*, or lyme grass, which starts forming communities with *Honckenya peploides* [34]. *Honckenya* grows close to the ground, keeping the soil's top-layer moist for tall-growing and extensively rooting *Leymus*, which, in turn, provides shelter for *Honckenya*. The third actor in this community are breeding gulls. The lyme grass dunes provide nesting material and shelter. The plants, in return, take advantage of the nutrients introduced by the birds.
We assign the first years of this new decade still to the system's r-phase since potential is slowly accumulated in form of biomass and species' richness, however, no close relationships among components have been formed yet and the future course of the system is not predictable. With the just described symbiosis forming, the system passes into its K-phase. The relationships among the components lead to a strong decrease in sensitivity to external variability and thereby to an increase in connectedness. Potential in form of biomass is comparably high whereas resilience is low. This is mainly due to the fact that symbioses have created strong dependencies among the species. For some years, the system is characterized by stability and constancy.

In 1985, the lesser black-backed gulls (*Larus fuscus*) arrive on the island. There is a sharp increase in the breeding population and thereby in the nutrients being introduced into the soil through excreta, lost bits of chick feed, and carcasses. Old colonizers, formerly unsuccessful due to the nutrient-poor conditions, reoccur. Besides, various new colonizers are brought to the island by the birds. The plants on the island, serving as nesting material and breeding space, are now exposed to destruction through the birds. During the following years, the future course of the ecosystem is formed with former established and newly introduced species competing. After some time, it becomes apparent that mainly grasses can benefit from the new conditions. Vegetation cover is extending and at the end of the decade, the gull colony region of Surtsey has turned into forb-rich grassland.
We consider the sudden population explosion of gulls as the event triggering the Ω-phase of the ecosystem. Environmental conditions change drastically, leading to a decline in some existing species' abundance and to a chance for new species to enter the system. Former connections are broken, new species have not yet built relationships among each other, provoking a decline in connectedness. The pressure to adapt to new conditions leads to an overall decrease in average species' potential. Stochasticity increases along with resilience. There is a fluent transition from Ω- to α-phase, being characterized by competition among species. With grasses settling down, the system enters its second r-phase, during which potential in form of biomass and species richness is accumulated. This phase eventually leads to another K-phase, shaped by wide, forb-rich grassland.
Note that a more precise division into the four phases is difficult in this case. The information provided in literature allows to distinguish periods of change and renewal (back loop of the cycle) and periods of growth and stability (front loop of the cycle) but phase changes within

this period cannot be reliably determined.

In summary, following our interpretation, the ecosystem on Surtsey runs through two adaptive cycles during the first three decades. After the formation of the island, different pioneer species occur and vanish again during the α-phase. Some shore plants get established in the r-phase and form strong relationships in the K-phase, when further colonization stagnates. The sudden increase in breeding gulls in 1985 triggers the Ω-phase. New components enter the system and compete with established ones during the α-phase. The following r-phase is characterized by the expansion of grasses. Eventually, continuous swards form, shaping the system during its K-phase.
In this case study, the Ω-phase results in a succession wave, enhancing vegetation and diversity. This illustrates the progression and advancement a system breakdown can cause.

In Section 5.2.1, we will return to the succession on Surtsey and derive our - so far descriptive - explanations from data. More precisely, we apply our method to species' abundance data collected in an experimental plot on the island between 1990 and 2018, capturing the local succession events in this period. However, in order to properly present our method, we first need to establish the theoretical foundation. We will start with an introduction to information theory in the following section.

2 Information Theoretic Framework

Our method to quantify the adaptive cycle is based on information theoretical concepts at two crucial points. Firstly, in the estimation of a system's network representation via Schreiber's transfer entropy, and secondly, in the computation of potential and connectedness, being variants of entropy and mutual information of the network's edges. We will therefore provide an introduction to the basic concepts of information theory in this section. Section 2.1 serves as an overview of the most fundamental notions of information theory, starting from a variable's (Shannon) entropy. After presenting some variants of entropy, we will consider the information structure between several variables, leading from the common measure of mutual information to transfer entropy. Information being transferred from other variables is not the only source of information. The total information composition is examined in Section 2.2. This requires, inter alia, the introduction of active information storage. Since many of the naturally occurring complex systems are of continuous nature, we will consider the continuous analogues of the information theoretical measures in Section 2.3.
Throughout the whole thesis, we follow the conventions that $0 \cdot \log(0) = 0$ and $\frac{0}{0} = 0$.

2.1 Basic notions

Let X be a discrete random variable taking values in the alphabet α_X. In this context, *discrete* means that α_X is finite. We denote the probability that X takes on a value $x \in \alpha_X$ by $p(x)$. Note that we distinguish probability distributions by their argument only, i.e. $p(x) = P(X = x)$, $p(y) = P(Y = y)$, $p(x, y) = P(X = x, Y = y)$, etc.

We will now present a fundamental measure of information content, the Shannon entropy. Imagine a message telling us that $X = x$ for some $x \in \alpha_X$. This message is very surprising or, equivalently, contains a lot of information, if $p(x)$ is small. If $X = x$ is very likely to happen, the message is neither surprising nor really informative. This property can be quantified by the *(Shannon) information content* or *local entropy* [20, Ch.3]

$$H_X(x) = -\log\left(p(x)\right).$$

Using the natural logarithm returns information in *nats*, base 2 yields information in *bits*. Averaging over all possible values of X yields its *Shannon entropy* [27, Ch.2].

Definition 1. *The (Shannon) entropy of a discrete random variable X over the alphabet α_X, following the probability distribution $p(x)$, is defined as*

$$H_X = -\sum_{x \in \alpha_X} p(x) \cdot \log\left(p(x)\right).$$

The entropy of X can be understood as the expected information content in the outcome

of X, or, in other words, as the expected degree of surprise in a message about the outcome of X. Considering the logarithm of base 2, $H(X)$ has a very concrete interpretation. Assume you want to encode the outcome of X in bits, hence, assign a unique string of bits $c(x)$ to every element $x \in \alpha_X$. Let $l(c(x))$ be the length of this string. An encoding which minimizes the expected length

$$\sum_{x \in \alpha_X} p(x) \cdot l(c(x))$$

is called *optimal encoding*. Then, $\lceil H(X) \rceil$ measures the average minimum length of $c(x)$ in an optimal encoding [20, Ch.3].

The idea of entropy can be naturally extended to two variables [27, Ch.2].

Definition 2. *Let X and Y be two discrete random variables over the alphabets α_X and α_Y, respectively, following the probability distributions $p(x)$ and $p(y)$, respectively. The joint entropy of X and Y is defined as*

$$H_{X,Y} = -\sum_{x \in \alpha_X} \sum_{y \in \alpha_Y} p(x,y) \cdot \log\left(p(x,y)\right).$$

Their conditional entropy is defined as

$$H_{Y|X} = -\sum_{x \in \alpha_X} \sum_{y \in \alpha_Y} p(x,y) \cdot \log\left(p(y|x)\right).$$

The individual summands are referred to as the respective local values.

Intuitively, conditional entropy quantifies the remaining uncertainty about the outcome of Y when the outcome of X is known. A short computation shows that [27, Ch.2]

$$H_{X,Y} = H_X + H_{Y|X}. \tag{1}$$

The shared information between two random variables is measured by the variables' *mutual information* [27, Ch.2].

Definition 3. *Let X and Y be two discrete random variables over the alphabets α_X and α_Y, respectively, following the probability distributions $p(x)$ and $p(y)$, respectively. The mutual information between X and Y is defined as*

$$\begin{aligned} I_{X;Y} &= \sum_{x \in \alpha_X} \sum_{y \in \alpha_Y} p(x,y) \cdot \log\left(\frac{p(x,y)}{p(x) \cdot p(y)}\right) \\ &= \sum_{x \in \alpha_X} \sum_{y \in \alpha_Y} p(x,y) \cdot \log\left(\frac{p(x|y)}{p(x)}\right) \\ &= \sum_{x \in \alpha_X} \sum_{y \in \alpha_Y} p(x,y) \cdot \log\left(\frac{p(y|x)}{p(y)}\right). \end{aligned}$$

An individual summand is referred to as local mutual information.

Mutual information symmetrically captures the expected reduction in uncertainty about the outcome of one variable if knowing the outcome of the other variable. This relation is reflected by the equality [27, Ch.2]

$$I_{X;Y} = H_X - H_{X|Y} = H_Y - H_{Y|X} = I_{Y,X}. \tag{2}$$

Together, Equations (1) and (2) yield

$$I_{X;Y} = H_X + H_Y - H_{X,Y}. \tag{3}$$

Equations (1), (2), and (3) hold for the local values of the measures as well.

The measure of *conditional mutual information* allows to distinguish between directly shared information and information which both variables gain from a third variable Z [20, Ch.3].

Definition 4. *Let X, Y, and Z be three discrete random variables over the alphabets α_X, α_Y, and α_Z, respectively, following the probability distributions $p(x)$, $p(y)$, and $p(z)$, respectively. The mutual information between X and Y conditioned on Z*

$$I_{X;Y|Z} = \sum_{z\in\alpha_Z} \sum_{x\in\alpha_X} \sum_{y\in\alpha_Y} p(x,y,z) \cdot \log\left(\frac{p(x|y,z)}{p(x|z)}\right)$$

is called conditional mutual information. An individual summand is referred to as local conditional mutual information.

Analogously to Equation (3), we obtain

$$I_{X;Y|Z} = H_{X|Z} + H_{Y|Z} - H_{X,Y|Z}. \tag{4}$$

Equation (4) applies to the local version of the measures as well.

Note that mutual information and conditional mutual information are always non-negative [20, Ch.3]. However, their *local* values can be negative. Consider

$$I_{X;Y}(x,y) < 0 \iff \frac{p(x,y)}{p(x)\cdot p(y)} < 1 \iff p(x|y) < p(x).$$

In this case, the occurrence of y decreases our expectation of the occurrence of x. Hence, in a situation where x and y occur together, y is *misinformative* about x. The summand

$$p(x,y,z) \cdot \log\left(\frac{p(x|y,z)}{p(x|z)}\right)$$

quantifies the expected amount of misinformation about x by y.

Having considered static variables so far, we will now focus on processes, i.e. sequences of random variables. In absence of a measure capturing *dynamical* and *directional* information exchange among processes, Schreiber proposed the measure of *transfer entropy* [67]. Let $X = (\dots, X_i, X_{i+1}, \dots)$ and $Y = (\dots, Y_i, Y_{i+1}, \dots)$ be two stationary discrete Markov processes of finite order k and l, respectively. Stationarity implies that both joint and individual probability distributions are not time-dependent. By discrete we mean that the alphabets α_X and α_Y underlying the random variables X and Y, respectively, are finite. Note that, in the following, we will distinguish the alphabets $\alpha_{X_i}, \alpha_{X_{i+1}}, \dots$ although they are all equal. This emphasizes the dynamical character of the measures and facilitates the understanding of the measures' estimators. The Markov orders tell us that

$$p(x_{i+1}|x_i, \dots, x_{i-k+1}) = p(x_{i+1}|x_i, \dots, x_{i-k+1}, x_{i-k}) \text{ and}$$
$$p(y_{i+1}|y_i, \dots, y_{i-l+1}) = p(y_{i+1}|y_i, \dots, y_{i-l+1}, y_{i-l}).$$

In the following, we will use the short form $x_i^{(k)} = (x_i, \dots, x_{i-k+1})$. If the generalized Markov property

$$p\left(x_{i+1} \,\middle|\, x_i^{(k)}\right) = p\left(x_{i+1} \,\middle|\, x_i^{(k)}, y_i^{(l)}\right) \tag{5}$$

holds, the state of Y has no influence on the transition probabilities of X. The degree to which the state of Y *has* an influence on the transition probabilities of X is quantified by Schreiber's *(apparent) transfer entropy* (TE) [67].

Definition 5. *Let $X = (\dots, X_i, X_{i+1}, \dots)$ and $Y = (\dots, Y_i, Y_{i+1}, \dots)$ be two stationary discrete Markov processes of order k and l, respectively. Denote by α_{X_i} the alphabet of X_i. Set $X_i^{(k)} = (X_i, X_{i-1}, \dots, X_{i-k+1})$ over the alphabet $\alpha_{X_i^{(k)}}$, and $Y_i^{(l)}$ analogously. The transfer entropy from Y to X is defined as*

$$T_{Y\to X} = \sum_{\alpha_{X_{i+1}}} \sum_{\alpha_{Y_i^{(l)}}} \sum_{\alpha_{X_i^{(k)}}} p\left(x_{i+1}, x_i^{(k)}, y_i^{(l)}\right) \cdot \log\left(\frac{p\left(x_{i+1} \,\middle|\, x_i^{(k)}, y_i^{(l)}\right)}{p\left(x_{i+1} \,\middle|\, x_i^{(k)}\right)}\right). \tag{6}$$

The individual summands are called local transfer entropies.

It can be easily seen that

$$T_{Y\to X} = I_{X_{i+1}; Y_i^{(l)} | X_i^{(k)}}.$$

As such, transfer entropy is always non-negative. Local transfer entropy is negative if

$$p\left(x_{i+1} \,\middle|\, x_i^{(k)}, y_i^{(l)}\right) < p\left(x_{i+1} \,\middle|\, x_i^{(k)}\right).$$

Hence, in this case, its absolute value measures the expected amount of misinformation about x_{i+1} by $y_i^{(l)}$. Since transfer entropy is a *directed* measure of statistical dependence

between two processes, we will from now on distinguish between the *source (process)* (Y in the above definition) and the *destination (process)* (X in the above definition). Following this terminology, transfer entropy can be understood as the average amount of information in the source Y about the next state of the destination X that was not already contained in the past of X itself. Whenever the source process Y is a *possible information contributor* of the destination process X [51], $T_{Y\to X}$ can be interpreted as *information transfer* from Y to X, giving insights about the emergent computation of the underlying system. Information transfer can be clearly distinguished from the frequently used notion of information *flow*, which captures direct causal effects [51].

We will now consider the amount of information in the outcome x_{i+1} of a variable X_{i+1} as the amount of information needed to *compute* state x_{i+1} at time i. This information can be assigned to different sources, inter alia the history of the process itself and the history of other processes, being possible information contributors. Introducing two additional information theoretical measures allows a *total information composition* for systems of multiple processes.

2.2 Total information composition

This review follows [69] and is based on the descriptions in [53]. Consider a system $\mathcal{V} = \{\dots, X, Y, Z, \dots\}$ of countably many processes which can be approximated by stationary discrete Markov processes. From now on, we will refer to the processes as the system's *agents*. The average information contained in the states of an agent X is captured by the agent's entropy

$$H_X = -\sum_{\alpha_X} p(x) \cdot \log\left(p(x)\right).$$

It measures the expected amount of information needed to predict x_{i+1} at time i. This information can be decomposed into three components.

The first component is the information being stored in the agent's past and being in use in computing its next state. It is quantified by the *active information storage* (AIS) [53].

Definition 6. *Let $X = (\dots, X_i, X_{i+1}, \dots)$ be a stationary discrete Markov process of order k. The active information storage of X is defined as*

$$A_X = \sum_{\alpha_{X_{i+1}}} \sum_{\alpha_{X_i^{(k)}}} p\left(x_{i+1}, x_i^{(k)}\right) \cdot \log\left(\frac{p\left(x_{i+1} \,\middle|\, x_i^{(k)}\right)}{p(x_{i+1})}\right).$$

An individual summand is referred to as local active information storage.

Clearly,

$$A_X = I_{X_{i+1}; X_i^{(k)}}.$$

As mutual information, active information storage is always non-negative. However, the local quantities are negative if

$$p\left(x_{i+1} \,\middle|\, x_i^{(k)}\right) < p(x_{i+1}),$$

measuring the expected amount of misinformation between the past $x_i^{(k)}$ and the next state x_{i+1}.

The information provided by other agents and not being contained in X's own past is comprised in the second component. We confine ourselves to agents whose information could possibly be processed by X in order to avoid artifacts. The subset of possible information contributors can be determined on basis of background knowledge of the system or using computational methods (compare [51]). Let $\mathcal{V}_X = \{\dots, Z^s, Z^{s+1}, \dots\} \subset \mathcal{V}$ be the set of all possible information contributors of X in the system except for X itself and

$$\mathcal{V}_{X,i} = (\dots, Z_i^s, Z_i^{s+1}, \dots).$$

Let $\alpha_{\mathcal{V}_{X,i}}$ be the alphabet of $\mathcal{V}_{X,i}$ and denote an element of the alphabet by $v_{X,i}$. The information being transferred to X from other agents is combined in the *collective transfer entropy* [53].

Definition 7. *Let $X = (\dots, X_i, X_{i+1}, \dots)$ be a stationary discrete Markov process of order k. The collective transfer entropy of X is defined as*

$$T_X = \sum_{\alpha_{X_{i+1}}} \sum_{\alpha_{X_i^{(k)}}} \sum_{\alpha_{\mathcal{V}_{X,i}}} p\left(x_{i+1}, x_i^{(k)}, v_{X,i}\right) \cdot \log\left(\frac{p\left(x_{i+1} \,\middle|\, x_i^{(k)}, v_{X,i}\right)}{p\left(x_{i+1} \,\middle|\, x_i^{(k)}\right)}\right).$$

An individual summand is called local collective transfer entropy.

In contrast to apparent TE, which captures only single-source transfers, collective TE captures single-source transfers as well as interaction-based transfers to X. Note that the collective transfer entropy is not the sum of the apparent transfer entropies from all sources but a sum of incrementally conditioned transfer entropies [53]. Analogously to the case of local AIS, negative local (collective) TE indicates that the sources' past states have been misinformative about the agent's next state.

Information in the agent's state neither being stored in its past nor being transferred from other agents is the third component and measured by the *local intrinsic uncertainty* [53].

Definition 8. *Let $X = (\dots, X_i, X_{i+1}, \dots)$ be a stationary discrete Markov process of order*

k. The intrinsic uncertainty of X is defined as

$$U_X = \sum_{\alpha_{X_{i+1}}} \sum_{\alpha_{X_i^{(k)}}} \sum_{\alpha_{\mathcal{V}_{X_i}^{(k)}}} -p\left(x_{i+1}, x_i^{(k)}, v_{x,i}\right) \cdot \log\left(p\left(x_{i+1} \,\middle|\, x_i^{(k)}, v_{x,i}\right)\right).$$

We refer to an individual summand as local intrinsic uncertainty.

Hence, the information needed to predict the next state of an agent is a composition of information being stored in the agent's own past, information being transferred from other agents, and intrinsic uncertainty. Formally, this can be expressed as [53]

$$H_X = A_X + T_X + U_X. \tag{7}$$

Equation (7) holds true for the local versions as well [53].

The local and non-local versions of the information-theoretic measures differ in their scope of application. The local measures are highly sensitive to short-term changes in the underlying time series, allowing a temporally more detailed analysis while at the same time increasing the amount of noise in the results. In contrast, the non-local measures yield smoother results, which is helpful in analyzing long-term development but can prevent the detection of small changes in the underlying data.

So far, we have only considered information theoretic measures of discrete random variables. We will now extend these definitions to continuous random variables.

2.3 Differential entropy

Information theoretic measures of continuous random variables are based on the definition of *differential entropy*, the continuous analogue of Shannon entropy ([27, Ch.8]).

Definition 9. *Let X be a continuous random variable with probability density function $f(x)$ and S_X the support of $f(x)$, i.e. the set where $f(x) > 0$. The differential entropy of X is defined as*

$$H_X = -\int_{S_X} f(x) \cdot \log\left(f(x)\right) dx.$$

Note that the differential entropy of X is not necessarily equal to the Shannon entropy obtained when discretizing X. The differential entropy of X changes with scaling of X and can be negative [49]. In contrast, the differential mutual information of X and Y, which we will define in the following, is equal to the mutual information of the discretized variables $X^{\triangle}$ and $Y^{\triangle}$ for the bin size limit $\triangle \to 0$ [49]. In particular, the two measures share the same properties.

Definition 10. *Let X and Y be continuous random variables with density functions $f(x)$ and $f(y)$, supports S_X and S_Y, respectively, and joint density function $f(x, y)$. The differ-*

ential mutual information between X and Y is defined as

$$I_{X;Y} = -\int_{S_X,S_Y} f(x,y) \cdot \log\left(\frac{f(x,y)}{f(x)\cdot f(y)}\right) dx\ dy.$$

Analogously, *continuous transfer entropy* can be defined [45]. Just like mutual information, it is always non-negative [82].

Definition 11. *Let X and Y be two stationary continuous Markov processes of order k and l. The continuous transfer entropy from Y to X is defined as*

$$T_{Y\to X} = \int_{S_{X_{i+1}}} \int_{S_{X_i^{(k)}}} \int_{S_{Y_i^{(l)}}} f\left(x_{i+1}, x_i^{(k)}, y_i^{(l)}\right) \cdot \log\left(\frac{f\left(x_{i+1}, x_i^{(k)}, y_i^{(l)}\right)}{f\left(x_{i+1}, x_i^{(k)}\right)}\right) dx_{i+1}\ dx_i^{(k)}\ dy_i^{(l)},$$

where $S_{X_{i+1}}$, $S_{X_i^{(k)}}$, and $S_{Y_i^{(l)}}$ are the supports of the respective density functions.

The main challenge in applying these measures to real-world data lies in the fact that probability or density functions underlying the data sets are usually not known. Hence, they have to be estimated on basis of the available samples. See [20, Ch.3 and Ch.4], [49], or [45] for a general overview of various estimation techniques.
Now that we have briefly introduced the information theoretic concepts being used in this thesis, we will return to the key question: how can we make the adaptive cycle computable?

3 Quantification of the Adaptive Cycle

After its first publication in 2001 [40], the idea of the adaptive cycle metaphor has entered several fields of research, in particular the field of socio-ecology. There have been various attempts to capture the adaptive cycle in terms of quantitative measurements. However, all of these approaches are *system-specific*. In this thesis, we develop a two-step universally applicable method to determine a complex system's position in the adaptive cycle. The method has been published by zu Castell and the author in [83].

In order to achieve universal applicability, our definitions of potential, connectedness, and resilience need to be defined on a very general representation of complex systems. We create such a representation in the first step of our method, making use of the abstract nature of information theory. Before going into detail, we want to outline the theoretical background of this first step.

Let $\mathcal{V}$ be a complex system. We identify each of its agents with a stationary Markov process $X = (\dots, X_i, X_{i+1}, \dots)$, specifying the agent's state at each time point. Assuming that every effective interaction among the agents leads to a transfer of information between them, transfer entropy as defined in (5) can be used to quantify interactions within the system. Following the notation of transfer entropy after Definition 5, every transfer determines a source and a destination agent. We consider the destination agent, being the one which processes information, as the active agent. Let $T_{Y\to X}$ be the (local) transfer entropy from agent Y to agent X. Considering the system's agents as nodes and the transfer entropy between them as edges yields a network representation which serves as a basis to compute potential, connectedness, and resilience independently of the concrete instantiation. While networks of *averaged* transfer entropy reflect the system's overall interaction structure, networks of *local* transfer entropy capture its interaction structure in the event of specific outcomes of the Markov processes.

In reality, the only information available about systems' agents X are series of states $\tilde{X} = (\tilde{x}_1, \dots, \tilde{x}_T)$ for a finite number of time points $1, \dots, T$. We assume stationarity of the underlying processes X. Since the probabilities/densities occurring in the definition of transfer entropy are usually not known, they have to be estimated on basis of the available samples. Let $\tilde{Y}$ be the realization of another agent. Transfer entropy from Y to X can be approximated via [45]

$$\tilde{T}_{Y\to X} = \sum_{i=\max\{k,l\}}^{N-1} \log\left(\frac{\tilde{p}\left(\tilde{x}_{i+1}|\tilde{x}_i^{(k)}, \tilde{y}_i^{(l)}\right)}{\tilde{p}\left(\tilde{x}_{i+1}|\tilde{x}_i^{(k)}\right)}\right), \tag{8}$$

where $\tilde{p}$ denote the probabilities/densities estimated on basis of $\tilde{X}$ and $\tilde{Y}$. Common estimation techniques include for example Gaussian and kernel estimation (see [49] for an

overview). The single summands represent estimations of the local transfer entropies.

The technique described above allows us to estimate one network, which then serves as a basis to compute the three systemic variables. However, one absolute value of potential, connectedness, and resilience each does not give us any insight about the system's position in the adaptive cycle. We need to know the *development* of the three systemic variables to determine the phase it is currently in. Hence, we need to extract a series of information networks, capturing the system's information *dynamics*. One possibility would be to consider networks of *local* transfer entropy, since they represent the system's interaction structure at specific time points. However, local values are very sensitive to noise in the underlying data. We estimate transfer entropy for certain time windows of data, creating a compromise between detailed dynamics and reliability. Hence, in order to estimate transfer entropy at time t ($\max\{k,l\}+1 \leq t \leq T$), setting a window size of w_t ($\max\{k,l\}+1 \leq w_t \leq T$), we calculate

$$\tilde{T}^t_{Y\to X} = \sum_{i=t-w_t+1+\max\{k,l\}}^{t-1} \log\left(\frac{\tilde{p}\left(\tilde{x}_{i+1}|\tilde{x}_i^{(k)},\tilde{y}_i^{(l)}\right)}{\tilde{p}\left(\tilde{x}_{i+1}\,\middle|\,\tilde{x}_i^{(k)}\right)}\right), \tag{9}$$

with the probabilities/densities $\tilde{p}$ being estimated on basis of data in the time window, i.e. $\tilde{X} = (\tilde{x}_{t-w_t+1},\dots,\tilde{x}_t)$ and $\tilde{Y} = (\tilde{y}_{t-w_t+1},\dots,\tilde{y}_t)$.

In the following, we will present our approach and its implementation in detail. We will start with the method's first step, the estimation of networks of information transfer (Section 3.1) and continue with the definitions of potential, connectedness and resilience in Sections 3.2 and 3.3. After a short examination of the three variables' behavior on random graphs (Section 3.4), we provide an overview of the method and illustrate its structure with a toy example in Section 3.5. Section 3.6 presents the R package QtAC (Quantifying the Adaptive Cycle), which enables a straightforward application of our method.

3.1 Estimation of networks of information transfer

This section is partly taken from [83]. Let $\mathcal{V}$ be a complex system whose agents X can be identified with stationary Markov processes $X = (\dots, X_i, X_{i+1}, \dots)$, specifying the agent's states at each time point. Assume that the only available information about each process is a finite realization $\tilde{X} = (\tilde{x}_1,\dots,\tilde{x}_T)$ at time points $1,\dots,T$. Let X and Y be two different agents of the system. In order to quantify their effective interaction, we estimate transfer entropy between them. At this point, the stationarity assumption is indispensable. It allows us to consider the data points $\{\tilde{x}_i | i = 1,\dots,T\}$ as samples of only one random variable. Omitting this assumption, a reliable estimation would require several realizations of X, which are, in reality, rarely available. The validity of the stationarity assumption of course depends on the concrete application example, however, it is in many cases justifiable for at least time windows of a certain length.

In order to estimate transfer entropy at time t, we use all samples falling within a time window preceding time t, i.e. $(\tilde{x}_t, \ldots, \tilde{x}_{t-w_t+1})$. The size w_t of this windows can either be fixed, or depend on the time t, i.e. $w_t = t$. In the first case, the window is shifted along with t to guarantee transfer entropy always being estimated on the same number of samples. Stationarity of the underlying processes has to be assumed for the fixed window size only. In the second case, the window starts at the beginning of the time series and is extended with increasing t. In this case, the full history of the time series is considered for estimating transfer entropy. The choice of the window size depends on the system under consideration and the specific question. In any case, it should be at least as large as the assumed order of the underlying Markov process.

Depending on the size of w_t and the data being available, it can be useful to increase the number of data points falling within every window by interpolation. To this end, we use the function `pchip` as being implemented in Matlab and R. Interpolation stabilizes the estimation in case of small window sizes. At the same time, interpolating too many points reduces stochasticity in the time series due to the deterministic component being introduced by the interpolation model. Thus, there is a trade-off between stochasticity and stability which has to be taken into account.

We estimate the networks of information transfer using the first Kraskov-Stögbauer-Grassberger (KSG) estimator `TransferEntropyCalculatorKraskov` as being provided with the JIDT toolkit [49]. It is based on the principles of a simple *kernel estimator*. The required probability density functions are estimated via kernel functions and used directly to compute local transfer entropy at each sample $\left(\tilde{x}_{i+1}, \tilde{x}_i^{(k)}, \tilde{y}_i^{(l)}\right)$. Averaging over the local values results in the transfer entropy between the two processes in the respective time window (compare Equation (8)). We use the KSG estimator since it is optimized to deal with small sample sizes. See [45, 48, 49] for details.
Table 1 displays those arguments of the estimation function, whose values will vary throughout the case studies presented in this thesis. We always use the default values for the parameters not mentioned here. When estimating transfer entropy from Y to X at time t, we use $(\tilde{y}_{t-w_t+1}, \ldots, \tilde{y}_t)$ as source data and $(\tilde{x}_{t-w_t+1}, \ldots, \tilde{x}_t)$ as destination data. Applying the function in the mode `computeAverageLocalOfObservations` yields non-local transfer entropy. The embedding lengths of past history k and l should be at least as large as the orders of the underlying Markov processes. This order can either be determined on basis of background knowledge of the system or be estimated using the Ragwitz optimization technique incorporated in the toolkit [49]. The so-called embedding delay $k_\tau \in \mathbb{N}$ is included via $x_i^{(k)} = (x_i, x_{i-\tau}, \ldots, x_{i-(k-1)\cdot\tau})$ and can be used to better empirically capture the state of the underlying variable. The delay u between source and destination denotes the time lag between the destination's next element x_{i+1} and the source's last element y_{i-u}. It should be increased according to the expected causal delay within the system.

	Description	Default
source	series of observations for the source process	
destination	series of observations for the destination process	
mode	local TE or average over local values	
k	embedding length of destination past history	1
k_τ	embedding delay for the destination variable	1
l	embedding length of source past history	1
l_τ	embedding delay for the source variable	1
delay u	time lag between source and destination	1

Table 1: Arguments of the Kraskov-Stögbauer-Grassberger estimator incorporated in the JIDT toolkit.

To distinguish actual interactions from random noise, we test the estimate via bootstrapping using the function `computeSignificance` incorporated in the toolkit. If the estimate is non-negative and below a given significance level, we accept it as weight of edge $e_{Y\to X}$. Repeating this procedure with all pairs of different components at fixed time t results in a weighted, directed graph

$$G^t = (\mathcal{V}, \{e_{Y\to X} | (Y, X) \in \mathcal{V} \times \mathcal{V}\}) \tag{10}$$

with weight function

$$\begin{aligned} &\omega^t \colon \mathcal{V} \times \mathcal{V} \to \mathbb{R}_+ \\ &\qquad e_{Y\to X} \mapsto \begin{cases} \tilde{T}^t_{Y\to X}, & \text{if the value is non-negative and significant,} \\ 0, & \text{otherwise,} \end{cases} \end{aligned}$$

as being our inferred model of interaction at time t. Given time series of abundances of length T for each component, we can estimate a sequence of interaction networks for time points $w_1, w_1 + 1, \ldots, T$.

Summarizing, the first step of our method infers models of information among the given variables in form of a series of networks $G^{w_1}, \ldots, G^T$, capturing the dynamics of the system's effective interaction pattern. The network G^t provides the basis for the computation of potential, connectedness, and resilience of the system at time t.

3.2 Definition of potential and connectedness

In order to quantify potential and connectedness of a complex system at a given time, we take recourse to information theoretic measures provided in the course of Ulanowicz's ecological ascendancy theory [74]. Ulanowicz was not the first to apply information theory

(IT) to ecology. Indeed, it was in 1955 that MacArthur presented an approach of how IT could be used to analyze networks of ecological flows [54]. He thereby provided an innovative framework for ecologists following the idea of Odum (see e.g. [61]) to consider an ecosystem as the ensemble of relationships among its components. In the subsequent years, however, IT was increasingly used in an autecological sense, applying it to distributions of numbers of organisms. Giving rise to ambiguity and yielding only few insights, disappointment arose and finally resulted in a broad rejection of IT in ecology [75]. In the seventies, Rutledge et al. revived and refined MacArthur's approach, paving the way for Ulanowicz, who was at this time seeking for a quantification of ecological succession.

We will now present Ulanowicz's quantitative approach to ecological succession, leading to our definitions of potential and connectedness. Afterwards, we will prove the measures' continuity.

3.2.1 Ulanowicz's ascendancy theory

In the late 20th century, several formal descriptions of ecological succession existed, among them Odum's 24 attributes of ecosystems in mature stages [61]. These attributes include a *large amount of organic matter*, a *well-organized community structure*, *narrrow niches*, and a *high information content*. However, a purely numerical description of ecological succession was still missing. Ulanowicz addressed this task by developing the ascendancy theory [74]. The theory is based on the assumption that the main driver behind succession is *autocatalysis*, a positive feedback mechanism consisting only of positive component interactions. Ulanowicz demonstrates that autocatalysis can explain various system behaviors like growth, selection, and competition. Speaking in terms of ecological networks, autocatalysis induces the transfer from loosely coupled, random exchanges to determinate, effective exchanges. It has both *extensive* effects, showing in an increase in total system activity, and *intensive* effects, which can be understood as focusing on autocatalytically effective processes. He combines the quantification of both effects in the measure of *ascendancy*, which we will now define.

Consider an ecosystem at a given time as the directed, weighted network G of physical flows e among its set of components $\mathcal{V}$, i.e.

$$G = (\mathcal{V}, \{e_{Y\to X} | (Y, X) \in \mathcal{V} \times \mathcal{V}\})$$

with weight function

$$\begin{aligned} \omega \colon \mathcal{V} \times \mathcal{V} &\to \mathbb{R}_{\geq 0} \\ e_{Y\to X} &\mapsto F_{Y\to X}. \end{aligned}$$

Then, the *total system throughput*

$$F = \sum_{(Y,X)\in\mathcal{V}\times\mathcal{V}} F_{Y\to X}$$

serves as a measure of total system activity and by this the extensive effects of autocatalysis. In order to quantify the intensive effects of autocatalysis, consider random variables A and B describing the flow of medium out of and into components, respectively. Recall that mutual information measures the constraint and thereby the deviation from indeterminacy between two variables (see Definition 3 in Section 2). Let A_Y be the event of medium leaving component Y and B_X the event of medium entering component X. Then, the mutual information between A and B is

$$I_{A;B} = \sum_{(Y,X)\in\mathcal{V}\times\mathcal{V}} p(A_Y, B_X) \cdot \log\left(\frac{p(A_Y, B_X)}{p(A_Y)\cdot p(B_X)}\right).$$

Using the estimators $p(A_Y, B_X) = F_{Y\to X}/F$ and

$$p(A_Y) = \sum_{X'\in\mathcal{V}} F_{Y\to X'}/F$$
$$p(B_X) = \sum_{Y'\in\mathcal{V}} F_{Y'\to X}/F,$$

we can estimate the mutual information via

$$\tilde{I}_{A;B} = \sum_{(Y,X)\in\mathcal{V}\times\mathcal{V}} \frac{F_{Y\to X}}{F} \cdot \log\left(\frac{F_{Y\to X}\cdot F}{\sum_{X'\in\mathcal{V}} F_{Y\to X'}\cdot\sum_{Y'\in\mathcal{V}} F_{Y'\to X}}\right).$$

Note that a summand of $\tilde{I}_{A;B}$ becomes maximal if

$$F_{Y\to X} = \sum_{X'\in\mathcal{V}} F_{Y\to X'} = \sum_{Y'\in\mathcal{V}} F_{Y'\to X},$$

hence, if the only edge leaving Y and the only edge arriving at X is the edge from Y to X. In this case, knowing that medium is leaving Y means knowing that medium is arriving at Y and the other way round. The transfer is determinate and focused. Scaling $\tilde{I}_{A;B}$ with the total system throughput F yields the system's *ascendancy*

$$A = \sum_{(Y,X)\in\mathcal{V}\times\mathcal{V}} F_{Y\to X} \cdot \log\left(\frac{F_{Y\to X}\cdot F}{\sum_{X'\in\mathcal{V}} F_{Y\to X'}\cdot\sum_{Y'\in\mathcal{V}} F_{Y'\to X}}\right).$$

Coming back to the characteristics of ecosystem maturation as described by Odum, Ulanowicz notes that all of them necessarily lead to an increase in ascendancy. He states the following principle [74, p.311]:

> "*In the absence of major perturbations, ecosystems exhibit a propensity towards a configuration of ever-greater network ascendancy.*"

Under this assumption, system's ascendancy can be understood as a quantification of succession.

The ascendancy of a system is always bounded from above by the system's aggregate indeterminacy or *capacity* [76]

$$K = -\sum_{(Y,X)\in\mathcal{V}\times\mathcal{V}} F_{Y\to X}\cdot\log\left(\frac{F_{Y\to X}}{F}\right).$$

Note that the capacity is a (scaled) entropy estimator of the random variable which describes the system's flows (see Definition 1). As such, it is high in the case of many, equally weighted flows.
The difference between capacity and ascendancy indicates the degree of disorder, indeterminacy, and inefficiency in the network. Those aspects prove to be advantageous in times of perturbations and thereby contribute to the system's stability and ability to survive. Ulanowicz understands capacity as a measure of the system's sustainability since it quantifies both efficient growth and stability.
In his computations of ascendancy and capacity, Ulanowicz usually uses 2 as base for the logarithm [74, 76].

Let us recall our heuristic definitions of potential and connectedness from Section 1. *Potential measures the magnitude of external variation a system can survive. Survival can involve deep internal structural changes.* Ulanowicz's measure of capacity captures exactly this idea. Sustainability requires the capability to survive external variation. Conversely, efficient growth and stability are essential for the survival in a changing environment.
Connectedness quantifies the internal controllability of a system, i.e. the degree to which it controls its own development. It contrasts the degree to which external variation forces the system into internal changes. A system of high ascendancy is characterized by effective, streamlined interactions, which create dependencies and mutual regulation among the agents and decrease sensitivity towards environmental variation. Hence, ascendancy can be understood as a measure of a system's connectedness. Ulanowicz himself made that connection between his theory and the adaptive cycle when describing a system of high ascendancy as a "catastrophe waiting to happen" [74, p. 311] - words that Holling used to characterize a system of high connectedness in [40].

We use Ulanowicz's capacity and ascendancy as measures of potential and connectedness, respectively. But we go beyond Ulanowicz's approach by applying his measures to networks of information transfer as defined in Section 3.1 instead of networks of physical flows. We identify a system $\mathcal{V}$ at a given time with the weighted, directed network G of information

transfers among its components following Equation (10). We define the system's *potential* at the given time as

$$P = -\sum_{(Y,X)\in\mathcal{V}\times\mathcal{V}} T_{Y\to X}\cdot\log_2\left(\frac{T_{Y\to X}}{T}\right)$$

and the system's *connectedness* at the given time as

$$C = \sum_{(Y,X)\in\mathcal{V}\times\mathcal{V}} T_{Y\to X}\cdot\log_2\left(\frac{T_{Y\to X}\cdot T}{\sum_{X'\in\mathcal{V}} T_{Y\to X'}\cdot\sum_{Y'\in\mathcal{V}} T_{Y'\to X}}\right).$$

Applying the measures to a system's information theoretic structure instead of its explicit interaction structure does not change the measures' meaning. The consequences of an effective interaction, be they positive or negative for the components involved, are reflected in suitable components' abundance data, on the basis of which the networks of information transfer are estimated. Every effective interaction will thus result in a transfer of information between the respective components. Hence, our approach builds on the effects of interactions, irrespective of their concrete instantiation. The change to information networks does not cause any information loss. On the contrary, as a network of information transfer only captures *effective* interactions among the components, it can yield an even more refined picture of the system's internal dynamics than networks of physical flows. A further advantage of the information theoretic approach is the practical applicability. In contrast to data on physical flows of a system, which is rarely available in practice, components' abundance data belongs to the most basic information about a system. The estimation does not even require homogeneous units. Hence, considering networks of information transfer instead of networks of physical flows significantly expands the application possibilities of our method.

It remains to verify the continuity of these measures with respect to edges whose weight is converging to zero.

3.2.2 Continuity of the measures

Let $N\in\mathbb{N}$ and $V=\{1,\dots,N\}$. Recalling the conventions $\frac{0}{0}=0$ and $0\cdot\log(0)=0$, potential and connectedness are defined as functions

$$\begin{aligned} P:\mathbb{R}_{\geq 0}^{N\times N} &\to \mathbb{R} \\ (x)_{ij} &\mapsto \sum_{(i,j)\in V\times V} x_{i,j}\cdot\log\left(\frac{x_{i,j}}{x}\right) \end{aligned}$$

and

$$\begin{aligned} C : \mathbb{R}_{\geq 0}^{N\times N} &\to \mathbb{R} \\ (x)_{ij} &\mapsto \sum_{(i,j)\in V\times V} x_{i,j} \cdot \log\left(\frac{x_{i,j}\cdot x_{**}}{x_{i*}\cdot x_{*j}}\right), \end{aligned}$$

where

$$x_{**} = \sum_{(i,j)\in V\times V} x_{i,j} \qquad x_{i*} = \sum_{j=1}^{N} x_{i,j} \qquad x_{*j} = \sum_{i=1}^{N} x_{i,j}.$$

Besides, define

$$\begin{aligned} x_{**}^{i,j} &= x_{**} - x_{i,j}, \\ x_{i*}^{i,j} &= x_{i*} - x_{i,j}, \\ x_{*j}^{i,j} &= x_{*j} - x_{i,j}. \end{aligned}$$

We want to show that the extension of the functions P and C from $\mathbb{R}_{>0}^{N\times N}$ to $\mathbb{R}_{\geq 0}^{N\times N}$ is continuous. We only have to verify continuity of one summand of P and C. The continuity of P and C, respectively, directly follows. Let us start with function P. Consider

$$\mathcal{P} = (\rho)_{ij} \in \mathbb{R}_{\geq 0}^{N\times N}$$

with $\rho_{s,t} = 0$ for some $(s,t) \in V \times V$. Let $(\mathcal{P}_n)_{n\in\mathbb{N}}$ such that

$$\mathcal{P}_n = (\rho_n)_{ij} \in \mathbb{R}_{\geq 0}^{N\times N} \ \forall n \quad \text{and} \quad \lim_{n\to\infty} \mathcal{P}_n = \mathcal{P}.$$

Let $\rho_{n_{s,t}} = \mathcal{P}_n(s,t)$ and $\rho_n^{s,t} = \rho_{n_{**}} - \rho_{n_{s,t}}$. We have

$$\begin{aligned} &\left|\rho_{n_{s,t}} \cdot \log\left(\frac{\rho_{n_{s,t}}}{\rho_{n_{s,t}} + \rho_n^{s,t}}\right)\right| \\ =& \left|\rho_{n_{s,t}} \cdot \log\left(\rho_{n_{s,t}}\right) - \rho_{n_{s,t}} \cdot \log\left(\rho_{n_{s,t}} + \rho_n^{s,t}\right)\right| \\ \leq& \underbrace{\left|\rho_{n_{s,t}} \cdot \log\left(\rho_{n_{s,t}}\right)\right|}_{\text{(A)}} + \underbrace{\left|\rho_{n_{s,t}} \cdot \log\left(\rho_{n_{s,t}} + \rho_n^{s,t}\right)\right|}_{\text{(B)}}. \end{aligned}$$

According to L'Hospital,

$$\text{(A)} \underset{n\to\infty}{\to} 0.$$

In order to determine the limit of term (B), we have to distinguish two cases. If $\rho_{**} > 0$, we

have

$$\begin{aligned}\lim_{n\to\infty}\left|\rho_{n_{s,t}}\cdot\log\left(\rho_{n_{s,t}}+\rho_n^{s,t}\right)\right| &= \left|\lim_{n\to\infty}\rho_{n_{s,t}}\cdot\log\left(\lim_{n\to\infty}\left(\rho_{n_{s,t}}+\rho_n^{s,t}\right)\right)\right| \\ &= \left|0\cdot\log\left(\rho^{s,t}\right)\right| \\ &= 0.\end{aligned}$$

If $\rho_{**}=0$, we know that for n large enough, $\rho_{n_{s,t}}$ and $\rho_n^{s,t}$ are small enough such that

$$1\geq\rho_{n_{s,t}}+\rho_n^{s,t}\geq\rho_{n_{s,t}}.$$

Hence,

$$\left|\log\left(\rho_{n_{s,t}}+\rho_n^{s,t}\right)\right|\leq\left|\log\left(\rho_{n_{s,t}}\right)\right|,$$

and thereby

$$(\mathrm{B})\leq\left|\rho_{n_{s,t}}\cdot\log\left(\rho_{n_{s,t}}\right)\right|\underset{n\to\infty}{\to}0.$$

The proof for function C requires similar arguments. Let

$$\begin{aligned}\rho_{n_{s*}}^{s,t} &= \rho_{n_{s*}}-\rho_{n_{s,t}} \text{ and} \\ \rho_{n_{*t}}^{s,t} &= \rho_{n_{*t}}-\rho_{n_{s,t}}.\end{aligned}$$

We have

$$\begin{aligned}&\left|\rho_{n_{s,t}}\cdot\log\left(\frac{\rho_{n_{s,t}}\cdot(\rho_{n_{s,t}}+\rho_n^{s,t})}{(\rho_{n_{s,t}}+\rho_{n_{s*}}^{s,t})\cdot(\rho_{n_{s,t}}+\rho_{n_{*t}}^{s,t})}\right)\right| \\ =&\left|\rho_{n_{s,t}}\cdot\log\left(\rho_{n_{s,t}}^2+\rho_{n_{s,t}}\cdot\rho_n^{s,t}\right)-\rho_{n_{s,t}}\cdot\log\left(\rho_{n_{s,t}}^2+\rho_{n_{s,t}}\cdot(\rho_{n_{s*}}^{s,t}+\rho_{n_{*t}}^{s,t})+\rho_{n_{s*}}^{s,t}\cdot\rho_{n_{*t}}^{s,t}\right)\right| \\ \leq&\underbrace{\left|\rho_{n_{s,t}}\cdot\log\left(\rho_{n_{s,t}}^2+\rho_{n_{s,t}}\cdot\rho_n^{s,t}\right)\right|}_{(\mathrm{A})}+\underbrace{\left|\rho_{n_{s,t}}\cdot\log\left(\rho_{n_{s,t}}^2+\rho_{n_{s,t}}\cdot(\rho_{n_{s*}}^{s,t}+\rho_{n_{*t}}^{s,t})+\rho_{n_{s*}}^{s,t}\cdot\rho_{n_{*t}}^{s,t}\right)\right|}_{(\mathrm{B})}\end{aligned}$$

At first, let us consider term (A). For n large enough, $\rho_{n_{s,t}}$ is small enough such that

$$1\geq\rho_{n_{s,t}}^2+\rho_{n_{s,t}}\cdot\rho_n^{s,t}\geq\rho_{n_{s,t}}^2.$$

Thereby,

$$\left|\log\left(\rho_{n_{s,t}}^2+\rho_{n_{s,t}}\cdot\rho_n^{s,t}\right)\right|\leq\left|\log\left(\rho_{n_{s,t}}^2\right)\right|$$

and hence,

$$(\mathrm{A})\leq\left|\rho_{n_{s,t}}\cdot\log\left(\rho_{n_{s,t}}^2\right)\right|\underset{n\to\infty}{\to}0.$$

Let us now address term (B). If $\rho_{s*} \cdot \rho_{*t} > 0$, we get

$$\begin{aligned}
&\lim_{n\to\infty} \left|\rho_{n_{s,t}} \cdot \log\left(\rho^2_{n_{s,t}} + \rho_{n_{s,t}} \cdot (\rho^{s,t}_{n_{s*}} + \rho^{s,t}_{n_{*t}}) + \rho^{s,t}_{n_{s*}} \cdot \rho^{s,t}_{n_{*t}}\right)\right| \\
&= \left|\lim_{n\to\infty} \rho_{n_{s,t}} \cdot \log\left(\lim_{n\to\infty}\left(\rho^2_{n_{s,t}} + \rho_{n_{s,t}} \cdot (\rho^{s,t}_{n_{s*}} + \rho^{s,t}_{n_{*t}}) + \rho^{s,t}_{n_{s*}} \cdot \rho^{s,t}_{n_{*t}}\right)\right)\right| \\
&= \left|0 \cdot \log\left(\rho^{s,t}_{s*} \cdot \rho^{s,t}_{*t}\right)\right| \\
&= 0
\end{aligned}$$

If $\rho_{s*} \cdot \rho_{*t} = 0$, we know that for n large enough, $\rho^{s,t}_{n_{s*}} \cdot \rho^{s,t}_{n_{*t}}$ is small enough such that

$$1 \geq \rho^2_{n_{s,t}} + \rho_{n_{s,t}} \cdot (\rho^{s,t}_{n_{s*}} + \rho^{s,t}_{n_{*t}}) + \rho^{s,t}_{n_{s*}} \cdot \rho^{s,t}_{n_{*t}} \geq \rho^2_{n_{s,t}}$$

and therefore

$$\left|\log\left(\rho^2_{n_{s,t}} + \rho_{n_{s,t}} \cdot (\rho^{s,t}_{n_{s*}} + \rho^{s,t}_{n_{*t}}) + \rho^{s,t}_{n_{s*}} \cdot \rho^{s,t}_{n_{*t}}\right)\right| \leq \left|\log\left(\rho^2_{n_{s,t}}\right)\right|.$$

We can conclude that

$$\text{(B)} \leq \left|\rho_{n_{s,t}} \cdot \log\left(\rho^2_{n_{s,t}}\right)\right| \underset{n\to\infty}{\to} 0.$$

We have now quantitatively defined two of three systemic variables. In order to determine the position of a complex system in the adaptive cycle at a given time, it remains to define Holling's and Gunderson's notion of resilience. We will approach this task in the following section.

3.3 Definition of resilience

In 1973, Holling introduced the notion of *resilience* in the context of ecosystems, defining it as "a measure of the persistence of systems and of their ability to absorb change and disturbance and still maintain the same relationships between populations or state variables" [41, p.14]. This understanding of resilience was revived in the Resilience Alliance's panarchy theory [39]. In quantifying resilience, we were inspired by an established measure in spectral graph theory, the *connectivity* of a graph [33]. However, this measure had so far mainly been used in the context of *undirected* graphs.

In the following, we will introduce the notions of Laplacian matrices and connectivity (Section 3.3.1) and subsequently transfer them to the case of directed graphs (Section 3.3.2). These sections build on the descriptions in [83]. Eventually, we will prove a relation between the directed Laplacian spectrum and the underlying graph's topology which justifies our choice of a definition for resilience (Section 3.3.3).

3.3.1 Graph theoretical preliminaries

The following two sections build on [83]. Let $G = [\mathcal{V}, E]$ be a weighted, undirected graph with $N \geq 1$ nodes and weight function $\omega \colon E \to \mathbb{R}_{\geq 0}$. We call

$$d_u = \sum_{v \in V} \omega(u, v)$$

the *degree* of a node u. The graph's *adjacency matrix* is defined as

$$A(u, v) = \omega(u, v) \; \forall u, v \in V,$$

its *degree matrix* as

$$D(u, v) = \begin{cases} d_u, & \text{if } u = v \\ 0, & \text{otherwise.} \end{cases}$$

From now on, we will follow the convention $D^{-1}(u, u) = 0$ if $D(u, u) = 0$. Multiplying $(D - A)$ with $D^{-\frac{1}{2}}$ from both sides, yields the *Laplacian matrix* of G:

$$\begin{aligned} L &= D^{-\frac{1}{2}} \cdot (D - A) \cdot D^{-\frac{1}{2}} \\ &= I - D^{-\frac{1}{2}} \cdot A \cdot D^{-\frac{1}{2}}. \end{aligned}$$

Therefore, we have

$$L(u, v) = \begin{cases} 1 - \frac{\omega(u,u)}{d_u}, & \text{if } u = v \text{ and } d_u \neq 0 \\ \frac{-\omega(u,v)}{\sqrt{d_u \cdot d_v}}, & \text{if } u \neq v \text{ and } d_u \neq 0,\, d_v \neq 0 \\ 0, & \text{otherwise.} \end{cases}$$

As the Laplacian matrix is symmetric, all of its eigenvalues are real. A short computation shows that all eigenvalues are non-negative and that 0 is always an eigenvalue of L [25, Ch. 1.4]. Let $\sigma_0 = 0 \leq \sigma_1 \leq \cdots \leq \sigma_{n-1}$ be the spectrum of L. It has been shown that the multiplicity of the eigenvalue 0 is equal to the number of components of G [25].

Our interest lies in the smallest non-trivial eigenvalue σ_G of the Laplacian matrix, often called its *connectivity* [33]. It can be understood as a measure of how "easily" a new component can be generated by deleting edges of G. Recall that the spectrum of a matrix is continuous with respect to the matrix's entries. Hence, if σ_G is close to 0, a slight change of the Laplacian matrix can shift σ_G to 0. Observe that the non-diagonal entries of the Laplacian matrix are continuous with respect to the underlying graph's edge weights. Therefore, we know that if σ_G is close to 0, a small perturbation, like the deletion of a low-weighted edge, can generate a new component. Whereas, if σ_G is high-valued, a great disturbance like the deletion of many or high-weighted edges might be needed to generate a new component.

Hence, σ_G quantifies the vulnerability of a graph to perturbation in form of edge deletion.

Let us recall our heuristic definition of resilience at a given time as *the magnitude of internal structural change which can be reversed by the system* (see Section 1). In the system's information network, such a change of internal processes could express itself in the omission of a transfer between one agent X and another agent Y. If an alternative path of information transfer between X and Y exists, there is a chance of it compensating the information loss. Whenever the omission of an edge provokes the generation of a new component, a compensation of the loss via existing structures is not possible. In this case, the system's internal processes will at least partially change.

However, the classical form of σ_G is insufficient for us as it is only defined for undirected graphs. We are interested in directed graphs (*digraphs*), considering the direction of transfers within a system as crucial for its identity. Therefore, we need to transfer these notions to the case of directed graphs. Several versions of the Laplacian matrix of a directed graph exist in literature [15, 26, 81], mainly differing in their normalization and the fact whether they are based on the out- or in-degrees of the graphs' nodes.

3.3.2 Directed Laplacian matrices and their eigenvalues

Let $G = [\mathcal{V}, E]$ be a weighted, directed graph with $N \geq 1$ nodes and weight function $\omega\colon E \to \mathbb{R}_{\geq 0}$. We define

$$d_{u,out} = \sum_{u \to v} \omega(u, v)$$

and

$$d_{u,in} = \sum_{v \to u} \omega(v, u)$$

the *out-* and *in-degree* of a node u, respectively. Let $c \in \mathbb{R}_{>0}$ be a standardization constant. We define the *directed Laplacian matrices* of G by

$$L_{out}(u,v) = c \cdot \begin{cases} \sqrt{d_{u,out}} - \frac{\omega(u,u)}{\sqrt{d_{u,out}}}, & \text{if } u = v \text{ and } d_{u,out} \neq 0, \\ \frac{-\omega(u,v)}{\sqrt{d_{u,out}}}, & \text{if } u \neq v \text{ and } d_{u,out} \neq 0, \\ 0, & \text{otherwise} \end{cases} \tag{11}$$

and

$$L_{in}(u,v) = c \cdot \begin{cases} \sqrt{d_{u,in}} - \frac{\omega(u,u)}{\sqrt{d_{u,in}}}, & \text{if } u = v \text{ and } d_{u,in} \neq 0, \\ \frac{-\omega(u,v)}{\sqrt{d_{v,in}}}, & \text{if } u \neq v \text{ and } d_{v,in} \neq 0, \\ 0, & \text{otherwise.} \end{cases} \tag{12}$$

Note that in the case of G being a network of information transfer following Definition 10, $\omega(u, u) = 0\ \forall u \in \mathcal{V}$, since we only consider transfer between *distinct* agents. However,

we provide a more general definition here, broadening the range of application possibilities.

Analogously to the undirected case, the Laplacian matrices have a relation to the adjacency matrix A and the directed degree matrices

$$D_{out}(u,v) = \begin{cases} d_{u,out}, & \text{if } u = v \\ 0, & \text{otherwise} \end{cases}$$

and

$$D_{in}(u,v) = \begin{cases} d_{u,in}, & \text{if } u = v \\ 0, & \text{otherwise.} \end{cases}$$

Define D_{out}^{-1} (and D_{in}^{-1} analogously) as

$$D_{out}^{-1}(u,u) = \begin{cases} D(u,u)^{-1}, & \text{if } D(u,u) \neq 0 \\ 0, & \text{if } D(u,u) = 0. \end{cases}$$

A short computation shows that

$$L_{out} = c \cdot D_{out}^{-\frac{1}{2}} (D_{out} - A), \quad \text{and} \quad L_{in} = c \cdot (D_{in} - A) D_{in}^{-\frac{1}{2}}.$$

From now on, whenever statements apply to L_{out} and L_{in} or D_{out} and D_{in}, we will subsume both matrices under L_* and D_*, respectively. We will write L_*^G in case we want to specify the graph G underlying L_*.

Eventually, we can formulate our definition of resilience. To this end, we want to find an analogue of the eigenvalue λ_G defined in the previous section. But we have to be aware of the differences between the two cases. Previously, we were considering symmetric matrices with real, positive eigenvalues. Now we are dealing with general matrices with complex eigenvalues. Therefore, we restrict ourselves to the absolute values of the real parts of the eigenvalues. Furthermore, by our definition, a directed graph has two Laplacian matrices, so our definition should respect both of them.

Let $\mathcal{V}$ be a system at a given time being identified with the weighted, directed network G of information transfers among its components following Equation (10). Let L_{in} and L_{out} be the Laplacian matrices of G. Given that the network contains at least one nontrivial transfer, we define

$$R = \min \{ |\mathcal{R}\,\sigma| : \sigma \in \mathrm{Spec}(L_{out}) \cup \mathrm{Spec}(L_{in}), \sigma \neq 0 \}.$$

as the system's *resilience*. If all transfers are trivial, the system's resilience is set to 0 to ensure continuity of the measure.

Example 1. *Let G be a complete graph with $N > 1$ nodes and uniform edge weight $s > 0$. Then,*

$$L_* = c \cdot \begin{pmatrix} \sqrt{s \cdot (N-1)} & \frac{-s}{\sqrt{s \cdot (N-1)}} & \cdots & \frac{-s}{\sqrt{s \cdot (N-1)}} \\ \frac{-s}{\sqrt{s \cdot (N-1)}} & \ddots & \ddots & \vdots \\ \vdots & \ddots & \ddots & \frac{-s}{\sqrt{s \cdot (N-1)}} \\ \frac{-s}{\sqrt{s \cdot (N-1)}} & \cdots & \frac{-s}{\sqrt{s \cdot (N-1)}} & \sqrt{s \cdot (N-1)} \end{pmatrix}.$$

This Laplacian matrix has eigenvalue 0 *with corresponding right eigenvector*

$$(1, \ldots, 1)$$

and eigenvalue

$$c \cdot \frac{\sqrt{s} \cdot N}{\sqrt{N-1}}$$

with corresponding eigenvectors

$$\{(1, -1, 0, \ldots, 0), \ldots, (1, 0, \ldots, 0, -1)\}.$$

Hence, the resilience of a complete graph with uniform edge weight s is

$$R(G) = c \cdot \frac{\sqrt{s} \cdot N}{\sqrt{N-1}}.$$

Remark 1. *Before computing a system's resilience, one should ask questions like 'Do I want the resilience to depend on the absolute edge weights? Hence, should a complete graph with uniform edge weight 2 be more resilient than a complete graph with uniform edge weight 1?' or 'Do I want the resilience to depend on the number of nodes? Hence, should a complete graph on 10 nodes be more resilient than a complete graph on 5 nodes?'. There is no right or wrong answer to these questions. The answer is depending on the specific context to be studied. The measure of resilience can be adjusted to the respective requirements by means of its standardization constant c. Especially when it comes to the comparison of resilience of different systems, standardization can be a helpful tool. Let M be the maximal edge weight of a graph G. Example 1 demonstrates that*

$$c = \frac{\sqrt{N-1}}{N} \text{ or } c = \frac{1}{\sqrt{M}}$$

are reasonable choices to standardize R regarding the number of nodes or the maximal edge weight, respectively.

Remark 2. *Note that in some of our earlier case studies, we use a symmetrically normalized*

version of the Laplacian matrices, namely

$$L_{out} = c \cdot D_{out}^{-\frac{1}{2}}(D_{out} - A)D_{out}^{-\frac{1}{2}}, \quad \text{and} \quad L_{in} = c \cdot D_{in}^{-\frac{1}{2}}(D_{in} - A)D_{in}^{-\frac{1}{2}}.$$

By now, we are only using the Laplacian matrices defined in Equations (11) and (12). They have the advantage that their eigenvalues change continuously with the edge weights of the underlying graph. For the case studies presented in this thesis, both versions qualitatively yield comparable results.

In the following, we will show that the spectra of directed Laplacian matrices are related to the underlying graph's topology in a similar way as the spectrum of the undirected Laplacian matrix. This relation justifies our choice of R as measure of a system's resilience.

3.3.3 The Laplacian spectrum related to the graph's topology

We will start with a rough estimate of the eigenvalues of L_{in} and L_{out}. For this purpose, we calculate the Gershgorin circles of these matrices (see for example [79]).
Let $u \in \mathcal{V}$. The center of the corresponding Gershgorin circle of L_{out} is located at $c \cdot \sqrt{d_{u,out}}$. Its radius is

$$\begin{aligned}
\sum_{v \in \mathcal{V}, v \neq u} |L_{out}(u,v)| &= c \cdot \sum_{v \in V, v \neq u} \frac{w(u,v)}{\sqrt{d_{u,out}}} \\
&= \frac{c}{\sqrt{d_{u,out}}} \sum_{v \in \mathcal{V}, v \neq u} w(u,v) \\
&= \frac{c \cdot d_{u,out}}{\sqrt{d_{u,out}}} \\
&= c \cdot \sqrt{d_{u,out}}.
\end{aligned}$$

Therefore, the real parts of the eigenvalues of L_{out} cannot be negative. Column-wise consideration of L_{in} shows that its Gershgorin circles have center and radius $c \cdot \sqrt{d_{in}}$. Hence, the real parts of L_{in}'s eigenvalues cannot be negative as well. Observe that, due to their position in the Gershgorin circles, for both L_{out} and L_{in}, there cannot be an eigenvalue with real value 0 except for 0 itself. Besides, due to the fact that all row sums of L_{out} and all column sums of L_{in} are 0, every Laplacian matrix has eigenvalue 0.

In the following, we want to examine the multiplicity of the eigenvalue 0 of normalized Laplacian matrices. To this end, we introduce the following notions.

Definition 12. *A directed graph $G = [\mathcal{V}, E]$ is called tree if there is a node $v \in \mathcal{V}$ such that for every other node $u \in \mathcal{V}$, there is exactly one directed path from v to u.*

Definition 13. *Let $G = [\mathcal{V}, E]$ be a directed graph. A spanning (forest) of G is a set of subgraphs $G_i = [\mathcal{V}_i, E_i]$, $i \in I$, of G such that every G_i is a tree and that $\bigcup_{i \in I} \mathcal{V}_i = \mathcal{V}$. We*

say that together, the trees G_i span the graph G. A spanning of G is called minimal if every other spanning contains at least as many trees.

In [80] and [81], it is shown that the multiplicity of the zero eigenvalue of $L = D_{out} - A$ is equal to the number of trees in a minimal spanning of the reversal of the underlying graph. We transfer this result to our version of directed Laplacian matrices, following the structure of the proofs of [80, Theorem 9 and 10].

We start by proving a lemma which is well known for unnormalized directed Laplacian matrices (see for example [81]). To this end, we first have to introduce some new notions.

Definition 14. *A directed graph (digraph) $G = [\mathcal{V}, E]$ is called strongly connected iff for all $u \neq v \in \mathcal{V}$, there exists a path from u to v.*

Definition 15. *The reversal of a digraph $G = [\mathcal{V}, E]$ is defined as $\bar{G} = [\mathcal{V}, \bar{E}]$, where an edge $(u, v) \in \bar{E}$ iff the edge $(v, u) \in E$.*

Lemma 1. *A digraph is strongly connected iff its Laplacian matrix is irreducible.*

Proof. We need to prove the statement only for L_{out} because L_{in} is just L_{out}^T of the reversal of the underlying graph and a graph is strongly connected iff the same holds for its reversal. Let L_{out} be reducible. Then there exists a permutation matrix M such that

$$ML_{out}M^T = \begin{pmatrix} L_{ss} & 0 \\ L_{ts} & L_{tt} \end{pmatrix},$$

where $L_{ss} \in \mathbb{R}^{s \times s}, s \in \{1, \ldots, N-1\}$. It becomes clear that there is a disjoint union $V = I \cup J$ such that

$$L_{out}(i, j) = 0 \ \forall i \in I = \{1, \ldots, s\},\ j \in J = \{s+1, \ldots, N\}.$$

Hence, there is no directed path from any node $i \in I$ to any node $j \in J$ and therefore, the underlying graph is not strongly connected.
We will now show the other direction. Let the underlying graph of L_{out} not be strongly connected. Then there exists a node u and a node v such that there is no directed path from u to v. Let V_v be the set of nodes with directed path to v, including v, and $\overline{V_v}$ its complement. Note that $\overline{V_v}$ is not empty as $u \in \overline{V_v}$. Clearly, there is no edge from a node in $\overline{V_v}$ to a node in V_v. After a possible reordering of the nodes, we can write L_{out} as

$$ML_{out}M^T = \begin{pmatrix} L_{ss} & 0 \\ L_{ts} & L_{tt} \end{pmatrix},$$

where the first s rows of the matrix correspond to the nodes in $\overline{V_v}$, the last $N - S$ ones to the nodes in V_v. Therefore, L_{out} is reducible.

□

Corollary. *The Laplacian matrix of a strongly connected graph has eigenvalue* 0 *of multiplicity one.*

Proof. Let L_* be the Laplacian matrix of a strongly connected graph. We consider

$$B = k \cdot I - L_*,$$

where $k > 2 \cdot c \cdot \max\{d_{u,*} | u \in V\}$. Clearly, all entries of matrix B are non-negative. According to Lemma 1, L_* and thereby B is irreducible. Therefore, the Perron-Frobenius Theorem tells us that the spectral radius of B is a simple eigenvalue of B (see for example [79]). Thanks to the choice of k, this is equivalent to 0 being a simple eigenvalue of L_*. □

Definition 16. *Consider a matrix $A \in \mathbb{R}^{N \times N}$, $N \in \mathbb{N}$. The matrix A is N-reducible if it is diagonal. For $1 \leq m < N$, the matrix A is m-reducible if it is not $(m+1)$-reducible and it can be written as*

$$A = M \begin{pmatrix} B_1 & B_{1,2} & \dots & & & B_{1,k+m} \\ & \ddots & & & & \\ & & B_k & B_{k,k+1} & \dots & B_{k,k+m} \\ & & & B_{k+1} & 0 & 0 \\ & & & & \ddots & 0 \\ & & & & & B_{k+m} \end{pmatrix} M^T, \tag{13}$$

where M is a permutation matrix and B_i are square irreducible matrices.

Remark 3. *Let L_* be a Laplacian matrix. Written in form (13), $B_{k+1}, \dots, B_{k+m}$ are the Laplacian matrices of strongly connected components of the underlying graph.*

Lemma 2. *A Laplacian matrix L_* is m-reducible iff the multiplicity of its eigenvalue* 0 *is m.*

Proof. Let L_{out} be the Laplacian out-matrix of a graph G. Being m-reducible, the matrix can be written in form (13), where $B_{k+1}, \dots, B_{k+m}$ are the Laplacian matrices of strongly connected components of the graph. According to Corollary 3.3.3, each of these matrices has a simple 0 eigenvalue. Hence, the multiplicity of eigenvalue 0 of L_{out} is at least m.
We know that for all i with $1 \leq i \leq k$, there exists $j > i$ such that $B_{i,j} \neq 0$, otherwise, L_{out} would be at least $m+1$-reducible. Hence, one of the row sums of B_i is positive and by [80, Theorem 1], B_i is non-singular, i.e. has no eigenvalue 0. For $1 \leq i \leq k$, let l_i be the number of rows of matrix B_i. Consider a left eigenvector v of L_{out}. Assuming that v corresponds to eigenvalue 0, one can show recursively that the first $\sum_{1 \leq i \leq k} l_i$ entries of v have to be 0. Therefore, the multiplicity of the eigenvalue 0 of L_{out} is maximally and thereby exactly m.

If L_{out} is not m-reducible, it is m'-reducible for some $m' \neq m$. Then the multiplicity of the eigenvalue 0 of L_{out} is m'.
In order to see that the statement is true for L_{in} of graph G, notice that the transpose of L_{in} is the Laplacian out-matrix of the reversal of G, i.e.

$$\overline{L_{in}^{G}} = L_{out}^{\overline{G}}.$$

□

Now we can relate this equality to the topology of the underlying graph:

Theorem 1. *The multiplicity of the eigenvalue* 0 *of a Laplacian matrix* L_{out} *is equal to the number of trees in a minimal spanning of the reversal of the underlying graph. Analogously, the multiplicity of the eigenvalue* 0 *of a Laplacian matrix* L_{in} *is equal to the number of trees in a minimal spanning of the underlying graph itself.*

Proof. Let L_{out} be the Laplacian out-matrix of a graph G. We know that the multiplicity of the eigenvalue 0 is equal to its order of reducibility. Let this order be m. Thereby, G has m strongly connected components, $B_{k+1}, \ldots, B_{k+m}$ such that there is no edge (u, v) with $u \in B_{k+i}$ and $v \neq B_{k+i}$ for $1 \leq i \leq m$. Hence, for any spanning directed forest of the reversal of G, each of these components must contain the root of a tree. Therefore, any spanning forest consists of at least m trees.
Since L_{out} is m-reducible, we know that for every $i \leq k$, there is some $j > i$ such that $B_{i,j} \neq 0$. It is easy to see that, starting from any node u, there is a directed path into one of the strongly connected components $B_{k+1}, \ldots, B_{k+m}$. Consequently, there is a path from any node u to the root being part of one of the components $B_{k+1}, \ldots, B_{k+m}$. Hence, there exists a spanning forest of the reversal of the graph with m trees.
If L_{out} is not m-reducible, it is m'-reducible for some $m' \neq m$. Then the number of trees in a minimal spanning of G is m'.
In order to show the analogue result for L_{in}, we just have to apply the proof to L_{out}^{G} and again use

$$\overline{L_{in}^{G}} = L_{out}^{\overline{G}}.$$

□

Let us interpret Theorem 1 in the context of our understanding of a system's resilience. A tree in the spanning forest of a system's information network can be understood as a set of agents being supplied with information tracing back to one source agent. The occurrence of another tree in the minimal spanning forest after a perturbation of the graph results from the fact that all paths between a set of agents and their former source agent have been separated. The agents are now supplied with information tracing back to (possibly several) other source agents. The overall information structure of the system has changed. This

would not be the case if there still existed paths between the agents and their source agent after the perturbation, hence, alternatives to the perturbed paths.
A tree in the spanning forest of the reversal of a system's information network can be interpreted as a set of agents supplying one destination agent with information. Whenever a perturbation is followed by the occurrence of another tree in the spanning forest, we know that all paths between a set of agents and their former destination agent have been separated. Again, a structural change which could, due to the lack of alternative paths, not be compensated. By considering both Laplacian matrices, we identify the weak point of the graph.
The occurrence of new trees in the minimal spanning forests of G and its reversal represent just one type of structural internal change. There are others which may not be captured by R. For example, one can easily construct a directed graph in which the deletion of an edge leads to a new component but not to an increase in the number of trees in the minimal spanning. However, with minimal spannings covering important aspects of a graph's overall topology, their structure is a comprehensive indicator for the graph's vulnerabilities. Indeed, R shows to reflect the cycling resilience of a system during its course through the adaptive cycle (see Sections 3.4 and 4.2).

In order to gain a first impression of the behavior of potential, connectedness, and resilience depending on the topology of the underlying graph, we examine the three systemic variables on a simple model of random graphs, so-called *Gilbert graphs* [37].

3.4 Potential, connectedness, and resilience of random graphs

Let $G \in G(N,p)$ be a Gilbert graph, i.e. a directed graph with N nodes, where each edge is of weight 1 (or *active*) with probability p and of weight 0 with probability $1-p$. Assume that G has no self-loops. We consider G as information network and its edges as channels of communication. Hence, the edge weight represents the strength of communication between two agents. The weights are described by the weight function $\omega\colon E \to \{0,1\}$. We denote the set of nodes by $\mathcal{V}$. Let

$$W = \sum_{(u,v)\in\mathcal{V}\times\mathcal{V}} \omega(u,v).$$

Recall the graph's potential

$$P = -\sum_{(u,v)\in\mathcal{V}\times\mathcal{V}} w(u,v)\cdot\log_2\left(\frac{\omega(u,v)}{W}\right).$$

In order to compute the expected potential of G depending on N and p, we define X_{uv} as the independent random variables describing the weight of the edge from node u to node v

and $X = \sum_{u,v\in\mathcal{V}} X_{uv}$. Hence,

$$P = -\sum_{u,v\in\mathcal{V}} X_{uv} \cdot \log_2\left(\frac{X_{uv}}{X}\right).$$

We then have

$$\begin{aligned}\mathrm{E}(P) &= \mathrm{E}\left(-\sum_{u,v\in\mathcal{V}} X_{uv} \cdot \log_2\left(\frac{X_{uv}}{X}\right)\right)\\ &= -\sum_{u,v} \mathrm{E}\left(X_{uv} \cdot \log_2\left(\frac{X_{uv}}{X}\right)\right),\end{aligned}$$

with

$$\begin{aligned}&\mathrm{E}\left(X_{uv} \cdot \log_2\left(\frac{X_{uv}}{X}\right)\right)\\ &= p \cdot \sum_{i=1}^{2\cdot\binom{N}{2}-1} p^i \cdot (1-p)^{2\cdot\binom{N}{2}-1-i} \cdot \binom{2\cdot\binom{N}{2}-1}{i} \cdot \log_2\left(\frac{1}{1+i}\right)\\ &= -\sum_{i=1}^{N\cdot(N-1)-1} p^{i+1} \cdot (1-p)^{N\cdot(N-1)-1-i} \cdot \binom{N\cdot(N-1)-1}{i} \cdot \log_2(1+i).\end{aligned}$$

This gives

$$\begin{aligned}\mathrm{E}(P) &= -\sum_{u,v\in\mathcal{V}} -\sum_{i=1}^{N\cdot(N-1)-1} p^{i+1} \cdot (1-p)^{N\cdot(N-1)-1-i} \cdot \binom{N\cdot(N-1)-1}{i} \cdot \log_2(1+i)\\ &= 2\cdot\binom{N}{2} \cdot \sum_{i=1}^{N\cdot(N-1)-1} p^{i+1} \cdot (1-p)^{n\cdot(N-1)-1-i} \cdot \binom{N\cdot(N-1)-1}{i} \cdot \log_2(1+i)\\ &= N\cdot(N-1) \sum_{i=1}^{N\cdot(n-1)-1} p^{i+1} \cdot (1-p)^{N\cdot(N-1)-1-i} \cdot \binom{N\cdot(N-1)-1}{i} \cdot \log(1+i).\end{aligned}$$

We expect $E(P)$ to increase for $p \in]0,1]$. In order to show this, we compute the derivative of $E(P)$. Setting $m \coloneqq N \cdot (N-1) - 1$, we receive

$$\begin{aligned}\frac{d}{dp}E(P) &= n \cdot (N-1) \cdot \sum_{i=1}^{m} \binom{m}{i} \cdot \log_2(1+i) \\ &\quad \cdot \left((i+1) \cdot p^i \cdot (1-p)^{m-i} - (m-i) \cdot p^{i+1} \cdot (1-p)^{m-1-i}\right) \\ &= N \cdot (N-1) \cdot \sum_{i=2}^{m} \underbrace{p^i \cdot (1-p)^{m-i} \cdot \binom{m}{i-1} \cdot \log_2(i)}_{\text{(A)}} \\ &\quad \cdot \underbrace{\left((i+1) \cdot \binom{m}{i} \cdot \log_2(i+1) - (m-i+1) \cdot \binom{m}{i-1} \cdot \log_2(i)\right)}_{\text{(B)}} \\ &\quad \underbrace{+2 \cdot p \cdot (1-p)^{m-1} \cdot m}_{\text{(C)}}\end{aligned}$$

The Terms (A) and (C) are obviously positive for $p \in]0,1[$. For term (B), we have

$$\begin{aligned}&(i+1) \cdot \binom{m}{i} \cdot \log_2(i+1) - (m-1+i) \cdot \binom{m}{i-1} \cdot \log_2(i) \\ &= \frac{m!}{(i-1)! \cdot (m-i)!} \cdot \left(\log_2(i+1) \cdot \frac{i+1}{i} - \log_2(i) \cdot \frac{m-i+1}{m-i+1}\right) \\ &\overset{(\star)}{=} \frac{m!}{(i-1)! \cdot (m-i)!} \cdot \left(\log_2(i+1) \cdot \frac{i+1}{i} - \log_2(i)\right) \\ &> 0\end{aligned}$$

for $p \in]0,1[$. Equality $(\star)$ follows from the term's properties as telescoping series. It remains to compute $\frac{d}{dp}E(P)$ at $p = 1$. We get

$$\begin{aligned}\frac{d}{dp}E(P)(1) &= N \cdot (n-1) \cdot \log_2(m) \cdot ((m+1) \cdot \log_2(m+1) - m \cdot \log_2(m)) \\ &> 0\end{aligned}$$

Hence, we have shown that the expected potential of a random graph $G \in G(N,p)$ increases

on $p \in [0,1]$. In other words, the expected potential increases along with the number of expected edges of weight 1. Coming back to information networks, this coincides with the perception of potential as a measure of the underlying system's possible future options. The more active channels of information, the broader the range of possible interaction structures. The left column of Figure 3 displays the expected potential for graphs of sizes $N = 5$, 10, and 25. Note that the values of expected potential increase along with the number of nodes N. This is due to the fact that potential is scaled with the total system throughput.

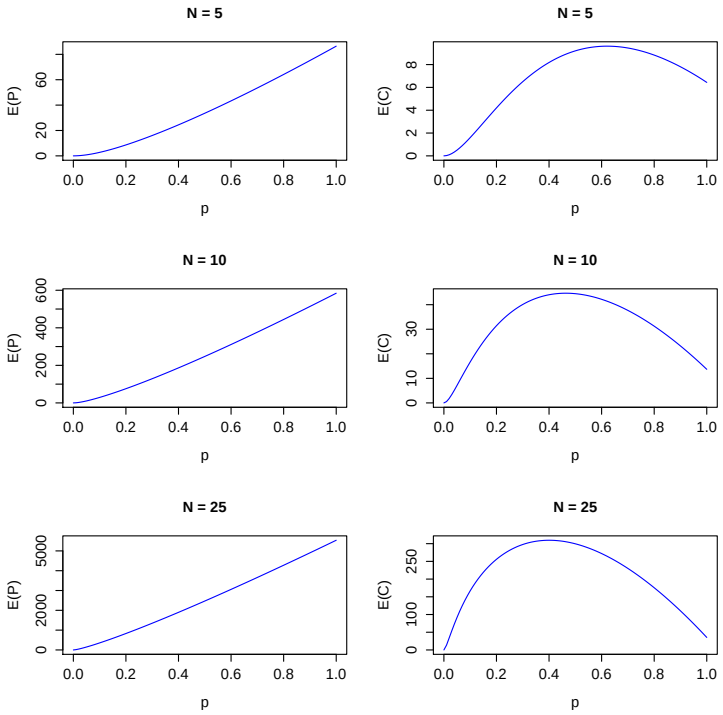

Figure 3: Expected potential $\mathrm{E}(P)$ and expected connectedness $\mathrm{E}(C)$ of Gilbert graphs $G \in G(N,p)$ as function of p for $N = 5,\ 10$, and 25.

We will now continue with the expected connectedness of Gilbert graphs. Set

$$W_{u*} = \sum_{v \in \mathcal{V}} w(u,v) \text{ and } W_{*v} = \sum_{u \in \mathcal{V}} w(u,v).$$

As a reminder, a graph's connectedness is defined as

$$C = \sum_{u,v \in \mathcal{V}} w(u,v) \cdot \log\left(\frac{w(u,v) \cdot W}{W_{u*} \cdot W_{*v}}\right).$$

Again, we write

$$C = \sum_{u,v \in V} X_{uv} \cdot \log\left(\frac{X_{uv} \cdot X}{X_{u.} \cdot X_{.v}}\right),$$

with $X_{u*} = \sum_{v \in V} X_{uv}$ and $X_{*v} = \sum_{u \in V} X_{uv}$. Combinatory considerations show that

$$\begin{aligned}
E(C) &= \mathrm{E}\left(\sum_{u,v \in \mathcal{V}} X_{uv} \cdot \log\left(\frac{X_{uv} \cdot X}{X_{u*} \cdot X_{*v}} \right) \right) \\
&= \sum_{u,v \in \mathcal{V}} \mathrm{E}\left(X_{uv} \cdot \log\left(\frac{X_{uv} \cdot X}{X_{u*} \cdot X_{*v}} \right) \right) \\
&= \sum_{u,v \in \mathcal{V}} p \cdot \sum_{k=1}^{2\cdot\binom{N}{2}-1} p^k \cdot (1-p)^{2\cdot\binom{N}{2}-1-k} \cdot \left(\sum_{i=\max\{0,m_1\}}^{\min\{k,N-2\}} \sum_{j=\max\{0,m_2\}}^{\min\{k-i,N-2\}} S_{i,j} \right) \\
&= N \cdot (N-1) \cdot \sum_{k=1}^{N\cdot(N-1)-1} p^{k+1} \cdot (1-p)^{N\cdot(N-1)-1-k} \cdot \left(\sum_{i=\max\{0,m_1\}}^{\min\{k,N-2\}} \sum_{j=\max\{0,m_2\}}^{\min\{k-i,N-2\}} S_{i,j} \right),
\end{aligned}$$

with

$$\begin{aligned}
S_{i,j} &= \binom{N-2}{i} \cdot \binom{N-2}{j} \cdot \binom{2 \cdot \binom{N}{2} - 2 \cdot (N-2) - 1}{k-(i+j)} \cdot \log\left(\frac{k+1}{(i+1)(j+1)} \right), \\
m_1 &= k - \left(2 \cdot \binom{N}{2} - 1 - (N-2) \right) = k + N \cdot (2-N) - 1, \\
m_2 &= k - \left(2 \cdot \binom{N}{2} - 2 \cdot (N-2) - 1 \right) - i = k + N \cdot (3-N) - 3 - i.
\end{aligned}$$

We use this representation of $E(C)$ to examine it numerically . The right column of Figure 3 shows $E(C)$ depending on p for $N = 5$, 10 and 25. The numeric evaluation shows that $E(C)$ has exactly one maximum in $[0, 1]$. The larger N, the smaller the value where the maximum is taken. Considering networks of information transfer, the fact that E(C) is maximal for intermediate values of p is in line with with Gunderson and Holling's understanding of connectedness. On the one hand, in order to reach a high internal controllability, a certain amount of active information channels is needed. On the other hand, too many active channels can generate redundancy and decrease efficiency in information processing and thereby exploitation of potential. Note that, just like in the case of expected potential, the values of expected connectedness increase with increasing number of nodes N due to the scaling.

To get an impression of the resilience of Gilbert graphs, we generated 100 random graphs for various constellations of p and N. Resilience of the graphs was computed using the standardization constant $c = 1$. Figures 4 and 5 display the results in form of boxplots. As could be expected, for $p \to 1$, resilience converges from below to $\frac{N}{\sqrt{N-1}}$, which is the resilience of a complete unweighted graph (recall Example 1). Clearly, the vulnerability of a graph with respect to edge deletions is minimal when all possible edges are active. In a certain distance to 0, which decreases with increasing N, the median approaches 1 from below (see Figure 5). This is due to the fact that for relatively small p, the graph's maximal weakly connected component is likely to consist of only two nodes and one active edge, yielding a resilience of 1. For $p \to 0$, the median will then converge to 0 as the probability

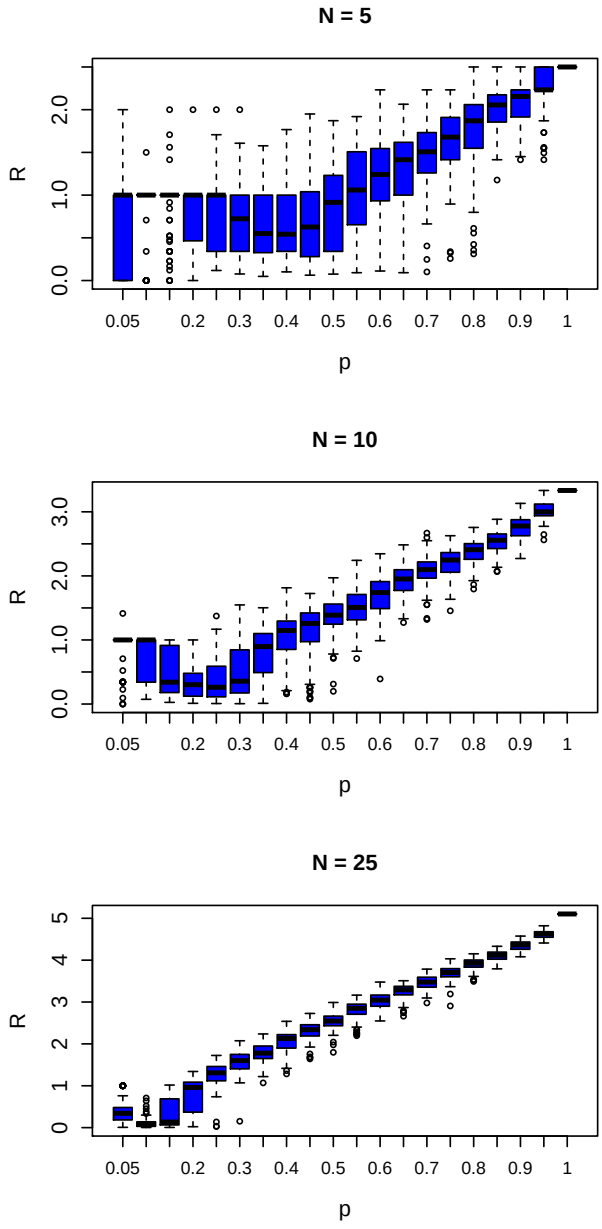

Figure 4: Boxplots showing the resilience R of Gilbert graphs $G \in G(N,p)$ for different values of p for $N = 5,\ 10$ and 25. For every combination of N and p, 100 graphs were generated.

of an edge appearing in the graph becomes smaller and smaller, leading by definition to a resilience of 0.

Studying the three systemic variables on unweighted random graphs helps in getting a

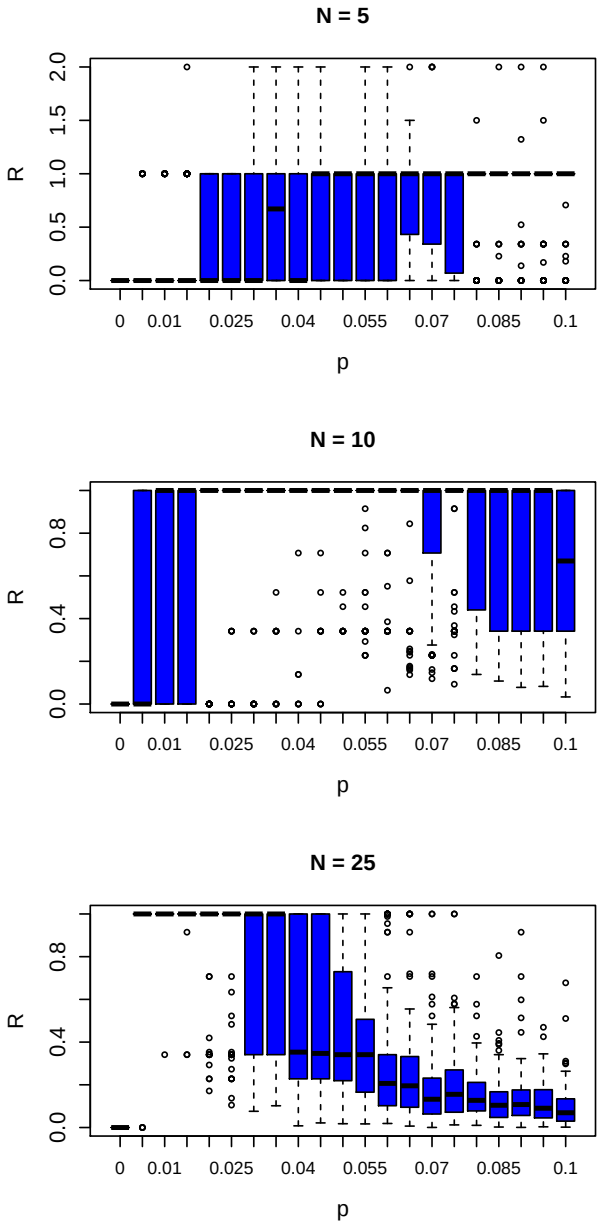

Figure 5: Boxplots showing the resilience R of Gilbert graphs $G \in G(N, p)$ for different values of p for $N = 5,\ 10$ and 25 and p close to 0. For every combination of N and p, 100 graphs were generated.

feeling for their behavior in a stochastic environment and their relation to the number of edges of the underlying graphs. The results coincide with our understanding of potential, connectedness, and resilience as defined by Gunderson and Holling and thereby support our

choice of definitions. However, such simple random graphs lack the specific topological structures of information networks of natural complex systems, which e.g. typically show certain degree distributions [21]. Hence, the question remains: can we observe a cyclic behavior of potential, connectedness, and resilience in the information networks of (naturally) developing systems? Do connectedness and resilience show the expected opposite behavior during the networks' development? And, taking one step back, is the interaction structure of a complex system indeed captured by its networks of information transfer? We will approach these questions in Section 4.

3.5 Overview of the method

Our method to quantify the adaptive cycle combines several ideas, concepts, and tools but eventually follows a simple structure. We will now provide a heuristic overview of the method in Table 2 and illustrate its functionality with the aid of a toy example. A similar example has been presented in [83].

Input	The method requires time series of system's components' abundance data. By abundance data, we mean any data capturing the effects of interactions among the components. Within a system, the data can be heterogeneous, i.e. the abundance of different components can be measured in different units. It is one of the advantages of the information theoretical approach that the results are not depending on the concrete instantiation of the system.
Step 1	In the first step, networks of information transfer are estimated. Precisely, pair-wise transfer entropy between the system's components at a given time is estimated on basis of a certain preceding time window of abundance data. By shifting the time window or extending it, networks for subsequent time points are achieved. Only transfers passing a certain significance level are taken into account.
Step 2	In the second step, the three systemic variables potential, connectedness, and resilience are computed for every information network.
Output	The method yields time series of potential, connectedness and resilience and thereby the course of the system through the adaptive cycle for a certain period of time. Next to the systemic variables, the information networks themselves can provide important insights into the underlying mechanisms and the role of individual components in the system's development.

Table 2: Structural overview of our method to quantify the adaptive cycle.

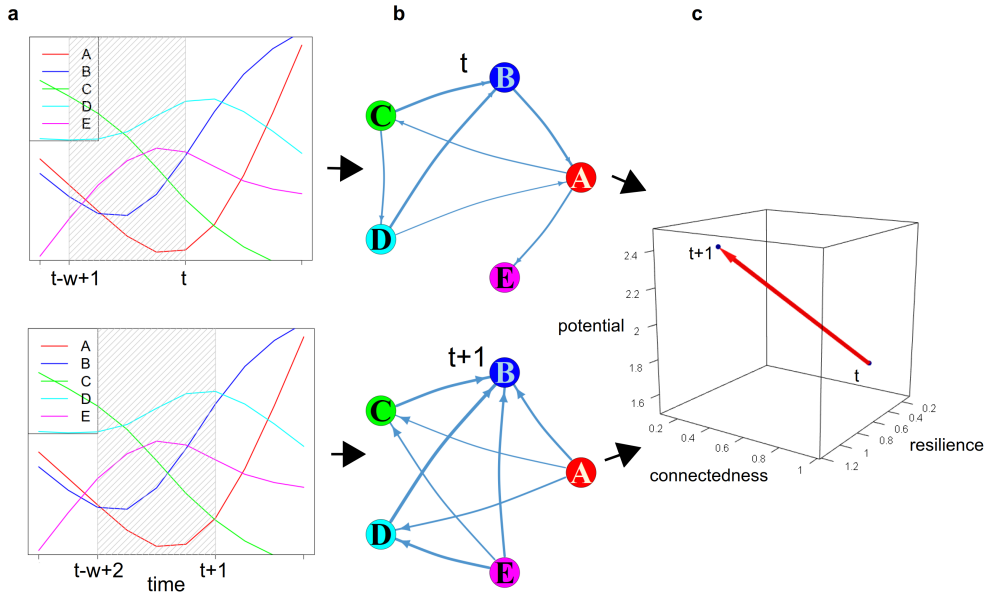

Figure 6: Illustration of the method's structure by means of a toy example. The figure is inspired by Figure 2 in [83]. (a) Time series of abundance data of the system's components A, B, C, D, and E. The figure displays the window shifting method with window size w, i.e. the time window serving as a basis for the estimations of information networks is shifted forward by one in order to receive the subsequent network. Time series in the toy example are of length 10, $w = 5$, $t = 6$, significance level is 0.05. (b) Networks of information transfer for time points t and $t + 1$. Here, and in all following plots of information networks, the edges' width is proportional to the information transfer's strength. (c) Three-dimensional plot of potential, connectedness, and resilience at time points t and $t + 1$.

Figure 6 demonstrates the structure of our method by means of a toy example. The system under consideration consists of five components, A, B, C, D, and E, whose time series of abundance were randomly generated. Figure 6(a) displays these time series. At first, a window size w has to be chosen. In order to estimate the course of the system through the adaptive cycle from time point t to time point $t + 1$, we then estimate pairwise transfer entropy based on the samples in window $(t-w+1, \ldots, t)$ and $(t-w+2, \ldots, t+1)$, respectively. The shaded areas mark the shifting window. Transfers passing a certain significance level are taken into account as edges in the resulting networks of information transfer, which are shown in Figure 6(b). Here, and in all subsequent network plots, edge width is proportional to the strength of the respective information transfer. Potential, connectedness, and resilience at time points t and $t + 1$ are computed as properties of the respective networks. Their

development between time point t and time point $t+1$ is displayed in 6(c). The three-dimensional plot shows that potential and resilience are increasing, while connectedness is decreasing. We will take a closer look at the corresponding networks to explain this behavior. The system's potential is higher at time point $t+1$ since more transfers increase the total system throughput and the capacity of the system to react to future changes. Resilience at time point t is lower since component E is connected with the rest of the system by one edge only, which renders the system vulnerable. A perturbation of edge $A \to E$ would fully decouple E from the system. Typically, the increase in resilience coincides with a decrease in connectedness. This decrease can be explained by the fact that the transfers are more equally distributed and thereby less constrained at time point $t+1$.

In order to enable a straightforward application of our method, we developed the R package QtAC, which we will present in the following section.

3.6 R package QtAC

The R package QtAC (Quantifying the Adaptive Cycle) provides an implementation of our quantification method. It is accessible via repository [66]. The repository contains a demo script including a sample application to a simulated bacterial community. The manual of the package can be found in Supplementary A of this thesis. Nevertheless, we will briefly present the main functions here.

In order to estimate a system's course through the adaptive cycle, the user needs to have time series of the system's components' abundance data in a tab separated file. The function `QtAC.TXT.reader` imports the data in R. The main function `QtAC` combines several steps. At first, the data is split up into windows of size `num_timepoints`, each of which shifted by one time point (the package does not yet provide the window expanding method). Note that the window size needs to be at least five, otherwise the main function will return an error. We set this minimum to avoid receiving statistically unreliable results. If the number of time points in a window is below 15, the amount of data in every window is tripled by means of a piecewise cubic spline interpolation. Now the networks of information transfer are estimated using the parameters `k`, `k_tau`, `l`, `l_tau`, and `delay`, which can be set by the user. See Section 3.1 for a description of the parameters. Furthermore, the significance of every transfer is calculated via a bootstrapping significance test. The number of surrogate samples `num_PermCheck` to generate the distribution in the significance test can be set by the user as well. The output of the main function is a list of adjacency and corresponding significance matrices for each time window. The significance matrices contain the significance of each estimation in the adjacency matrix. The adjacency matrices can be filtered according to a user-defined significance level `signfac` by means of the function `QtAC.Signfactor`. The three systemic variables of the (filtered) adjacency matrices can be computed using `QtAC.maturation`. Concerning resilience, the user can choose between two

normalization variants and several standardizations of the underlying Laplacian matrices. The two normalization variants are `res_norm = "continuous"`, i.e.

$$L_{out} = c \cdot D_{out}^{-\frac{1}{2}} (D_{out} - A), \quad \text{and} \quad L_{in} = c \cdot (D_{in} - A) D_{in}^{-\frac{1}{2}},$$

and `res_norm = "symmetric"`, i.e.

$$L_{out} = c \cdot D_{out}^{-\frac{1}{2}} (D_{out} - A) D_{out}^{-\frac{1}{2}}, \quad \text{and} \quad L_{in} = c \cdot D_{in}^{-\frac{1}{2}} (D_{in} - A) D_{in}^{-\frac{1}{2}}.$$

Let M be the maximal information transfer at the corresponding time point. Then a common choice for the standardization constant `res_stand` is $c = \frac{1}{\sqrt{M}}$ (`"maxweight"`) in the continuous version and $c = \frac{1}{M}$ (`"maxweight2"`) in the symmetric version. A standardization with respect to the number of nodes N is possible via $c = \frac{\sqrt{N-1}}{N}$ (`"nodes"`). In the continuous version, a standardization with respect to both nodes and maximal transfer is possible via `"maxweightnodes"`, i.e. $c = \frac{\sqrt{N-1}}{N \cdot \sqrt{M}}$.

QtAC offers various options of visualizing the results. The adjacency matrices can be plotted in form of networks using `QtAC.network`. Layout of the network and several graphical parameters can be chosen by the user. The development of potential, connectedness, and resilience can be plotted over time using `QtAC.2dplot`. Besides, the variables can be plotted with respect to each other in two dimensions using `QtAC.2dmixplot` or in three dimensions using `QtAC.3dplot`.

At the time of submission of this thesis, QtAC allows a quick and uncomplicated first analysis of a system's maturation process in the sense of the adaptive cycle. However, various variants and subtleties of the method have not been incorporated in the package yet. At first, only the window shifting method is implemented. Another example would be the inclusion of statistical tests for the choice of the estimation parameters `k`, `k_tau`, `l`, `l_tau`, and `delay` as being provided in the JIDT toolkit [49]. In particular, it should be possible to set the parameters component-dependently. Furthermore, the consideration of networks of *local* transfer entropy can be useful as well. These and further refinements will be subject of future work.

4 Validation of the Method

Our method to quantify the adaptive cycle is based on several assumptions. In this section, we will provide case studies supporting them. Effectively, the proper functioning of our method depends on the correctness of three assumptions:

1. We assume that a complex system can be understood as a computing entity whose effective interaction structure is captured in the transfer entropy among its components. In other words: every effective interaction leads to a transfer of information.
2. We assume that our definitions of potential, connectedness, and resilience capture Gunderson and Holling's conception of these notions.
3. We assume that the adaptive behavior of a system is reflected in the interactions among its components, i.e. that the system's interaction structure shows distinguishable, phase-specific patterns.

The understanding of biology as information processing, or, in other words, computation, has been around for many decades (see e.g. [18, 30, 58]). Effectively, the structure of DNA inspires to consider life itself as processing of genetic code [42]. The computational approach builds on the idea that on a certain level of abstraction living entities and systems follow the same information theoretical principles as information-processing machines. Hence, the same language can be used to describe the information dynamics of a human cell or an ecosystem as well as the logical functioning of a computer. In this language, information processing can be divided into the component operations of information storage, transfer, and modification [52]. Accordingly, the total information of a computing entity consists of information being stored in its own past, information being transferred from other entities and information being modified [50].

The common mathematical framework for studying information processing is information theory. This theory provides the notions of active information storage and transfer entropy, which serve as measures of information storage and transfer, respectively. Information modification has for example been measured by means of separable information [52]. Understanding the information dynamics of living entities or systems can provide important insights into the mechanisms underlying their behavior. Within the last years, there have been multiple applications of this concept to complex biological systems, including neural and ecological systems, see for example [77, 78]. In order to support the rationality of the first assumption, we examine the distributed computation of a simulated bacterial community in Section 4.1. It demonstrates, inter alia, the usability of abundance-based information transfer in capturing a system's interaction structure.

In Section 4.2, we address the second assumption. In order to further justify our definitions of potential, connectedness, and resilience, we investigate the variables' behavior in a

classical adaptive cycle scenario. To this end, we simulate the development of an information network following Gunderson's and Holling's descriptions in [39].

Having validated our information theoretical approach and our concrete choice of definitions, we can address the third assumption in Section 4.3: is the adaptive behavior of a system reflected in the system's mere interaction structure? For this purpose, we apply our method to a purely interaction-based model, the Tangled Nature Model as being provided by Christensen et al. [24]. The occurrence of the typical cyclic pattern in the system's connectedness and resilience demonstrates that interactions indeed capture a system's adaptive development in the sense of the adaptive cycle metaphor.

4.1 Justification of the information theoretic approach

This chapter is except for smaller modifications taken from [69]. The human intestinal microbiota is of growing interest due to its effects on host physiology and health. Nevertheless, there are still large gaps in the understanding of the molecular mechanisms and the functional role of its members [19]. In the following case study, we consider the bacterial system as computing entity, allowing us to examine its development by means of established information theoretical tools. Here, our focus will be on the following question: does the information transfer among components reflect the system's interaction structure?

In order to cope with the high complexity of the intestinal microbiota and the limits of in-vivo data, we take two steps.

- We confine ourselves to the simplified human intestinal microbiota (SIHUMI). It consists of seven species representing metabolic activities that are shared among all hosts: *Anaerostipes caccae, Bacteroides thetaiotaomicron, Bifidobacterium longum, Blautia producta, Clostridium ramosum, Escherichia coli*, and *Lactobacillus plantarum*. This community has been cultivated successfully in in vivo experiments [16].

- We consider an *in silico* SIHUMI community. This enables us to compare our results with the underlying metabolic activity of the community at every time point. Such data is difficult to collect in vivo. Besides, a simulation allows controlled perturbations of the system and provides time-series long enough for a reliable statistical analysis.

Using BacArena [14], we simulate the metabolic activity of individual bacteria of the seven SIHUMI species in a nutrient-enriched environment for 184 time steps (see [56] for the reconstructed metabolic models used). The models were manually curated and checked using published experimental data. The bacterial species were selected according to their relevance and abundance within the human gut microbiota to represent a simplified human intestinal microbiota (SIHUMI). The simulation comprises production and consumption of nutrients, reproduction as well as extinction of the individuals. It comprises all relevant fermentation

paths, interacting with chemical parameters of the substrate. After time points 35, 62, and 121, nutrients are added to the environment. These feeding events allow us to examine the reaction of the system to external intervention. We extracted the metabolic activity of the species using the function `plotSpecActivity`. The cross-feeding fluxes were estimated via `findFeeding3`. The function `plotSubCurve` was used to determine the amount of substances in the media. The functions yield values in mmol/g_dw, where g_dw denotes the dry weight of all living microbes. See [69] for details on the simulation.

The following description is based on the notation introduced in Sections 2.1 and 3.1. We consider every bacterial species as agent of a computing system. All information theoretical estimations are based on the species' abundance. Recall that the abundance of a species reflects the internal dynamics as it modifies according to the species' success or failure of its interactions. Be it a lost competition or the benefits of a mutualism, both will effect the species' abundance and thereby be memorized. We applied the Ragwitz optimization method as provided in Lizier's JIDT toolkit [49] to each agents' time series in order to estimate its Markov order. As the history length k should be *at least* as long as the Markov order of the underlying random process [49], we set the maximal value of the estimated Markov orders, 10, as common k. When computing local AIS of an agent X, we used the whole time series as basis for the probability estimation. Analogously, when computing local TE between two agents, we used their whole time series to compute their (joint) probability. In order to gain non-local measures, we used a window size of $w_t = 30$. The window size was chosen as a compromise between a statistically large enough sample size and the analytical requirement to display the first feeding time. Being commonly set to 1, we decided to increase the delay u to 2 in this case. Our choice is due to the fact that nutrients produced by species in one time step are not available to other species until the next time step. Hence, changes in abundance and thereby metabolic activity of a species can be taken into account by other species two steps later at the earliest. We determined the significance of the transfer entropies and rejected all entropies with p-value above 0.05. Table 3 shows an overview of the data and parameters used in the case study.

Our results support the following three hypotheses:

- Hypothesis 1: Environmental changes are reflected in sudden decreases of local active information storage.
- Hypothesis 2: Transfer entropy captures commensalistic and competitive interactions among the system's components.
- Hypothesis 3: In an interaction, the agent mainly *receiving* information is generally more successful than the agent mainly *sending* information.

Hypothesis 1 is clear from a mathematical point of view. Sudden environmental changes lead to unexpected changes in a species' abundance and therefore to a decrease of local active

system	simplified human intestinal microbiota
components	bacterial species
number of components	7
type of abundance data	number of individuals
length of time series	184
window size w_t	30
interpolated window size	30
history lengths k, l	10
delay u	2
significance level	0.05

Table 3: Data and parameters of the SIHUMI case study. The parameters refer to the computation of (average) transfer entropy.

information storage. But also translated to a real-world scenario, this relation is plausible. If the environmental conditions change, a living entity's development will be less predictable from its past development than under stable environmental conditions. Hypothesis 2 supports the information theoretical approach of our method. It can be expected under the assumption that, in reality, every interaction leads to a transfer of information and that these dynamics can be found in the model as well.

Hypothesis 1: Environmental changes are reflected in sudden decreases of local active information storage. Figure 7(a) shows that species' abundances are strongly varying around the external feedings after time steps 35, 62, and 121. Two effects are of interest for us. Firstly, there are species' abundances which decrease strongly before feedings due to a lack of certain essential nutrients in the environment and then stabilize after the feedings. Examples of these species are *Bacteroides* at the first feeding or *Bifodobacterium* at the second feeding. Second, there are species' abundances which increase strongly after feeding events, see e.g. *Bifidobacterium* or *Anaerostipes* after the third feeding. In both cases, the feeding events lead to sudden changes in abundance development since these species are primary users of the new resources. Hence, we can expect the information composition of the system to reflect the feeding. In order to gain an overview of the whole system's long-term information dynamics, we averaged all species' AIS, collective TE, and E at every time step, displayed in Figure 7(b). The time series start at time step 30 since we are considering the average of the local values over the last 30 time steps.

The system's (averaged) AIS shows a cyclic behavior with clearly defined local minima. The first minima are located right after the first and right at the second feeding event. The third minimum around time step 80 coincides with a sudden increase of several species' abundance following a mainly constant period. Concurrently to the third feeding after time

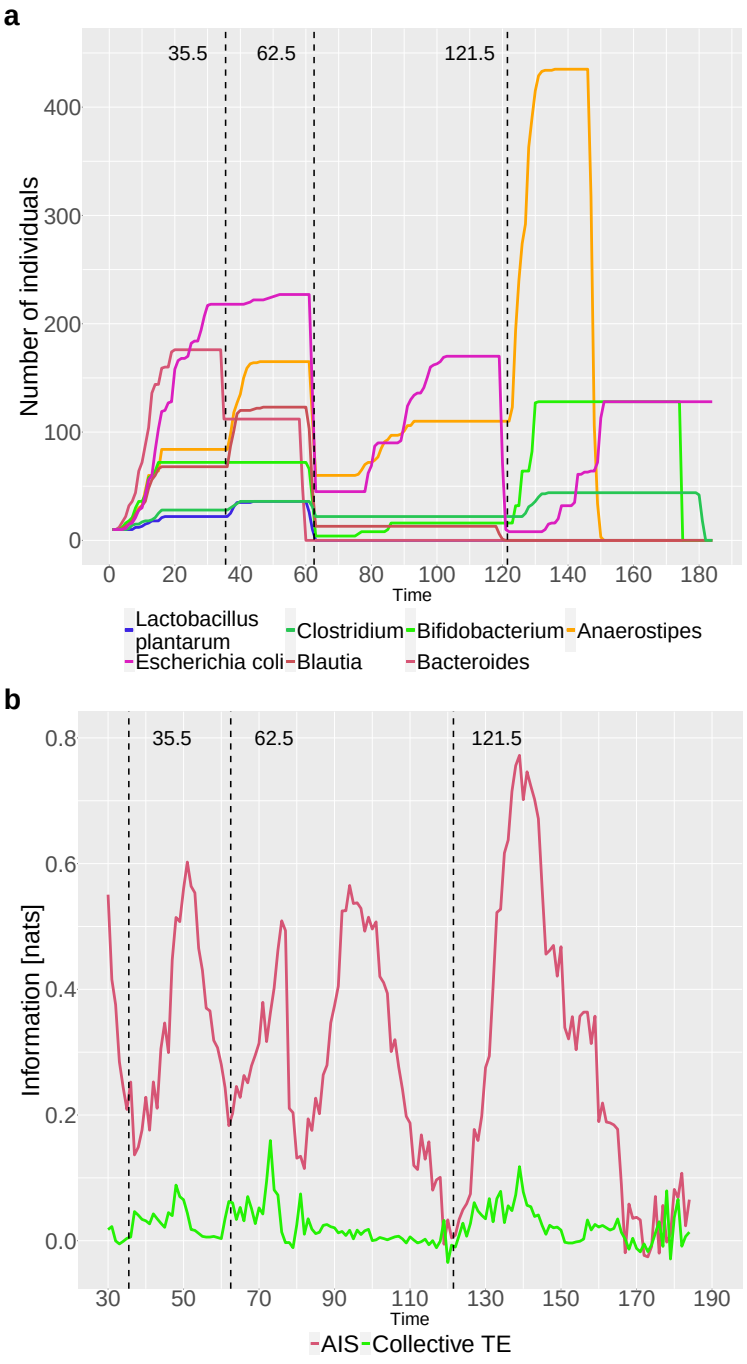

Figure 7: Information composition in the SIHUMI community. Dashed lines show the feeding events. (a) Abundance of the seven species. (b) AIS and collective TE averaged over all species.

step 162, there is another local minima in AIS. From time step 170 on, with some extinction events interrupting a rather stable phase, the system's AIS stays in another local minimum.

The system's collective TE does not show such a clear cyclic behavior but we can see a certain pattern: Whenever AIS has a local minima, collective TE has small local maxima. At the third feeding event and toward the end of the simulation, collective TE takes even higher values than AIS. This goes with the common understanding of these two measures. In times of unpredictability, the species' past development is rather misleading when trying to determine their next state and other species' development becomes more informative. In this case study, unpredictability is induced through lack of nutrients and the subsequent feeding events. The phenomenon that information transfer alternates with information storage in complex systems has been found in other complex systems as well, see e.g. [77].

Let us now take a more direct look into the relation between abundance and AIS by considering *local* AIS of *single* species (Figure 8 (a) and (b)). However, we have to be aware of the fact that the outcomes contain a higher amount of noise than the twice averaged outcomes we considered before. This is also a result of a certain amount of random Gaussian noise added to the data in the estimation process, which is essential for the estimator to work properly in all data situations [48, 49]. Note that the time series start at time step 10 due to the chosen history lengths k and l.
Figure 8(a) shows that the AIS of *Bifidobacterum* is mostly positive, except for four times. The first time is concurrently to the second feeding, when the abundance of *Bifidobacterium* decreases strongly. The second time is around time step 85, when the abundance of *Bifidobacterium* shows a short but steep increase. After the third feeding, the abundance of *Bifidobacterium* strongly increases in two steps, reflected by two negative values of AIS. Note that the first feeding has no significance effect on the AIS of *Bifidobacterium* since its abundance is not affected at all.
Let us compare the AIS of *Bifidobacterium* with the AIS of *Clostridium* (Figure 8(b)). *Clostridium's* mainly positive AIS is also interrupted by four negative local minima. The first one is right at the beginning, around time step 15, when the species' abundance suddenly increases in its slope. At the first feeding, the AIS of *Clostridium* decreases strongly due to the increase in abundance but it remains positive. The second and third negative minima are concurrent to the second and third feeding. While the first of these two minima reflects the strong decrease right before the feeding, the second minimum reflects the increase after the third feeding. Towards the end of the simulation, the AIS of *Clostridium* becomes negative again as a result of its sudden decrease in abundance. Note that the AIS of *Bifidobacterium* did not get negative during its extinction. This is due to the fact that we only measure AIS of living species and the abundance of *Bifidobacterium* decreases to zero in one time step.
Examination of the local measures confirms our hypothesis: Environmental changes, in our example artificially induced through sudden addition of nutrients to the media, are reflected

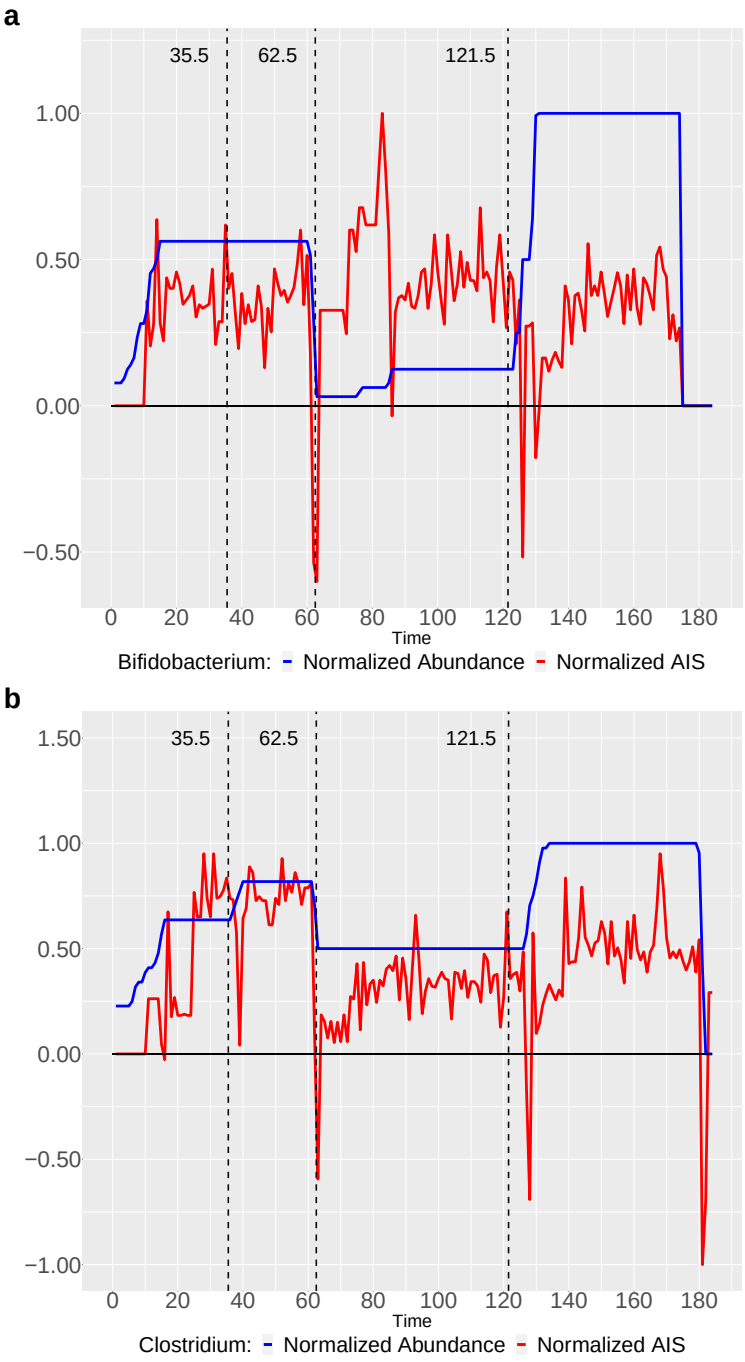

Figure 8: Local AIS of single species. (a) Comparison of *Bifidobacterium's* local AIS and abundance. (b) Comparison of *Clostridium's* local AIS and abundance.

in the species' abundance and thereby in strong decreases in AIS.

Hypothesis 2: Transfer entropy captures commensalistic and competitive interactions among the system's components. There are various types of interactions among the species in the simulated SIHUMI community. Two of the most common ones are commensalism and competition. In a commensalistic interaction, one of the agents profits from the presence of the other one while the other one neither profits nor suffers. This happens in our case when one of the species is feeding on nutrients being produced by another species. A competition takes place when two species are competing for the same, possibly rare, nutrient. We found that transfer entropy reflects both these interactions.

Let us start with examples of commensalism. Figure 9(a) shows the sum over all (apparent) transfer entropies from and to Bacteroides. In the following, we will denote this quantity by *total information transfer*. We distinguish between the information transfer *arriving* at a species, its *information inflow*, and the transfer *leaving* a species, its *information outflow*. Note that the plot starts at time step 30 since it shows values averaged over the last 30 time steps.
In the case of *Bacteroides*, the information outflow clearly exceeds the inflow. Recalling the definition of transfer entropy, the impact of *Bacteroides'* development on the other species' development is significantly higher than the other way round. This phenomenon can easily be traced back to the metabolic activity of *Bacteroides*. *Bacteroides* is producing a considerably higher amount of products than all the other species (see Figure 9(b)). For many nutrients, the amount produced by *Bacteroides* exceeds the amount externally added as well. *Bacteroides* is the main provider of nutrients like hydrogen, formate, and succinate. The fact that those nutrients are among the main feeding components of almost all of the other species explains the strong information outflow of *Bacteroides*. This dominance of outflow becomes particularly apparent in the case of *Anaerostipes* (see Figure 10(a)). This is due to the fact that *Anaerostipes* is strongly depending on the succinate production of *Bacteroides* between the first and second feeding. Indeed, during this period of the simulation, succinate is the second largest feeding component of *Anaerostipes* (compare Figure 11(a)) and by far most of it is provided by *Bacteroides* (see Figure 10(b)).

E.coli serves as another example of commensalism. Figure 12(a) shows an interesting pattern in the information transfer of *E.coli*: a strong dominance of outflow abruptly turns into a dominance of inflow around time points 50 and 140. The explanation of this phenomenon requires some understanding of *E.coli's* metabolic activity. Within the SIHUMI community, *E.coli* is the only facultative anaerobe. On anaerobic conditions, which set in shortly after the feeding times (see Figure 13(a)), formate is released as a product of *E.coli's* fermentation process (see Supplementary Figure 11(b)). Right after the first feeding, *E.coli* becomes the community's main formate producer. The fact that all the other species except for *Bacteroides* and *Clostridium* are consuming formate during this period explains the con-

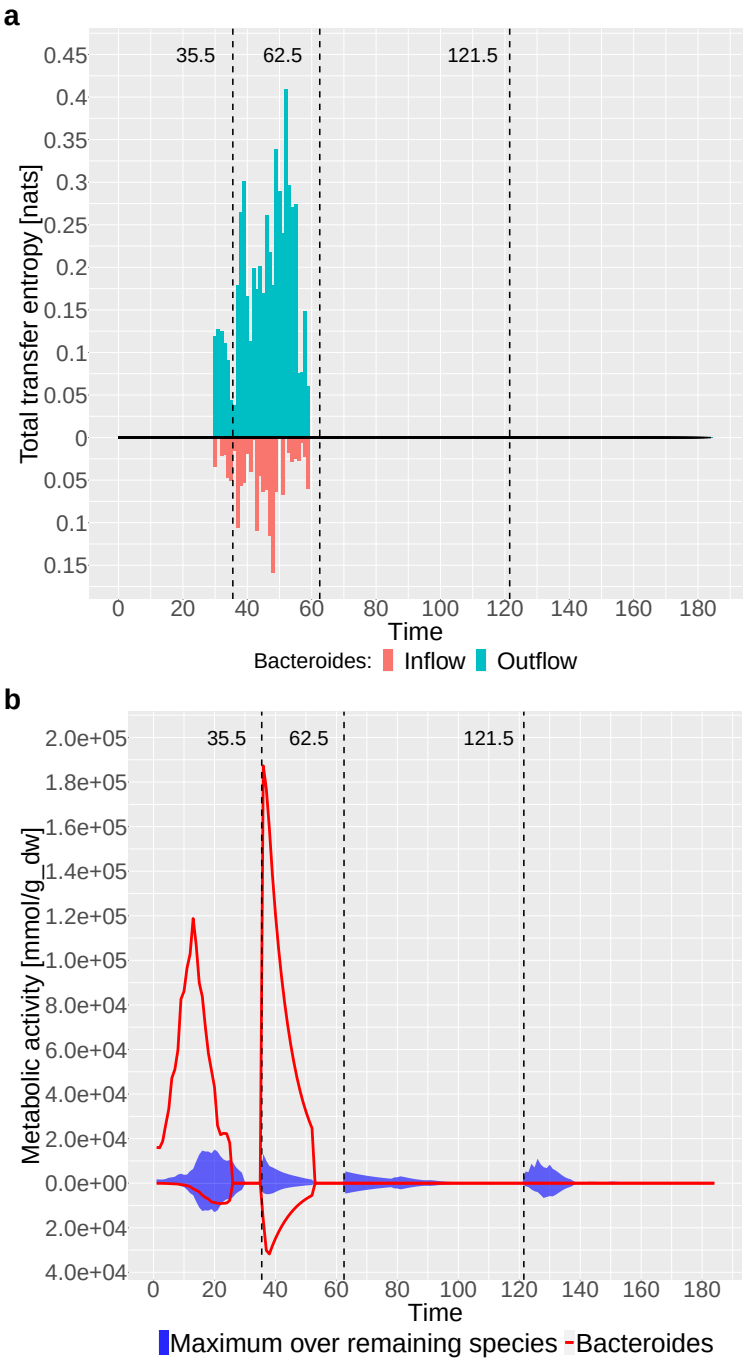

Figure 9: Information theoretic and metabolic activity of *Bacteroides*. (a) Total TE from and to *Bacteroides*. (b) Comparison of *Bacteroides'* and the maximum over all other species' metabolic activity. Consumption is shown below the x-axis, production above the x-axis.

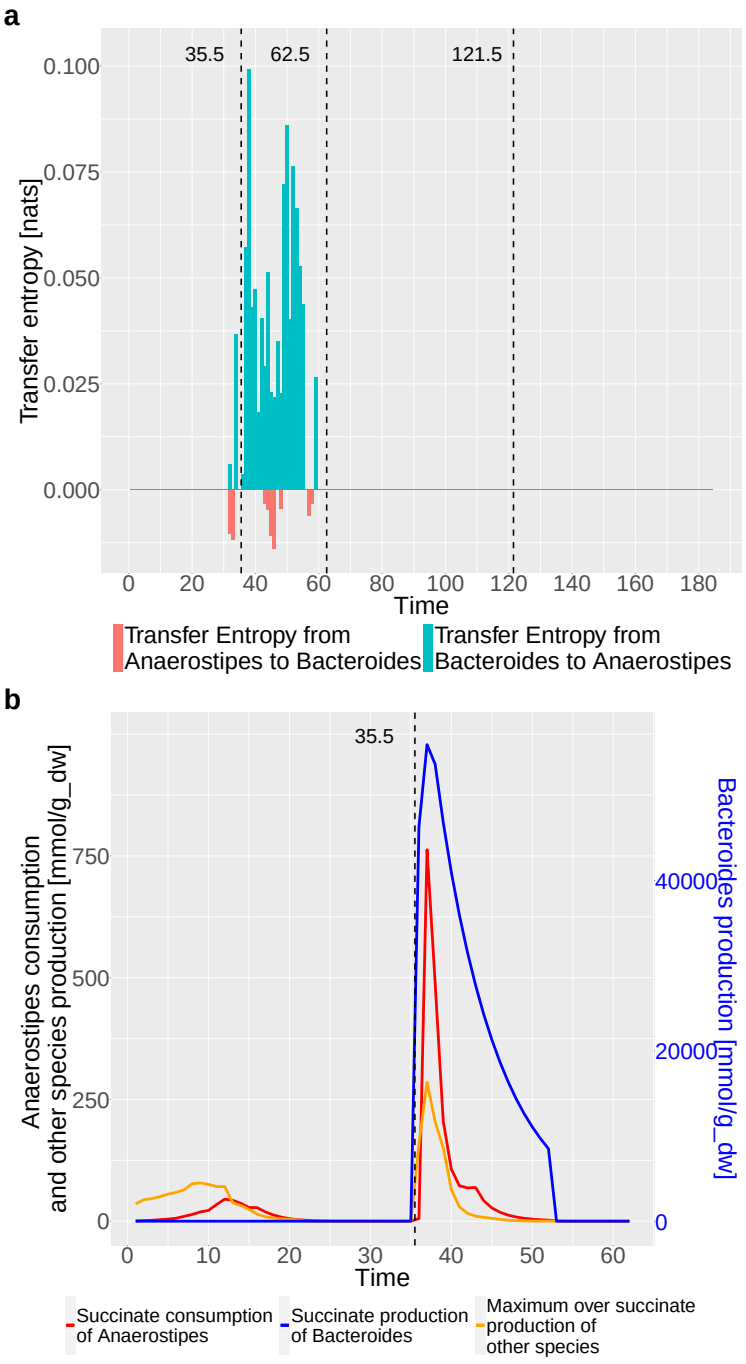

Figure 10: Information theoretic and metabolic activity between Bacteroides and Anaerostipes. (a) TE between *Bacteroides* and *Anaerostipes*. (b) *Anaerostipes'* consumption of succinate compared to the other species' production of succinate.

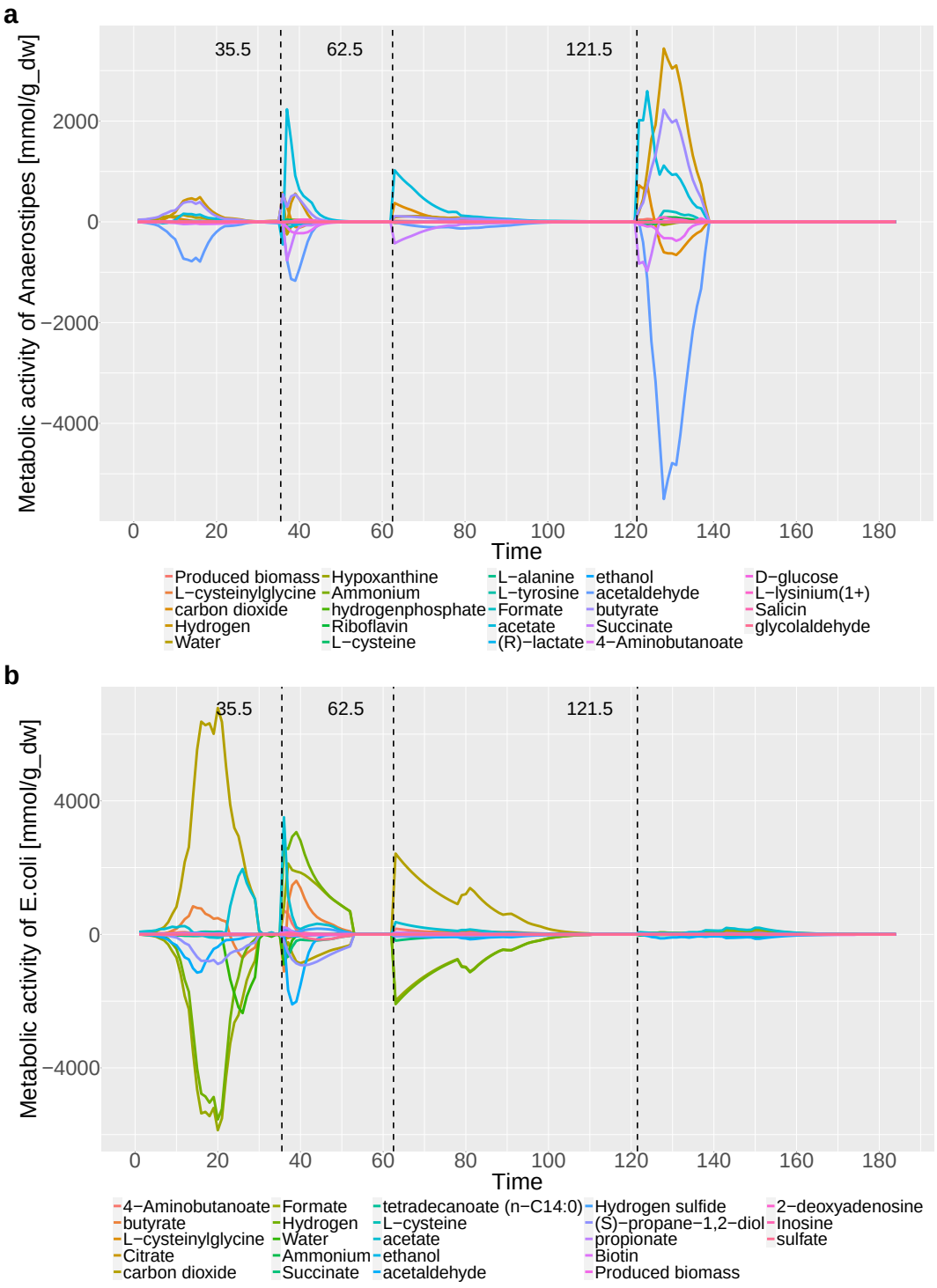

Figure 11: Metabolic profile of *Anaerostipes* and *E.coli*. Consumption is shown below the x-axis, production above the x-axis. Only the most varying substances each are displayed. (a) Consumption and production by *Anaerostipes*. (b) Consumption and production by *E.coli*.

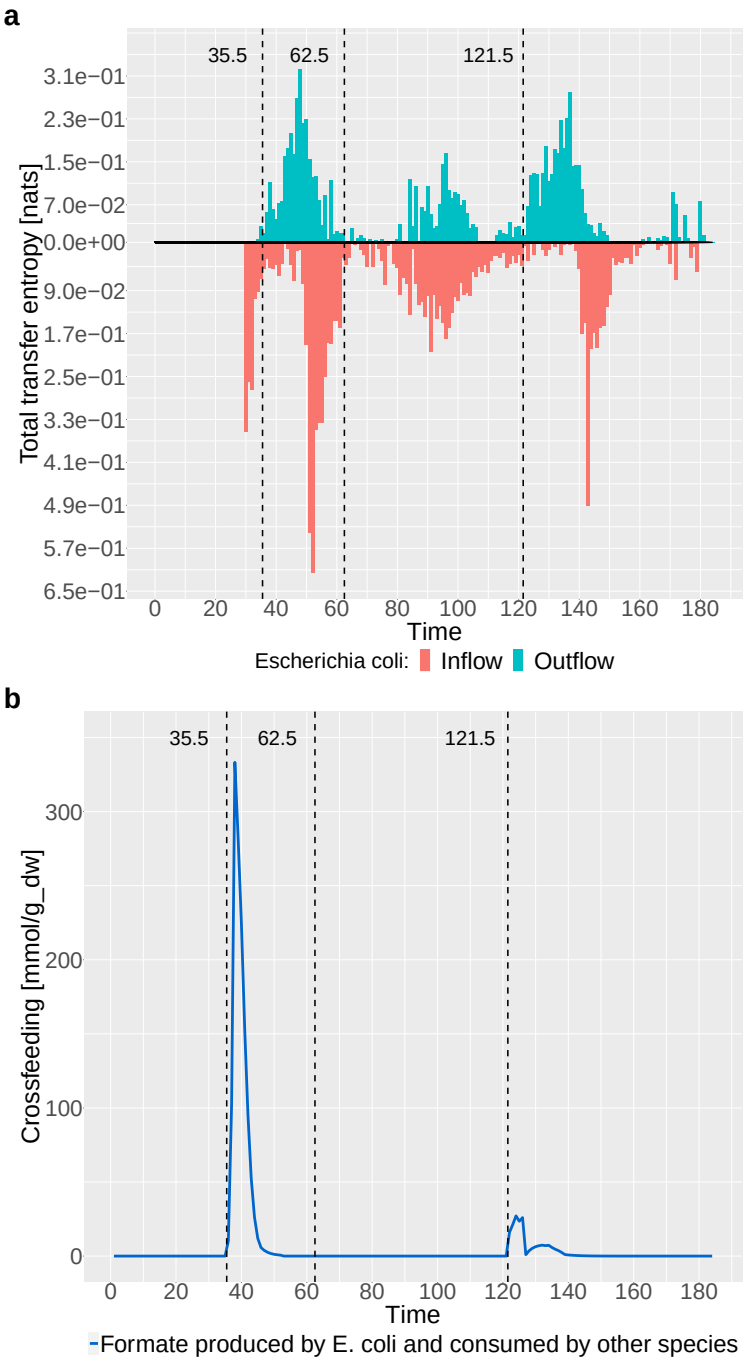

Figure 12: Information theoretic and metabolic activity of *E.coli*. (a) Total TE from and to *E.coli*. (b) Amount of formate being produced by *E.coli* and consumed by other species.

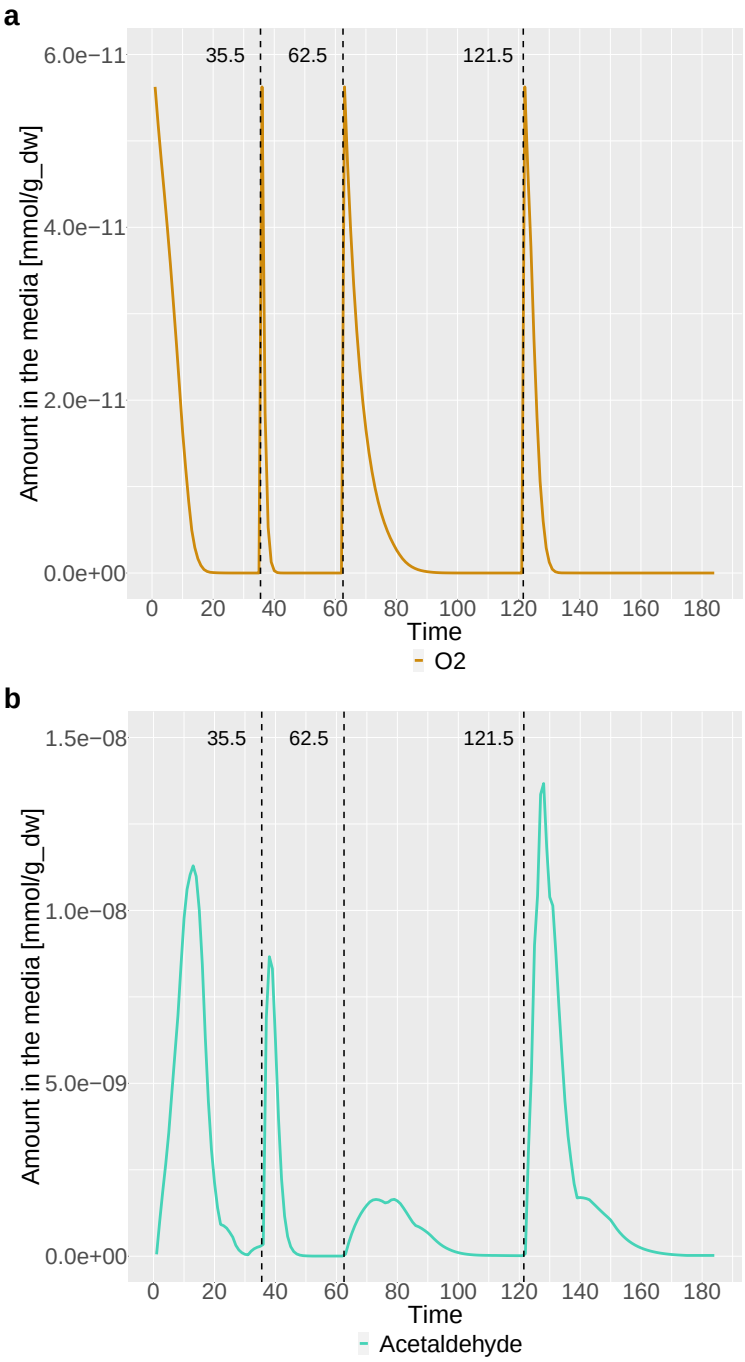

Figure 13: Amount of certain nutrients in the media. (a) Amount of oxygen in the media. (b) Amount of acetaldehyde in the media.

current dominance of information outflow. Figure 12(b) shows that around time step 50, the amount of formate being produced by *E.coli* and consumed by other species has decreased to zero again, turning the dominance of information outflow into a dominance of inflow. After the third feeding, *E.coli* starts producing formate again, which is mainly consumed by *Anaerostipes* and *Clostridium* now. This interaction results in a strong dominance of information outflow again. With the two species stoppping their formate consumption around time step 140 (see Figure 12(b)), *E.coli's* dominance of information outflow is abruptly changing into a dominance of information inflow.

There is a strong competition for acetaldehyde (see Figure 14) between *Anaerostipes* and *Clostridium*. Acetaldehyde is the main feeding component of both species and, as can be seen in Figure 13(b), a limiting factor shortly after the feedings. Following the third feeding, *Anaerostipes* significantly increases its consumption of acetaldehyde and becomes *Clostridium's* main competitor. This interaction is reflected in a high information transfer from *Anaerostipes* to *Clostridium* (see Figure 15(b)).

Hypothesis 3: In an interaction, the agent mainly *receiving* information is generally more successful than the agent mainly *sending* information. Let us take a closer look at some of the interactions just presented, starting with *Bacteroides*. From a metabolic view, *Bacteroides* is highly productive. However, from an information theoretic view, it is mainly passive, since only *receiving* information transfer indicates active processing. This lack of active adaptation to the other species' development is reflected in the abundance of *Bacteroides*. It increases quicker than the abundances of the other species during the first steps. It seems to have an initial advantage when the others are not yet established. This advantage gets lost as soon as all the others are established: *Bacteroides* is the first species to start decreasing in abundance again. The decrease happens right before the first feeding. The feeding is able to prevent a further decrease but there is no increase in abundance. Shortly before the second feeding, all the individuals die abruptly.

In contrast, consider *Clostridium*. Throughout the whole simulation, *Clostridium* is one of the least abundant species. Nevertheless, it does not become extinct until three steps before the end of the simulation. Figure 15(a) shows that the information inflow of *Clostridium* is clearly dominating its outflow. Compared to *Bacteroides*, being a clear outflower to get extinct quickly, *Clostridium* can compete with the other species on the long run.

Finally, recall the competition between *Clostridium* and *Anaerostipes*. There is a clear dominance of information transfer from *Anaerostipes* to *Clostridium*. While Anaerostipes gets extinct around time step 150, *Clostridium* maintains its population size for another 30 time steps.
These examples and several more suggest that the act of receiving information transfer from

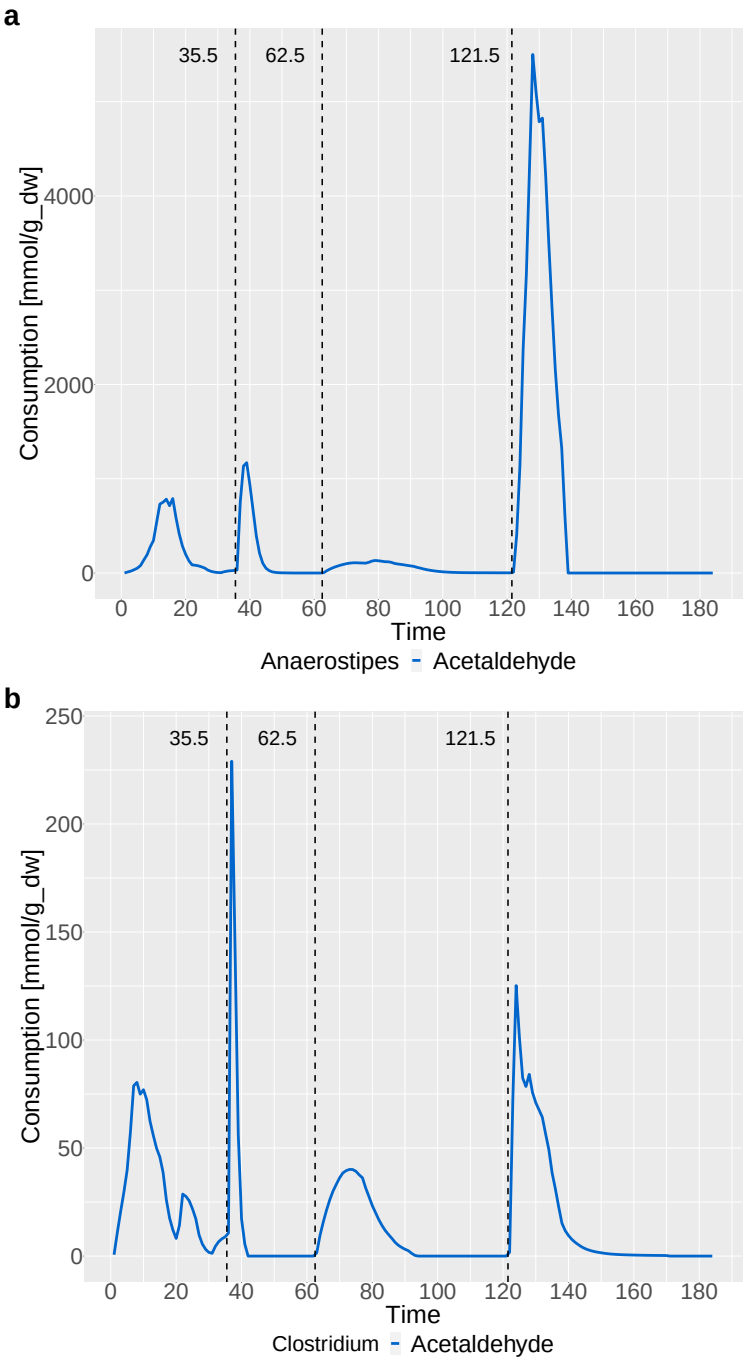

Figure 14: Acetaldehyde consumption of single species. (a) Acetaldehyde consumption by *Anaerostipes*. (b) Acetaldehyde consumption by *Clostridium*.

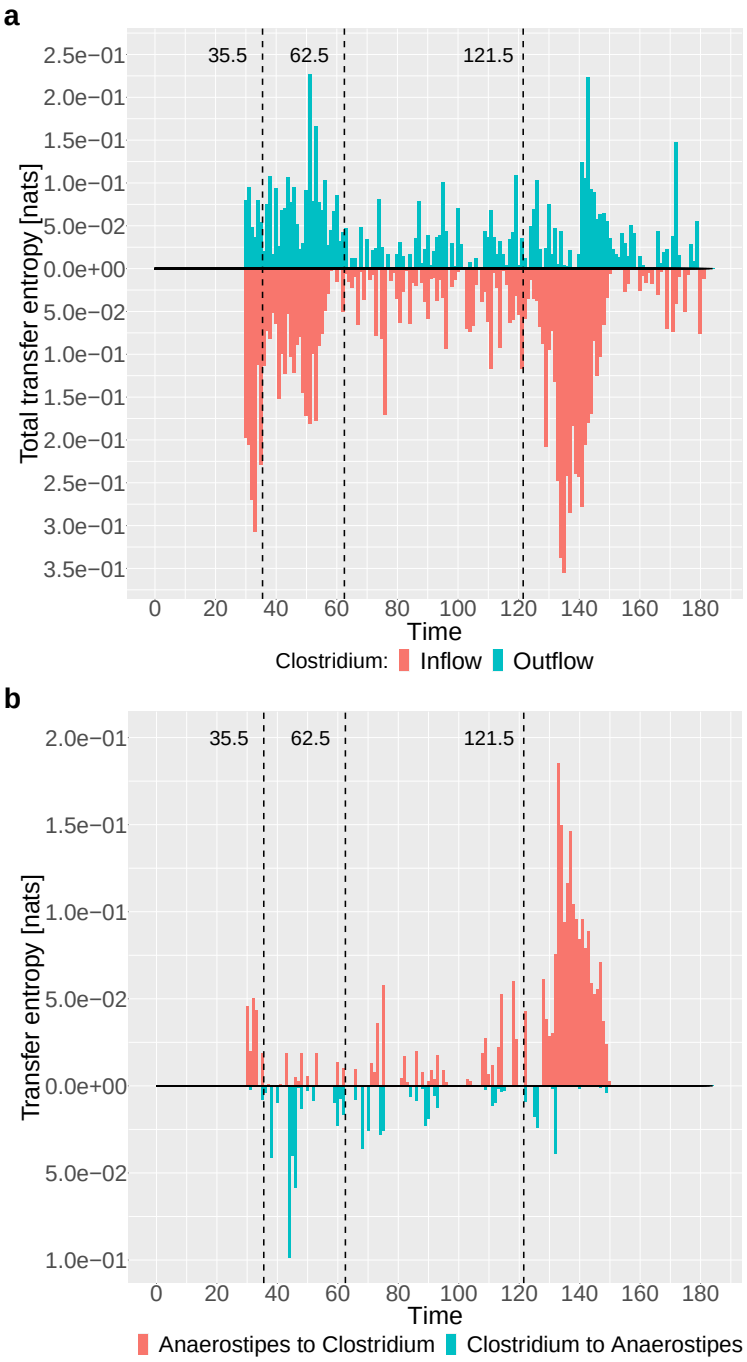

Figure 15: Information theoretic role of *Clostridium*. (a) Total transfer entropy from and to Clostridium. (b) Transfer entropy between Anaerostipes and Clostridium.

other species can be understood as an active adaptation process, thereby benefiting the chances of survival in the community.

This case study nicely illustrates that considering complex systems as computing entities can be a fruitful approach to system analysis. Effective interactions, in this case competition for nutrients and feeding among each other, are clearly reflected in the abundance-based transfer entropy among the system's components. Examples like this further enhance our confidence in the information theoretic approach of our method.
Having transferred time series of abundance into networks of information transfer, the next crucial step in our method is the computation of the networks' potential, connectedness, and resilience. In the following chapter, we will address the question whether our measures do indeed agree with Gunderson and Holling's understanding of these complex notions.

4.2 Interplay of the systemic variables

The core of our method to quantify the adaptive cycle is the computation of its three defining variables, potential, connectedness, and resilience. In Sections 3.3 and 3.2, we presented and explained our choice of definitions. From a theoretical point of view, this choice should be comprehensible at this point. However, we still need to demonstrate the suitability of the three measures in practice. To this end, we will simulate the development of a complex system's information network during a classic course through the adaptive cycle. The simulation will be designed on basis of Gunderson and Holling's descriptions of phase specific system properties given in [39]. Table 4 summarizes these properties and their meaning with regard to a system's information network.

According to Table 4, the topological evolution of a system's information network is likely to alternate between a slow contraction to a few, high-weighted edges during r/K phase and an abrupt expansion to many, low-weighted edges at the onset of the Ω-phase. We call this developmental pattern "contract and spread". In this section, we simulate a series of graphs which follows this pattern, building on the principle of *overexploitation*. Overexploitation denotes the mechanism that an interaction between components of a system becomes inoperable or unprofitable due to overuse.
Note that, although the "contract and spread" pattern is the classic way of how the information network develops during a course through the adaptive cycle, other patterns of development are in accordance with the descriptions in Table 4 as well. We will see examples of such alternative patterns throughout this thesis.

We are simulating the interactions (and thereby the transfer of information) between the N components of a system in an agent-based model type approach. We want to outline the main ideas before describing the implementation in detail. Heuristically, the interactions follow the principles below.

Phase	General system properties	Network properties
α-phase	"internal regulation is week" "low connectivity among variables" "unexpected associations and recombinations"	quickly changing, low-weighted edges
r-phase	"subset of species begins to develop close interrelations" "intense activity" "future starts to be more predictable"	increasing weight on a subset of edges growing consistency in network topology
K-phase	"extreme and growing rigidity" "streamlining operations"	high consistency in network topology focus on a few high-weighted edges
Ω-phase	"connections are broken" "resources are released" "sudden explosive increase in uncertainty"	disappearance of high-weighted edges occurrence of new edges

Table 4: Properties of a system during the different phases of the adaptive cycle as given by Gunderson and Holling in [39, pp.41-46] and translated into the language of network topology.

- Interactions can be positive/negative for both interaction partners or positive for one and negative for the other partner.
- If a component has a positive interaction with another component, the probability of choosing this component as cooperation partner again increases. Though, the probability of this cooperation turning out positively decreases (overexploitation).
- If a component has a negative interaction with another component, the probability of choosing this component as cooperation partner again decreases to zero. The probability of this cooperation turning out positively increases.
- If the probability to choose a component is zero, this component is only taken into account as a cooperation partner again when there are no other options left.
- Each of the components is assigned a "capital" C, which it invests into its interactions. A component's capital increases after positive interaction and decreases after negative interaction. The amount of gain/loss is equal to the amount of capital invested in the

respective interaction. We call the amount of capital invested into an interaction the interaction's *strength*.

These rules are implemented as follows. We create a uniformly distributed random matrix P of size $N \times N$, whose (i,j)-th entry contains the probability that an interaction between i and j is positive for component i. Analogously, its (j,i)-th entry contains the probability that an interaction between i and j is positive for component j. The stochastic matrix R stores component i's probability to choose component j as interaction partner in its (i,j)-th entry. An interaction with oneself is not possible. Initially, the probability to choose an interaction partner is equally distributed. Furthermore, in every simulation step, we compute the matrix K to store the *strength* of the interactions. With C_i being the capital of component i, we set $K(i,j) = C_i \cdot R(i,j)$. Hence, each component invests its whole capital in its interactions, proportionally to the interaction probabilities. We consider K as adjacency matrix of the information network of the system. In addition, three constants $0 \leq c, c_p, c_C \leq 1$ have to be chosen. Their function will become clear later.
The simulation performs S rounds, each of which follows the same routine. Based on the probabilities in matrix R, every component i randomly selects an interaction partner j. Every component can thereby be part of several interactions, the one it has chosen itself and the ones for which it has been chosen as interaction partner. Based on the probabilities $P(i,j)$ and $P(j,i)$, two coins are tossed for every interaction, deciding whether the interaction is positive or negative for i and j. In random order, which is determined anew after each round, the interactions chosen by the components are executed as follows. We refer to the execution of one interaction as one simulation step.
Assume component i has chosen component j as interaction partner. If the interaction between i and j is positive for component i, the capital C_i of i increases to $C_i + C_i \cdot R(i,j)$, whereas $P(i,j)$ decreases to $\max\{P(i,j) - c_P, 0\}$. The probability for i to choose j again, $R(i,j)$, increases to $\min\{R(i,j) + c_C, 1\}$. The other entries in $R(i,:)$ decrease uniformly to maintain row sum 1. If the interaction is negative for component i, the capital decreases by $C_i \cdot R(i,j)$, whereas $P(i,j)$ increases by c_P. The entry $R(i,j)$ is set to zero. The other non-zero entries of $R(i,:)$ increase uniformly. There is one exception to this procedure: if $R(i,j)$ is equal to one, component i's capital is set to the initial value, representing a restart after the last interaction possible has turned out to be negative.
Subsequently, the same interaction is executed for j. If the interaction between i and j is positive for j, the capital C_j of j increases to $C_j + C_j \cdot R(j,i)$, whereas $P(j,i)$ decreases to $\max\{P(j,i) - c_P, 0\}$. The probability $R(j,i)$ for j to chose i again increases to $\min\{R(j,i) + c_C, 1\}$. The other entries in $R(j,:)$ decrease uniformly. If the interaction is negative for component j, the capital decreases by $C_j \cdot R(j,i)$ whereas $P(j,i)$ increases by c_P. The entry $R(j,i)$ is set to zero, the other non-zero entries of $R(j,:)$ increase uniformly. The exceptional rule described above applies analogously for j.
Finally, components i and j reinvest their capital in their interactions, hence, the matrix K

is computed based on the new values of $R(i,j)$, $R(j,i)$, C_i, and C_j. We compute potential, connectedness, and resilience of matrix K, completing one step of the simulation. Hence, the simulation yields time series of networks and systemic variables of length $S \cdot N$.

Our simulation produces series of networks showing the desired "contract and spread" behavior for a broad range of parameters. An exemplary series of 64 networks can be found in Supplementary B, the corresponding parameters are listed in Table 5. At the beginning of the simulation, the network has many edges, resembling a complete graph. The number of edges reduces and the edges' weight increases until time point 11. From time point 12 on, there is an opposite trend: the number of edges suddenly increases again and the network approaches its initial topological structure. The network contracts again until time point 25, where only a few edges are left. From time point 25 to time point 26, the second turnaround takes place. The network becomes more dense again and keeps this structure for more than ten time points. From time point 40 on, the edges clearly start contracting again. Starting at time point 48, the number of edges increases slightly, followed by a strong increase at time point 54. At time point 55, the network resembles a complete graph again. Summing up, we identify three contracting periods followed by spreading events, or, in the language of Gunderson and Holling, three runs through the adaptive cycle.

N	5
S	16
C	10
c	0.5
c_P	0.1
c_C	0.1

Table 5: Parameters used in the overexploitation simulation underlying Figures 16 and 17.

What behavior of the three systemic variables do we expect? Following the descriptions of the adaptive cycle metaphor, connectedness should increase during the contracting periods due to the accumulation of overall capital and the rising constraints, whereas resilience should decrease due to the network's growing vulnerability. Potential should increase as long as the effect of increasing capital outweighs the effect of the decreasing number of edges. The sudden breakdowns should be reflected by a decrease in connectedness and an increase in resilience. The behavior of potential during breakdowns is again dependent on the weighting of the different effects but we expect an overall decrease. Figure 16 shows that the development of potential, connectedness, and resilience fulfills our expectations. Considering the system's connectedness, three clear breakdowns can be detected: the first at time point 12, the second at time point 26, and the third at time point 48. The system's potential shows a similar behavior. Both variables capture, besides the pure topology of the graph, the increasing total capital during contraction periods and its decrease at spreading

events. Resilience, typically opposite to connectedness, slowly decreases during times of contractions and suddenly and strongly increases at times of breakdowns.

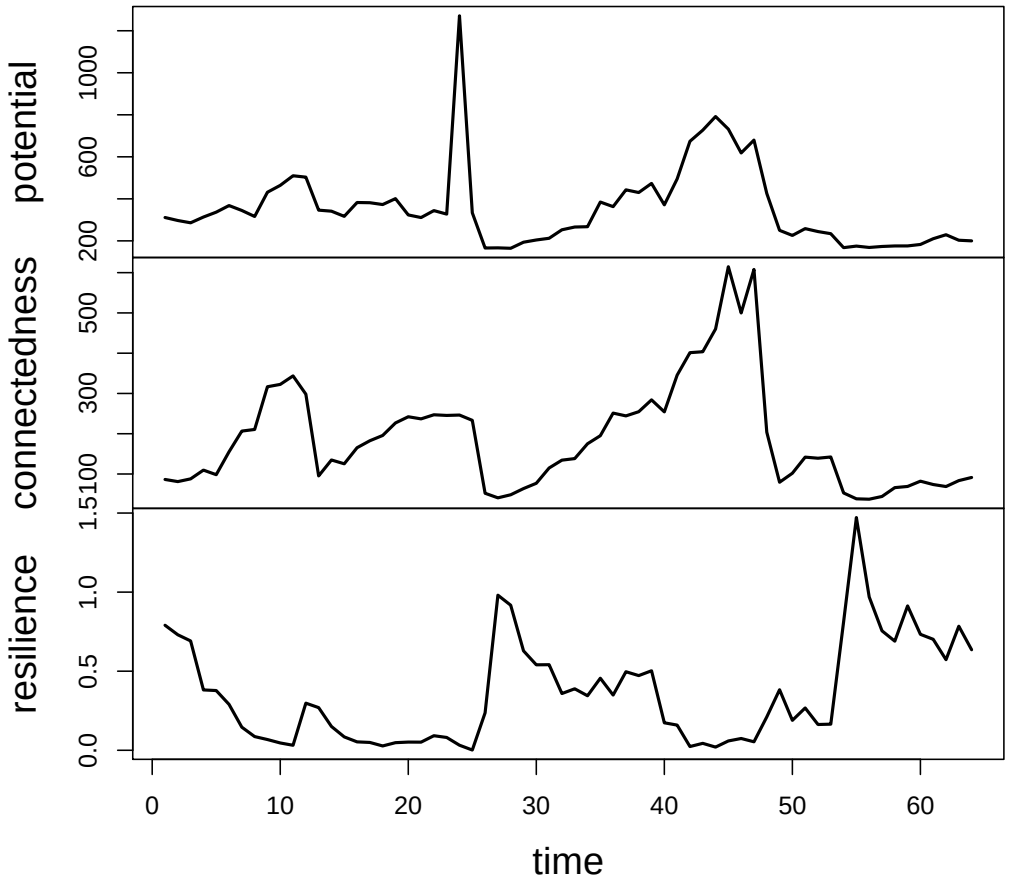

Figure 16: Potential, connectedness, and resilience of the first 64 time points of one run of the simulation. The corresponding networks are displayed in Supplementary B.

Figure 17 displays the output of a second realization. Here we used the same parameters as in the first realizations (see Table 5), except for the number of time steps, which we set to $S = 20$. The interplay of the three systemic variables indicates two clear cycles, with the first taking place at time point 32, the second at time point 70. In both cases, resilience suddenly increases while connectedness strongly decreases. The networks shown exemplify the network's topology before and after the breakdowns. Before the breakdowns, at times of high connectedness and potential, the network has a comparably low number of edges,

some of which are significantly stronger than others, (compare networks 29 and 63). After the breakdowns, the networks resemble complete graphs with rather equally weighted edges (compare networks 32 and 70). This topology is reflected in the networks' high resilience and low connectedness. Both connectedness and potential indicate a smaller third breakdown around time point 50. But it does not result in a complete graph-like topology like at time points 32 and 70, therefore it is not clearly reflected in the network's resilience. The situation is similar to the period between time points 48 and 54 in the first realization: connectedness has just declined but resilience is still comparably low. Considering the corresponding networks, one can see that they are less constrained than before time point 48, hence the lower connectedness, but they do not receive their complete graph-like topology before time point 55.

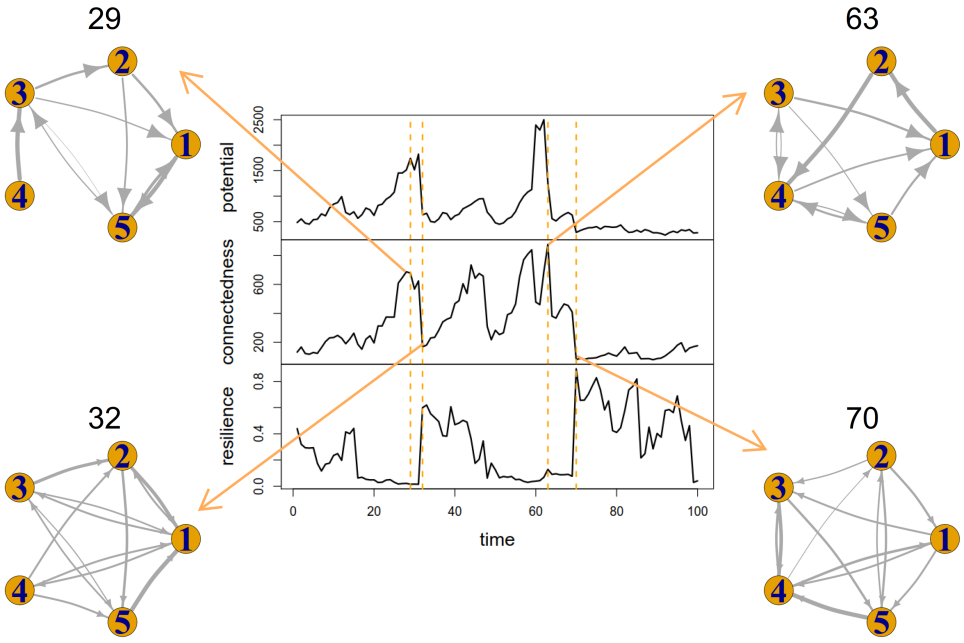

Figure 17: Potential, connectedness, and resilience of a second run of the simulation. The corresponding network is shown for time points 29, 32, 63, and 70.

The results just presented demonstrate that the three systemic variables behave as expected in a *particular* adaptive cycle network development scenario. They therefore contribute to the validation of the variables' definitions. However, as already mentioned, other development scenarios with very different topological properties can be in accordance with the adaptive cycle metaphor as well. We will see an example in the following section, addressing the question whether the adaptive behavior of a system can be extracted from

purely interaction-based data.

4.3 Capturing cyclic development in an interaction-based model

The following section is except for smaller modifications an excerpt of [83]. The Tangled Nature Model (TNM) [24] is an abstract model of co-evolutionary interactions. It simulates the development of a community of genotypes, being represented by binary vectors of a fixed length. Each of the genotypes provides an opportunity for individuals of this type to be born, mutate, reproduce, or die. The probability for these events is based on an underlying interaction pattern among the genotypes which is randomly generated at the beginning of the simulation. The model yields time series of abundances of representatives of genotypes. We consider each genotype as an agent of a system. Since there is no metabolism being modeled, it is the interactions only, which drive the dynamics of the simulation and potential does not differ from connectedness. Therefore, we will restrict our analysis to only two of the systemic variables, namely connectedness and resilience. Note that the model has been shown to generate alternating phases of stability and change [24]. It therefore provides an ideal testing scenario for our assumption that the interaction structure of a complex system captures its cyclic adaptive behavior.

We chose a genome space of size 32 and simulated an evolution of 5000 time steps. The simulation is based on the code provided by Jensen & Palmieri [24]. See Suppl. Table 1 for a list of the parameters used. During the whole simulation, 24 different genotypes occurred. For the estimation of the information networks, we used a window size of $w_t = 100$. History lengths and delay were set to 1. Only transfers passing a significance level of 0.01 were taken into account. Resilience was computed by means of symmetrically normalized Laplacian matrices, being standardized with respect to the maximal edge weight M via $c = \frac{1}{M}$. An overview of the data and parameters used in this case study can be found in Table 7.

Considering the development of connectedness and resilience of the simulated system, one can immediately observe an antagonistic cyclic behavior (Figure 18(a)) with connectedness peaking while resilience drops and vice versa. This behavior perfectly matches with the variables' anticipated development. Taking a closer look at breakdowns, two different kinds of breakdown can be identified (see Figure 18(b)). One type of structural change occurs right before the composition of the genome space changes (1), while the other arises in the middle of a compositionally stable phase (2). The first case literally follows the adaptive cycle metaphor: release and a subsequent phase of reorganization are characterized by structural changes of the system. The second type seems to be non-intuitive at first glance. However, an Ω-phase does not need to result in compositional changes. A structural breakdown of organization can also manifest itself in internal reorganization. The external structure of the system thereby appears to remain unaffected. Examples of such an internal crisis are abundant in both ecology and socio-economical systems.

system	community of genotypes
components	genotypes
number of components	24
type of abundance data	number of individuals
length of time series	5000
window size w_t	100
interpolated window size	100
history lengths k, l	1
delay u	1
significance level	0.01
normalization type	symmetric
standardization constant c	$\frac{1}{M}$

Table 6: Data and parameters of the TNM case study.

Let us now consider the networks of information transfer underlying the systemic variables. A clear pattern in the development of the information networks reflects the different phases of the cycle. As exemplarily shown for time step 3121 (see Figure 18(c)), the network of information transfer does only have a few edges in times of higher resilience. From step to step, these edges quickly change and do not exhibit any pattern of continuity. This is typically the case during phases of release and reorganization. Recall that the transition from K- to Ω-phase is characterized by connections being broken, low connectivity among variables, and unexpected associations and recombinations appearing (see [39, p. 45 et seq.]). In contrast, in times of lower resilience, the network reveals many edges (see, e.g., the network at time step 3376 in Figure 18(c)). Here, the edges range from very low-weighted edges, representing weak transfers of information, to temporally more constant, heavy-weighted edges, reflecting strong transfers and thereby more closely connected components. This matches the description of the four phases by Gunderson & Holling [39] There are structural differences to the development scenario in Section 4.2. However, as already mentioned, their descriptions allow different developmental patterns of systems' information networks.

In this case study, we extracted the typical cyclic, antagonistic pattern of connectedness and resilience from a purely interaction-based model following simple rules of co-evolutionary development. These results support our assumption that the adaptive behavior of a system indeed expresses itself in the lowest common denominator of all complex systems, i.e the interactions among its components.

Having validated the main ideas underlying our method, we will now demonstrate its broad field of application by means of three different case studies.

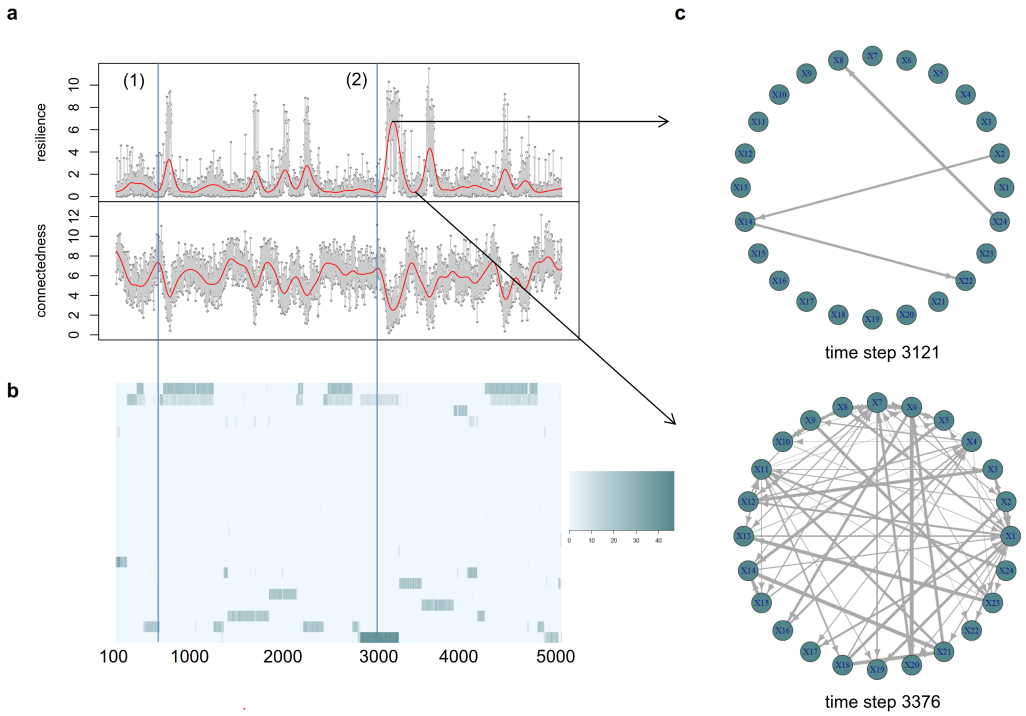

Figure 18: Information theoretical analysis of a Tangled Nature Model system. (a) Resilience and connectedness of the system (genome size of 32) over 5000 time steps. (b) Occupation of genome space. The blue lines mark two different kinds of breakdowns. After 1), the composition of the genome space changes. Breakdown 2) happens in the middle of a stable phase. (c) Networks of information transfer of the simulated system at time steps 3121 and 3376.

5 Cases of Application

Complex systems are as diverse as our world itself. No less diverse are our questions when it comes to understanding specific complex systems. The strength of our method lies in its generality. In the last section, we already saw it being applied to a simulated microbiome and a model of co-evolutionary interactions. Now, it is time to illustrate its use in investigating real-world systems. By means of an economic example, we demonstrate the method's capability in *comparing* systems (Section 5.1). Here, the concrete question is: How does the development of three European countries differ from each other during the Euro crisis? Subsequently, in Section 5.2, we go more into detail, showing our method's ability to *explore* complex systems. Exploration does not end with the consideration of a system's course through the adaptive cycle. It includes the examination of the cycle's specific underlying driving forces. We can gain insight into these forces by studying the estimated information networks themselves. The development of nodes' positions in the network contains important information about the role of single components or interactions in the transition between the adaptive cycle's phases. We will illustrate this analysis technique by means of two ecological systems.

Recall that it is important to keep in mind that we cannot and should not expect any real system to exactly follow the idealistic pattern of the adaptive cycle. The metaphor should rather be seen as a description of the baseline development of a system which can be taken as background for a detailed analysis of a given instantiation of the system. In particular, deviations from the ideal allow to identify specificities in system development which are due to the particular interaction patterns given in a concrete situation.

5.1 Comparing economic systems during the Euro crisis

This section is except for smaller modifications an excerpt of [83]. In the second decade of the 21st century, Europe was shaken by a financial crisis. In the following case study, we will analyze and compare the development of three European countries during this crisis. Considering each country as an economic system, classical economic variables such as export, import and gross national product can be considered as agents. We complemented this set of monetary variables with logistic variables such as the amount of goods transported by road or by railway to incorporate logistic capacity. Variables such as final consumption expenditure of households, motorization rate, or people at risk of poverty or social exclusion reflect the prosperity of a country. Additionally, environmental indicators such as greenhouse gas emissions are considered. Our data set comprises yearly quantities of 19 economic variables from 2004 to 2015, being obtained from the Eurostats database [3]. The data is provided in the supplementary material. See Suppl. Table 3 for a complete list of the variables used. The units of the variables are heterogeneous, ranging from Euro over tonnes to the number of individuals. We used an expanding window size of $w_t = t$, starting at $t = 7$, and

an interpolated window size of 18 for the estimation of the information networks. History lengths and delay were set to 1. Only transfers passing a significance level of 0.01 were taken into account. Symmetrically normalized Laplacian matrices standardized with respect to the maximal edge weight M via $c = \frac{1}{M}$ were used for the computation of resilience. See Table 7 for an overview of the data and parameters used.

system	European country
components	economic variables
number of components	19
type of abundance data	heterogeneous
length of time series	12
window size w_t	t (starting at 7)
interpolated window size	18
history lengths k, l	1
delay u	1
significance level	0.01
normalization type	symmetric
standardization constant c	$\frac{1}{M}$

Table 7: Data and parameters of the Europe case study.

Retrospectively, European countries were split into two major classes, the Northern countries representing creditor states, and Southern/peripheral countries, representing the debtor states. These two groups drifted into the crisis under different prerequisites and consequently played very different roles. As a representative of the former group, we chose Germany. For the debtor group, we chose Greece and Italy. Greece has a special position among the southern countries. In contrast to other debtor states, the Greek crisis was a genuine sovereign debt crisis right from the beginning, and it is one of only two countries in which dept restructuring became necessary to overcome the crisis [36]. In contrast, Italy represents a Southern state without international intervention or control during the study period.

Let us start with the consideration of Germany. Figure 19(a) shows a classical Ω-phase during 2010 to 2011. A breakdown in potential and connectedness is accompanied by an increase in resilience. This phase of economic decline can also be seen at the financial market. Note that an increase in returns from ten-year government bonds (see Figure 19(d)) reflects decreasing trust in the governments capacity to act at the onset of the crisis [32]. From 2011 to 2013, potential and connectedness recover, indicating a clear r/K phase. This increase goes along with a loss of resilience, leading to a second breakdown in 2013. These phases can also be followed in the development of government bond yields, decreasing from 2011 to 2013 followed by another increase until the first months of 2014. From 2014 to 2015, the

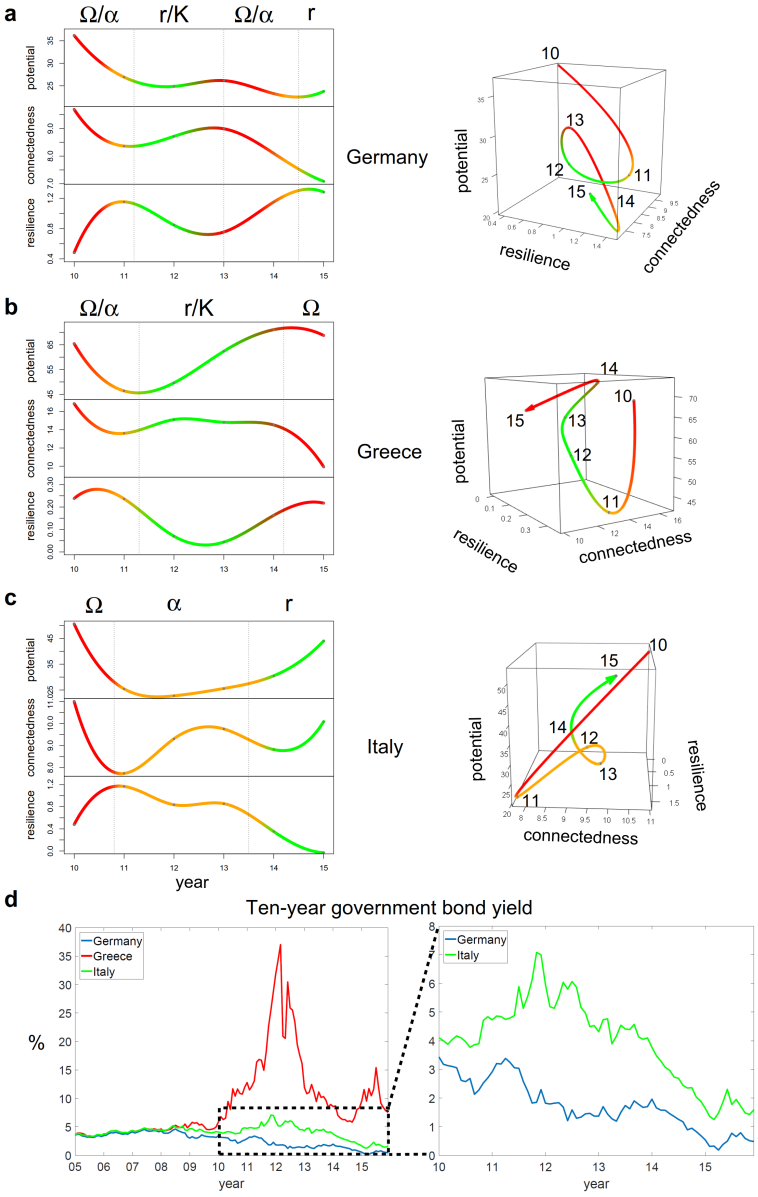

Figure 19: Information theoretical analysis of European countries during the Euro crisis. (a)-(c) Development of potential, connectedness, and resilience of Germany, Greece, and Italy considered as economic systems. (d) Ten-year government bond yield of Germany, Greece, and Italy [9]. The labels mark the month January of the respective year.

yields decreased again with the system starting into another α-phase. Overall, Germany runs through a complete adaptive cycle during these years. This well matches the fact that Germany has not been hit by the Euro crisis so hardly. Like most of the Northern countries, Germany had a finance surplus when the global financial crisis started, which allowed the

country to take-in the role of a creditor [36].

From a system point of view, the development of the Greek economy shows a similar behavior (Figure 19(b)). After a breakdown in 2010–11, a classical r-phase can be identified from 2011 to 2012, with potential and connectedness increasing and resilience decreasing. Considering yields of ten-year government bonds (Figure 19(d)), the conclusion would be partially opposite. The beginning of the r-phase from 2011 to 2012 is coming along with a steep increase in yields, showing the fact that the markets lost their trust in the Greek economy. Recall that at the end of 2009, Greece's credit ratings have been downgraded after the Greek government had disclosed an extraordinary high budget deficit [35]. In the following, financial assistance programs have been approved (e.g. "Six-Pack of reforms" in December 2011 [35]) aiming at the stabilization of the economy. From our system perspective, these external actions seem to have had a stabilizing and growth encouraging effect from 2011 onwards, being reflected in strongly increasing potential and more or less constant connectedness. Thus, through the intervention of the European community, actual market development as being captured by economic performance indicators and thereby by our three systemic variables has been decoupled from the financial assessment of the country's economy, as being reflected in governmental bonds. After a second financial assistance package in March 2012 [35], potential further increases until 2014. However, connectedness slightly declines from 2012 on, resilience increases from 2013 on. Hence, while potential still indicates that the system is in its r/K phase, connectedness and resilience more and more indicate a system breakdown. This 'atypical' behavior might indicate the fact that the exploitation phase has been triggered externally. Due to the formation of a new government, European payments were suspended from August 2014 to July 2015 [4]. With internal control taking over again in that period, a second breakdown can be seen, with potential and connectedness decreasing and resilience increasing. This breakdown is now indeed being reflected in a second peak in governmental bond yields.

In the form of Italy, we will now consider a debtor state which has not been subject to external intervention. From 2010 to 2011, the systemic variables show the same behavior as in the other two countries: Potential and connectedness decrease along with an incline in resilience (Figure 19(c)). At the same time, yields of ten-year government bonds increased (Figure 19(d)). We identify this period as a classical Ω-phase. During the following three years, yields first continued increasing and subsequently decreased again. This is accompanied by an in- and decrease in connectedness and an overall slight decrease in resilience. Potential remains low during the whole period. We interpret this period as comparatively long α-phase. This matches the fact that, although a bailout could be avoided, structural reforms and austerity measures progressed slowly [44]. The country faced massive increases in unemployment and poverty, and populist and anti-establishment parties were strengthened in the sequel [36]. A particularly strong decline in governmental yields can be observed between 2014 and 2015, leading to a local low at the beginning of 2015. Indeed, 2014 is the year

where potential and connectedness start increasing again while resilience strongly decreases. Here, we identify a classical r-phase. In summary, the systemic analysis well matches the economic situation of the country and the financial assessment via governmental bonds.

In the following two case studies, we will exploit the full potential of our method by including the information networks themselves into the analysis. To this end, we return to the metaphor's original source of inspiration, ecosystems.

5.2 Exploring systems

In the following, we will investigate the development of two ecosystems. First, a vascular plant community on a volcanic island near Iceland (Section 5.2.1) is presented. Second, we consider a plant community in the prairie-forest ecotone of Kansas (Section 5.2.2). The two systems differ in a crucial aspect: while the plant community of Iceland is largely unspoiled, the experimental plot in Kansas is exposed to human intervention in form of triennial spring burns. We analyze their development from the adaptive cycle point of view, taking into consideration the networks of information transfer themselves. Knowing the systems' characteristics during and at the transition of the cycle's phases is the key to understanding the systems' development.

5.2.1 Systemic analysis of a developing plant community on the island of Surtsey

We will now come back to the vascular plant system on the volcanic island of Surtsey, whose first years of development have been generally described in Section 1. The following case study is taken from [70] in large parts. It provides a detailed analysis of a particular plant community on the island, aiming to locally explore the succession events following 1990. Our analysis is based on time series of vascular plant species' abundance data collected in a 10x10m plot (Plot 1) on the Southern part of Surtsey. The plot is within a sea-gull nesting site on sand-filled sheet lava (see Figure 20(d)). During the observation period, twelve different species were recorded (Table 8).

Data has been collected biennially in July by the Icelandic Institute of Natural History from 1990 to 2018. Next to species' abundances, the number of sea-gull nests within the plot was counted from 2004 onwards. This quantity is included into our analysis in form of the variable nesting density (ND). For more information on data collection and the approach to monitoring, see [55]. Precipitation data has been obtained from the weather station on Stórhöfði, the main island in the Vestmannaeyjar archipelago, about 18 km away from Surtsey (provided by the Icelandic Institute of Natural History in January 2019).

The estimations of information networks are based on windows of a fixed size of $w_t = 6$. By interpolation, we increased the number of data points in every window to 18. History

Species	**Abbreviations**
Cerastium fontanum	CF
Cochlearia officinalis	CO
Festuca rubra	FR
Honckenya peploides	HP
Leymus arenarius	LA
Matricaria maritima	MM
Poa annua	PA
Poa pratensis	PP
Puccinellia distans	PD
Sagina procumbens	SP
Stellaria media	SM
Taraxacum	T

Table 8: Species of vascular plants recorded in Plot 1 between 1990 and 2018.

length and delay were set to 1. An estimated transfer was taken into account only if its significance was ≤ 0.1. We used symmetrically normalized Laplacian matrices, standardized with respect to the maximal edge weight M via $c = \frac{1}{M}$ to compute the system's resilience. Table 9 summarizes features of the data and the parameters used in this case study.

system	vascular plant community
components	plant species and nesting density
number of components	13
type of abundance data	heterogeneous
length of time series	15
window size w_t	6
interpolated window size	18
history lengths k, l	1
delay u	1
significance level	0.1
normalization type	symmetric
standardization constant c	$\frac{1}{M}$

Table 9: Data and parameters of the Surtsey case study.

Since data has been provided on a biennial basis, we decided to confine ourselves to merge the two phases of predictability into a single r/K-phase and the phases of stochasticity into an Ω/α phase, correspondingly. Doing so, analyzing the community of vascular plants and sea-gull nests on the study plot reveals four clearly distinguishable phases. Our observation

period starts with a clear r/K-phase in 2000 – 2004. While potential and connectedness increase, resilience decreases (see Figure 20(a and c)).

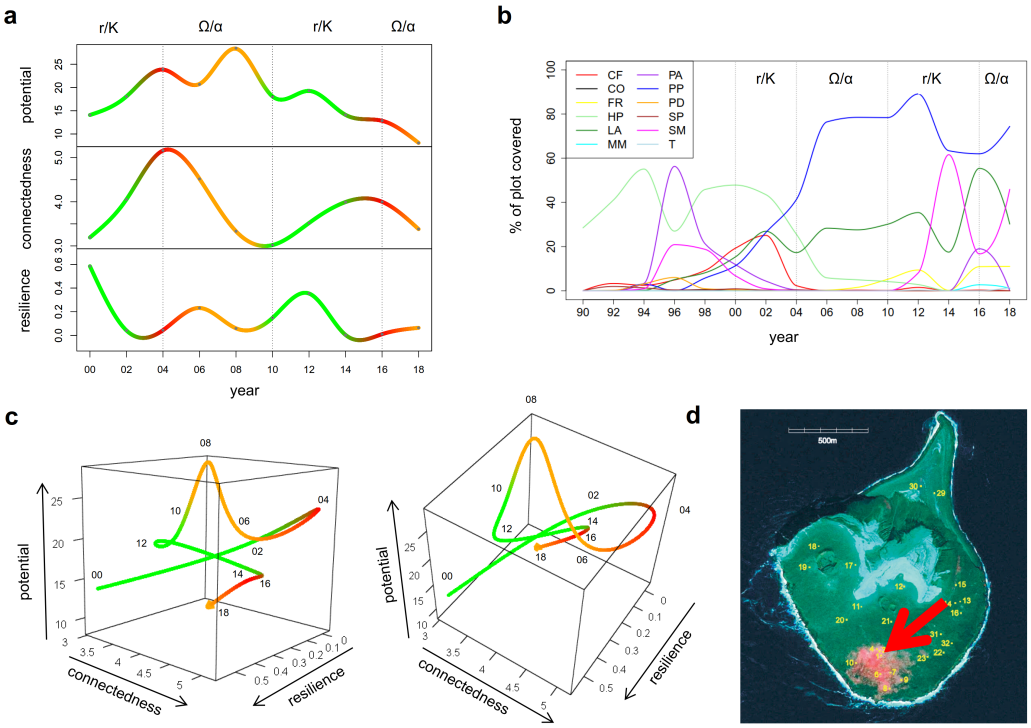

Figure 20: (a) Potential, connectedness, and resilience of the vascular plant system in the monitoring plot. (b) Percentage of the monitoring plot covered by the different plant species. (c) Three-dimensional plot of potential, connectedness, and resilience of the vascular plant system in two different perspectives. (d) Bird's-eye view of Surtsey with the red arrow displaying the location of the monitoring plot. Edited version of Figure 2 in [55].

The following period from 2004 to 2010 can be interpreted as an Ω/α-phase, primarily indicated by monotonously decreasing connectedness. Potential shows an overall decrease, resilience an overall increase during this period. However, their development is not monotonous. Potential peaks in 2008 while resilience is concurrently at a local minimum.

The period from 2010 to 2016 reveals a second r/K-phase. This conclusion is mainly supported by the increase of connectedness. An associated loss of resilience follows slightly delayed, as starting in 2012. Potential does not follow the idealistic pattern of the adaptive cycle. Although the system does increase its inner level of organization, it cannot build up potential. Such atypical development hints towards external drivers, hindering the system from fully exploiting its capabilities.

Finally, the years 2016 and 2018 indicate a second Ω/α-phase of reorganization. All three variables show the classical behavior as expected by theory. However, we will not discuss

this last phase in detail since it seems to be still ongoing. Overall, the system runs through two adaptive cycles during the study period. In the following, we will provide a deeper analysis of the first three of the observed phases. Here, the decrease in potential during the second r/K phase is of special interest.

The first r/K phase – the end of an era. Let us first consider species composition during the period 2000 – 2004. Robust species being capable of surviving under harsh conditions still prevail. At the beginning of the period, *Honckenya peploides* and *Leymus arenarius*, along with *Cerastium fontanum*, together make up more than 80% of land cover. Towards the end of the period, the contribution of these early colonizers decreases down to less than 50%. In 2004, *Poa pratensis* has gained dominance. This perennial grass outcompetes annual community members such as *Poa annua* and *Sagina procumbens*. Plant community composition exhibits a clear transition from early pioneers and opportunistic species towards a grassland community. The well-established association of *Honckenya* with *Leymus* (compare Section 1), which has been important in establishing sustainable plant life on the island [34], starts to give way to experts of higher competition under stabilized environmental conditions. This development is associated to the increasing nutrient content of the soil, which can be traced back to the growing population of breeding birds on the island [55].

Switching to the networks of information transfer, we gain insight into the inner functioning of the plant community. Strikingly, *Stellaria media* takes a central position in the network in 2000, 2002 and 2004 (see Supplementary F). Note that there is a net-inflow of information into *Stellaria*, indicating that the species is actively taking into account the other species' development (see Figure 21(c)). This might come as a surprise considering the fact that *Stellaria's* abundance is monotonously decreasing during this period. However, we have to keep in mind that the information structure of the system is computed on basis of the twelve preceding years. Indeed, Figure 20(b) shows a peak phase of *Stellaria* in the middle and late nineties. The active role of *Stellaria* during this period of upcoming change can be ecologically underpinned. Being a short-lived, annual plant of typically high growth rate and capable of producing seeds rapidly and abundantly [38], *Stellaria* can take the opportunity being opened by the transition from an early pioneering plant community towards establishing a grassland ecosystem. *Stellaria* can be considered as indicator of a transition in community composition. Note that 2004 is the first time in eight years of plant communities on the plot (data provided by the Icelandic Institute of Natural History) that plant cover falls below 100%.

H. peploides, which was a driver of community development in the early period of land capturing [34, 55], is taking a peripheral position in the information networks during these first years (see Supplementary F). Just like *Stellaria*, *Honckenya* shows a net-inflow of information, reflecting its active adaptation to the environment. With the environment opening

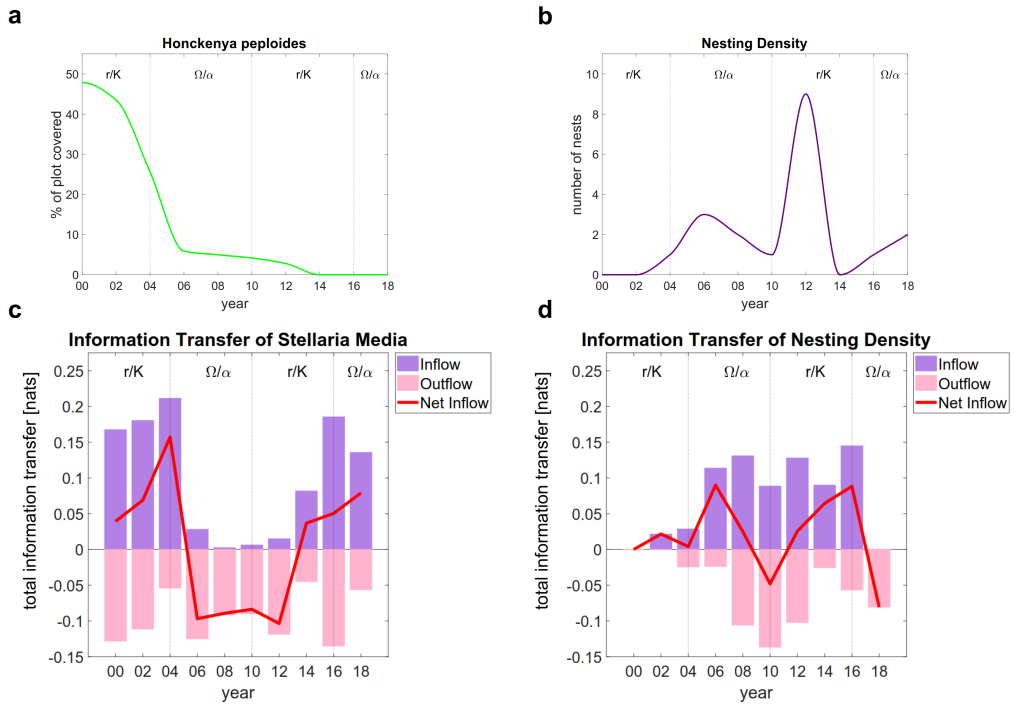

Figure 21: (a) Percentage of monitoring plot covered by *H. peploides*. (b) Number of nests in the monitoring plot. Recall that no data was collected before 2004. (c) Information transfer from and to *S. media* with the red line marking the net transfer. (d) Information transfer from and to nesting density with the red line marking the net transfer.

up for competition, *H. peploides's* lower competitiveness hereafter leads to a decrease in abundance.

Resilience during this first period clearly is low, since stability has been provided by associations of the pioneers *Honckenya* and *Leymus* during the early phase of community development. These connections are now dissolving with the decline of *Honckenya*. At the same time, warrantors of the period to come have not yet established themselves strongly enough. The system indeed is facing a new era to come.

The first breakdown – from pioneers to perennials. The years 2004 to 2008 mark a period of dramatic change on the island. *"During 1999 - 2005, colonization declined to 0–3 species per year indicating that it was leveling off. This was however followed by a sharp increase in 2006 and 2007 with 5 new species found on the island each year. In addition, a few species, which had been unsuccessful colonizers on the island in the past, have invaded the island again."* [55, p.62] A plausible trigger for this breakdown is the accumulated effect of the gulls having been breeding on this part of the island for several years. The birds

serve both as provider of nutrients (in particular nitrogen), as well as source of seeds [55]. Thereby, they change the environmental conditions for all components of the system. We can find clear signals on the role that nesting density played in the breakdown of the system and the resulting Ω/α phase.

There is a remarkable difference between the network in 2004 and the network in 2006 (see Supplementary F). Surprisingly, *H. peploides* gains the most central position in the system. For the first time, its information outflow dominates its inflow, indicating the transition from an active role to a passive one (recall the definition of information transfer). In the same year, the decrease in abundance of *Honckenya* slows down considerably (Figure 21(a)).

Meanwhile nesting density obtains a role as active player in 2006 (compare Figure 21(d)), reaching a central position in 2008 (see Supplementary F). Its information in- and outflow are comparably high in this year, indicating both an active adaptation to the plant species' development and, the other way round, a strong influence on these species' development. This phenomenon can be explained by the fact that, on the one hand, the birds are depending on the vegetation in building their nests and raising their chicks, and, on the other hand, the specialized and demanding species of the second succession wave rely on the nutrient input by the birds. Furthermore, the effect of bird damage has to be considered. In 2010, at the end of the α-phase, information outflow is dominating (see Figure 21(d)), capturing the strong influence of the breeding birds on the vegetation.

During 2006 and 2010, the plot is dominated by the higher competitive species *P. pratensis* and *L. arenarius*. Both plants together contribute almost all of surface cover during this period (see Figure 20(b)). Towards the end of the period, *Festuca rubra* is entering the scene. Just like *L. arenarius* and *P. pratensis*, it forms dense mats by extensive lateral spread above and below ground [55]. During this period, it takes a central and active position in the information networks (see Supplementary F). In 2010, the network stabilizes as being indicated by a rather balanced set of edges with more equally distributed flows of entropy. This indicates the end of the Ω/α phase and the start of a new period of growth.

On a system level, the accumulated nutrients and the newly established plant colonizers lead to an increase in potential in the α-phase between 2006 and 2008. The subsequent loss of potential is typical for a system's late α-phase. Resilience develops contrarily to potential: it classically increases during the breakdown between 2004 and 2006, decreases when potential is accumulated and continues increasing at the end of the α-phase.

The second cycle – a plan being failed The second r/K phase lasts from 2010 to 2016. Connectedness increases while resilience declines antagonistically, although with a delayed start. Surprisingly, potential does not follow the expected pattern. Despite a small increase at the beginning, the system constantly looses potential from 2012 onwards. We are thus faced with an atypical phase of exploitation and conservation.

Almost all species are decreasing in abundance between 2012 and 2014 with *Honckenya* and *Cerastium* becoming extinct at the plot. It is *S. media* only that can increase during this year, profiting from released nutrients through dead plant material and indicating the opening of unexpected opportunity. While at the first occurrence, *Stellaria*'s appearance marked a period of internal system change, this time lack of rain being an environmental factor is perturbing the system during its move of exploitation. Figure 22 shows the mean rainfall during the vegetation period as being measured at Stórhöfði weather station, 18km away from the island of Surtsey. In 2012, precipitation has been at a long term minimum of less than 50mm. Although the amount of precipitation was comparably low in 2007, the plants have, according to personal correspondence with Borgþor Magnússon from the Icelandic Institute of National History in October 2020, never shown such severe drought symptoms before. This might be, inter alia, due to the fact that the drought in 2012 is hitting the plant community at the onset of its exploitation phase. In addition, a peak in the population of birds in 2012 (see Figure 21(b)) presumably provides additional stress for the plants given the dry conditions during that summer. Thus, the system (temporarily) has to invest into managing extreme environmental conditions rather than building up potential for future growth.

While the system has been shaped under humid climatic conditions and moderate disturbance through birds, the plant community is suddenly confronted with completely unexpected conditions. The plan laid out during the late α-phase is doomed to fail. The community is exhibiting features of a system finding itself in conditions it has not been adapted to. Under these circumstances, the system is vulnerable, indicated by its extremely low resilience. Indeed, towards the end of the period, resilience reaches an estimated minimum in 2015. We note in passing that no data has been taken during odd numbered years. Thus, the exact point of change of the system cannot be determined within a year's precision.

Concerning the entropy networks, *Festuca rubra* and *L. arenarius* show an active and central role from 2012 onwards (see Supplementary F). Both species are capable of dealing with harsh conditions due to their extensive root system and might therefore suffer less from the dry summer. From 2014 on, *S. media's* inflow of information increases strongly, matching its preceding growth in abundance. However, it cannot take a central position in the network before 2016, the year of the second breakdown. The system seems to start into another Ω-phase, indicated by decreasing potential and connectedness and increasing resilience. The breakdown is clearly visible in a decentralization of the information network's topology (see Supplementary F).

Summing up, the systemic assessment of the plant community under the adaptive cycle's point of view coincides with the ecological assessment. There are two large breaks during the observation period, namely a restructuring of the community composition around 2006 and a drought hitting the system in 2012. The community restructuring is reflected by a systemic breakdown. Here, the corresponding information networks clearly indicate the

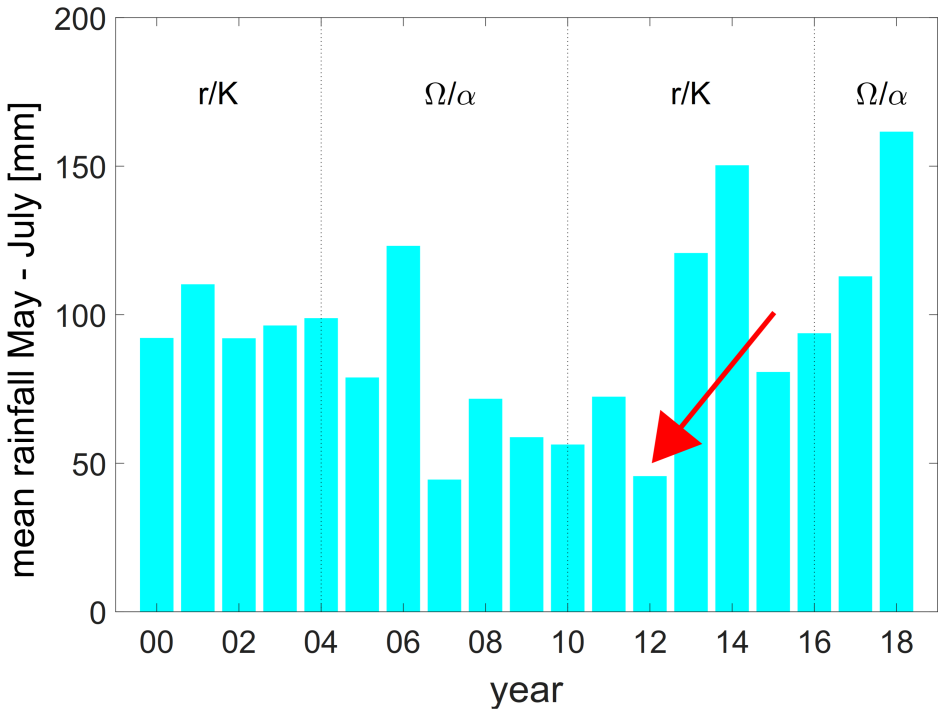

Figure 22: Mean rainfall measured at the weather station on Stórhöfði from May to July.

driving position of nesting density. The drought is reflected by a decrease in potential during the system's r/K-phase, hence, by a deviation from the expected behavior of the systemic variables. Moreover, the role of single species, like *S. media* as indicator of change, is emphasized.

5.2.2 A prairie-forest ecotone under human intervention

In the following case study, we will examine the development of a plant community in the prairie-forest ecotone of Eastern Kansas. This case study is except for smaller modifications an excerpt of [83]. The data underlying this case study was collected yearly in the course of a succession experiment in an experimental plot in Kansas from 2002 to 2015. We excluded those species which appeared at most once during the observation period, covering less or equal ten percent of the experimental plot. In this way, we took 39 out of 47 species into account, including grasses, forbs, shrubs, trees, and vines. Their relative abundances have been measured every June. In 2008, 2011 and 2014, intentional spring burns have been executed shortly before data collection. For details on the experiment and data collection, see [6, Exper. 1, Unit 13]. For a complete list of the plant species and their features used in the ecological interpretation see Suppl. Table 2.

For the estimation of the information networks, we used a window size of $w_t = 6$ and an interpolated window size of 18. History lengths and delay were set to 1. Only transfers passing a significance level of 0.05 were taken into account. The system's resilience was computed by means of symmetrically normalized Laplacian matrices, standardized with respect to the maximal edge weight M via $c = \frac{1}{M}$. The parameters used are summed up in Table 10. We computed the nodes' unscaled eigencentrality using the function `eigen_centrality` as being provided by the R package igraph.

system	plants community
components	plant species
number of components	39
type of abundance data	percentage of plot covered
length of time series	14
window size w_t	6
interpolated window size	18
history lengths k, l	1
delay u	1
significance level	0.05
normalization type	symmetric
standardization constant c	$\frac{1}{M}$

Table 10: Data and parameters of the Kansas case study.

In order to gain an overview of the system's dynamics, we start with a consideration of the three characteristic variables. Figure 23(a) and (c) shows that their development indicates a clear division into four phases. At the beginning, from 2007 –2008, we can identify a classical Ω-phase, with potential and connectedness strongly decreasing and resilience increasing. Supposedly, this breakdown results from the preceding spring burn, releasing resources and breaking connections. Within the next two years, the system is not able to considerably regain potential or connectedness. At the same time, resilience monotonously decreases. This changes abruptly with the spring burn in 2011, which naturally leads to a strong increase in resilience. Now the three variables are in a classical initial situation for another r/K phase: resilience is high, while potential and connectedness are low. The following climax phase leads to a peak in potential and connectedness in 2013. The subsequent breakdown in potential and connectedness coincides with the third intervention in 2014. Interestingly, resilience increases one year earlier, from 2013–2014, but not during the supposed breakdown. From 2014–2015, with potential and connectedness still decreasing, resilience still does not fully recover. We will come back to this atypical behavior of the systemic variables during the second breakdown.

Now that we have an overview of the system's dynamics, the networks of information

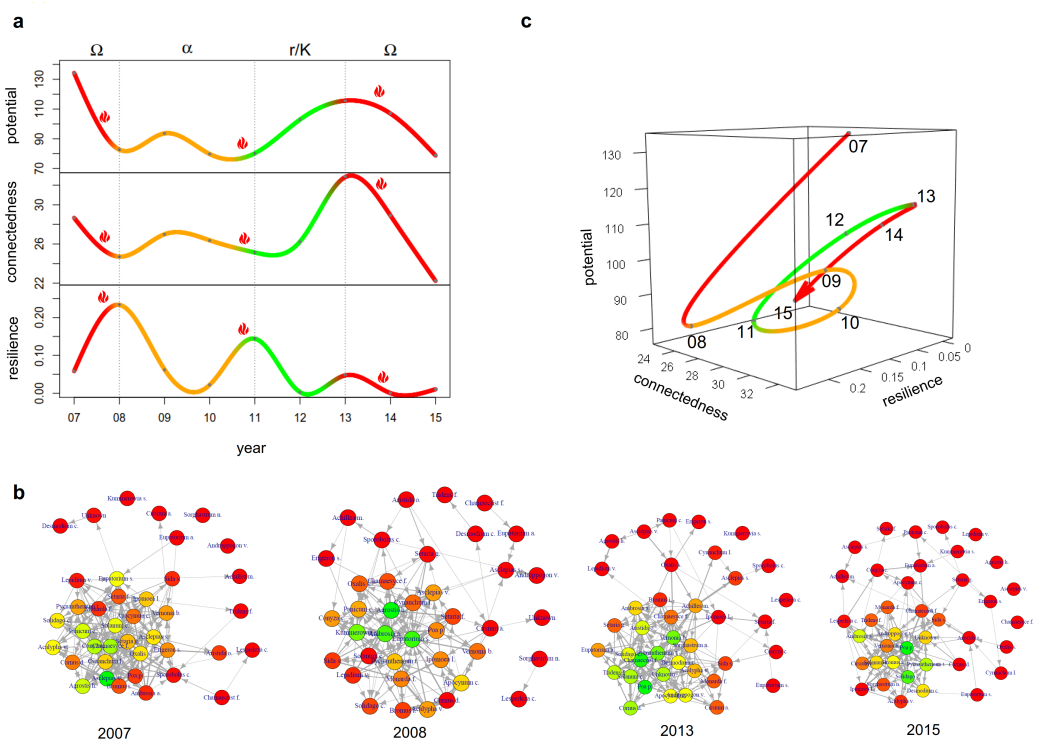

Figure 23: Information theoretical analysis of a prairie-forest plant community being exposed to human intervention. (a) Potential, connectedness and resilience of the system during the study period. For every year, the labels mark the month June, when data was collected. The flames indicate the times of the spring burns. (b) Networks of information transfer of the plants' community in 2007, 2008, 2013, and 2015. The nodes are colored according to their eigencentrality. Red marks low values of eigencentrality, orange eigencentrality of medium height, and green high values of eigencentrality. (c) Three-dimensional plot of potential, connectedness, and resilience of the system.

transfer will give us deeper insights into the mechanisms and structures driving this behavior (see Figure 23(b)). Considering the overall topology of the networks, a clear pattern in recognizable. At times of high connectedness (e.g. n 2007 and 2013), the network is characterized by a large number of nodes showing high eigencentrality. In contrast, at times of low connectedness (e.g. in 2008 and 2015), there are fewer nodes of high eigencentrality. At the same time the number of loosely connected nodes increases. Hence, there is a large central core of strongly connected nodes, which partly dissolves when the system collapses during its Ω-phases. Since the structure of the core appears to be closely related to the dynamics of the system, further information on the system's driving forces can be drawn from the core's composition. Partitioning the set of nodes according to their centrality over time, five groups of plants can be identified (see Figure 24). Group 4 is characterized by high centrality values at the beginning of the study period, only, whereas Group 2 shows the

opposite behavior. Group 1 and Group 3 exhibit comparably high eigencentrality all over the study period, with the former being lower at the beginning and the latter towards the end. Finally, Group 5 comprises species which are of small centrality all the time.

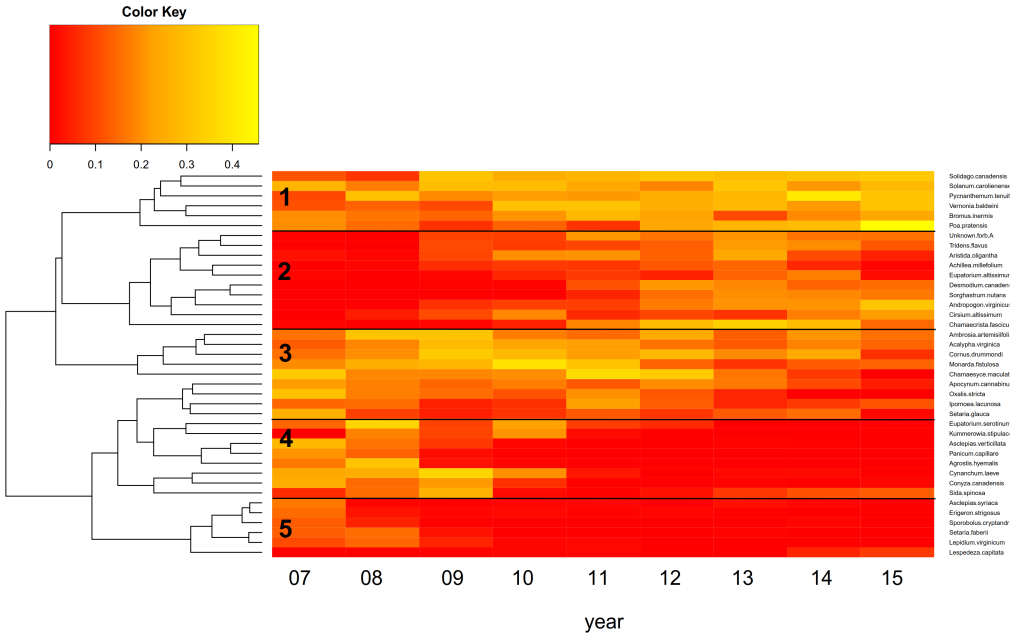

Figure 24: Heatmap showing the eigencentrality of the species in the networks of information transfer from 2007 to 2015. The species are divided into five groups according to the pattern of their eigencentrality development.

Taking a closer look at the ecological features of the plants in either group (see Suppl. Table 2), this pattern can be explained. The first two groups contain considerably more perennial and fire tolerant species than the other groups. Hence, these species should be expected to gain importance throughout the sequence of fire interventions. This is indeed the case since both groups' eigencentrality increases toward the end of the study period. Furthermore, the species in the first and third group tend to have higher growth rate and higher vegetative spread rate. These features should favor a long-term central role under repeated interventions. This coincides with the permanently high eigencentrality of these groups. Comparing both properties with respect to the groups' eigencentrality, being perennial and fire tolerant (Group 2) seems to be beneficial over time, while higher reproduction capabilities (Group 3) cannot cope with repeated fire intervention on a longer term. Note that these findings are not immediately visible in raw abundance data.

Finally, let us return to the atypical breakdown in 2013. It is the only time that resilience increases without the spring burn as external trigger and during the subsequent breakdown of potential and connectedness, it still remains low compared to the preceding years. This phenomenon seems to have natural reasons. Regional climate data shows that total precipitation has been extraordinary low in 2012. In the first half of 2013, the situation seems to relax slightly. But in June, when data was collected, total precipitation again dropped significantly below normal (Figure 25). Thus, the plants have been exposed to an unusual high drought stress during the system's r/K-phase. On top of that, the central core during this phase mainly consists of species of comparably low drought tolerance. The breakdown starting in 2013 with the increase in resilience is thus likely to be caused by increased vulnerability of the plants. Just like in the Surtsey case study, the system finds itself in a situation it has not been adapted to during its α- and early r-phase. The twofold perturbation eventually results in the atypical situation of low potential, connectedness, and resilience in 2015. This last observation nicely shows the difficulty in analyzing ecosystems under experimental intervention scenarios. Effects due to the planned disturbance always also interact with systemic effects under natural conditions. Nevertheless, our approach allows to dissect the two types of perturbation.

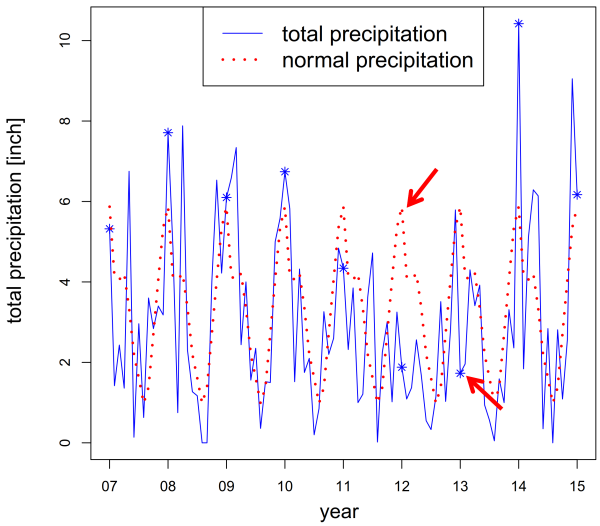

Figure 25: Precipitation in Lawrence, Kansas. The plot shows the total precipitation in Lawrence, where the experimental plot is located. In comparison, the normal precipitation for this area is shown [8]. The stars label the month June of the respective year.

So far, we could detect adaptive behavior in various complex systems, supporting the general idea of the adaptive cycle metaphor. Taking a step back, the question for the

mechanisms and drivers behind this pattern naturally arises. We will address this question in the following section.

6 Drivers of the Adaptive Cycle

The results of this section are part of [68]. The adaptive cycle metaphor describes complex systems' development as alternating phases of change and stability, leading to an antagonistic cyclic behavior of connectedness and resilience. While stressing its metaphorical character, our analyses of various real-world systems generally confirm this description. The information networks underlying the systemic variables usually show a typical "contract and spread" pattern. The contraction periods are reflected in increasing connectedness, interrupted by temporary small decreases only, capturing local spreading events. Eventually, the contraction period is terminated by a global spreading event, leading to a sudden and strong decrease in connectedness. This pattern reiterates constantly. In contrast to connectedness, resilience slowly decreases during the contraction period and strongly increases during a global spreading event. In real-world complex systems, various different internal and external processes shape a system's specific dynamics of change. However, we hypothesize that the observed pattern can result from the interplay of only two (antagonistic) processes, which are an inherent part of general complex systems' dynamics:

- A (cascading) adaptation process, driven by optimization goals, manifesting in increasing connectedness and decreasing resilience (compare Ulanowicz' ascendancy theory [74]).
- Random perturbations of the same type, provoking breakdowns of connectedness and increases of resilience.

In particular we do not think that the extent of a system's breakdown is necessarily related to the strength of the trigger. The crucial factor is the state of the system in the moment of the trigger. This idea has formed the basis of earlier models, see for example Per Bak's work on self-organizing criticality [11].

In this section, we will support our hypothesis by means of an agent-based model solely based on the just described processes of adaptation and perturbation. More precisely, we model the development of a complex system's information network, with the nodes being the model's agents. There are two aspects which distinguish our model from most of the existing ones:

- We do not make any assumptions about the specific optimization goal(s) of the system. We only model the *result* of such an optimization process, reflected in a concentration of the information structure and thereby in an increase of connectedness.
- We model *dynamically changing* networks of information transfer.

Observe that this model and the one defined in Section 4.2 clearly differ in the first aspect. The latter is build on the assumption that agents tend to increase their capital through

positive interactions, thereby explaining the increase of connectedness. Some notes on the second aspect: there are various network-based models examining information-theoretic dynamics in relation to network topology (see e.g. [46, 47, 50, 59]). In order to generate dynamic behavior, they for example assign Boolean functions to the nodes [50] or consider particle swarm optimization on the networks [46]. Hence, the values assigned to the nodes change throughout a simulation while network topology remains fixed.

In Section 6.1, we will describe our model in detail. Simulations of the model support our hypothesis that the interplay of adaptation and perturbation processes lead to the pattern of change described in the adaptive cycle metaphor (Section 6.2). Section 6.3 underpins the hypothesis mathematically. In this course, we define the event of a *phase change*, denoting a profound reorganization of the simulated information network, and show that the interplay of the two processes almost surely leads to a phase change. Furthermore, we examine the expected frequency of phase changes in the system under the influence of the different parameters of the model.

6.1 Description of the model

The model produces a sequence of networks consisting of N nodes $\{x_1, \ldots, x_N\}$ and directed, weighted edges between them. The edges represent the information being transferred among the agents. We say that an edge *exists* if its weight is non-zero. In the following, a *random* selection means a selection according to the uniform distribution. A positive integer *maximal weight* W, a sensitivity threshold θ ($0 \leq \theta \leq 1$), and a perturbation probability q ($0 \leq q \leq 1$) are selected. In the initial graph, every edge exists with probability p and, if existent, is assigned a random, positive, integer weight between 1 and W. We denote the weight of the edge e_{ij} from node i to node j by w_{ij}. There are no self-loops. We assign the *eigenvector centrality* to every node x_i, computed as

$$C(x_i) = \sum_{j \neq i} w_{ij} \cdot d_{in}(x_j),\ 1 \leq i \leq N.$$

For a node x_i, we call the set of nodes $\{x_j | w_{ij} \neq 0\}$ its *out-neighbors* and the set $\{x_j | w_{ji} \neq 0\}$ its *in-neighbors*. We call the transition from network at time point i to the network at time point $i+1$ the ith *step*. Every step consists of an adaptation phase (initial adaptation try and possible triggered adaptation cascade) and a perturbation phase.

- For the initial adaptation try, a node x_i is randomly chosen, where the probability P to choose x_i is indirectly proportional to its eigenvector centrality, i.e.

$$P = \begin{cases} \frac{1}{C(x_i) \cdot \sum_{j=1}^{N} C(x_j)^{-1}} & \text{if } C(x_i) \neq 0 \\ 0 & \text{otherwise.} \end{cases}$$

Note that in modeling complex systems' evolution, it is common practice to choose the in some sense "weakest" agent for mutation (see e.g. [12]), which is reflected in the selection process above. An out-neighbor x_j of this node and a node $x_k \neq x_i$ (not necessarily an out-neighbor of x_i) are selected randomly. If $x_j = x_k$, nothing happens. If $x_j \neq x_k$, the in-degrees of these two nodes are compared. If $d_{in}(x_k) \leq d_{in}(x_j)$, nothing happens. If $d_{in}(x_k) > d_{in}(x_j)$, the edge e_{ij} is deleted and its total weight w_{ij} is added to the edge w_{ik}. Well call this shift *adaptation*. This accounts for the goal of an adaptation being the increase the adapting node's eigencentrality. When an adaptation has taken place, x_i is called *adapted node* and an adaptation cascade is started.

- The adaptation cascade always follows the same principle: whenever an in-neighbor of an adapted node is connected "closely enough" with the adapted node, it tries an adaptation itself. To be precise, let x_l be an in-neighbor of a just-adapted node x_i. If

$$\frac{w_{li}}{d_{out}(x_l)} \geq \theta,$$

x_l carries out an adaptation try. The in-neighbors of adapted nodes carry out their adaptation tries in random order and the cascade continues until it "dries out" by itself. The idea behind this mechanism is that agents of a system have a certain sensitivity toward changes in their environment, which in this case is constituted by their neighboring nodes. If an agent's environment changes, a new strategy might be more profitable, leading to adaptation moves of the agent itself. The sensitivity of the agents will be one of the parameters of our model. Note that for very small θ, it can be reasonable to set an upper limit for the number of adaptations to prevent extremely long or infinite adaptation cascades.

- With probability q, a perturbation is executed after the adaptation phase. In the perturbation phase, an edge is chosen randomly. The edge is deleted, i.e. its weight is set to 0. Its previous weight w is distributed by randomly assigning w independent weight units among all edges (existing and not yet existing) which leave the starting node of the deleted edge. In particular, edge weights are always integers. The idea behind this mechanism is the fact that in real-world systems, existing pathways of interaction or communication can suddenly become unusable due to environmental or internal changes. We say that a node is *perturbed* when one of its outgoing edges is perturbed.

The two phases of adaptation and perturbation can be understood as antagonistic. While the phase of adaptation will in general increase order and coherence, perturbation will increase chaos and randomness. Note that, with a growing number of agents, scaling might become necessary to balance the two processes and to make effects visible. There are various

ways of scaling the processes. For example, one can apply the initial adaptation try to a suitable fraction of nodes instead of to a single node only. Besides, the perturbation can affect several edges instead of only one edge. Observe that for fixed N, W, p, q, and θ, our model defines a Markov process on

$$\{0, \ldots, (N-1) \cdot W\}^{N \times N}.$$

6.2 Simulation of the model

We will now present simulation results demonstrating that our model indeed generates the desired network dynamics. For all of the following plots, the system consists of seven agents. The initial probability for every edge to exist is $p = 0.8$ and the maximum weight is $W = 6$. If a perturbation takes place, seven random edges are perturbed in random order. The maximal number of adaptations in an adaptation avalanche is set to 35. The plots start at step 10 in order to exclude initial noise.

First of all, the simulation produces - in a large range of parameters - the typical "slowly contract and quickly spread" pattern of the network's topology and the consequent antagonistic behavior of its systemic variables. See Figure 26 for an exemplary development. Here, the sensitivity threshold is $\theta = 0.3$ and the perturbation probability $q = 0.1$. We can see an overall increase in connectedness until time step 59. This increase is suddenly interrupted by a strong decrease, followed by another slow increase. Resilience behaves contrarily. It shows an overall decrease until time step 59 and strongly increases during the system's breakdown. During the whole simulation, decreases in connectedness are accompanied by increases in resilience. At times of high connectedness, the underlying network does typically have fewer, comparably thick edges, while networks at times of low connectedness do resemble complete networks. Networks 59 and 61 represent these two types of topology. In terms of the adaptive cycle metaphor, we would call the period from time step 10 to 59 r/K-phase. It ends with the sudden entry into an Ω/α-phase, eventually leading into another r-phase.

Figure 27 shows the influence of an increasing number of perturbations on this pattern. For better comparability, we fixed the times of perturbations at every 100th, 50th, 20th, and second time step. It becomes clear that in the case of rare perturbations, their average effect on connectedness is larger than in the case of frequent perturbations. In Figure 27(a), every perturbation leads to a typical system breakdown, while in Figures 27(b) and (c), only some of the perturbations result in a strong decline of connectedness. In Figure 27(d), with perturbations happening at every second step, the typical "slowly contract and quickly spread" pattern has turned into an irregular "contract and spread" pattern.

Beyond our hypothesis, we made two interesting observations. The first concerns the effects of perturbations of systems' connectedness. Perturbations hitting the system in times of low connectedness can lead to a strong *increase* in connectedness. Figure 28 illustrates

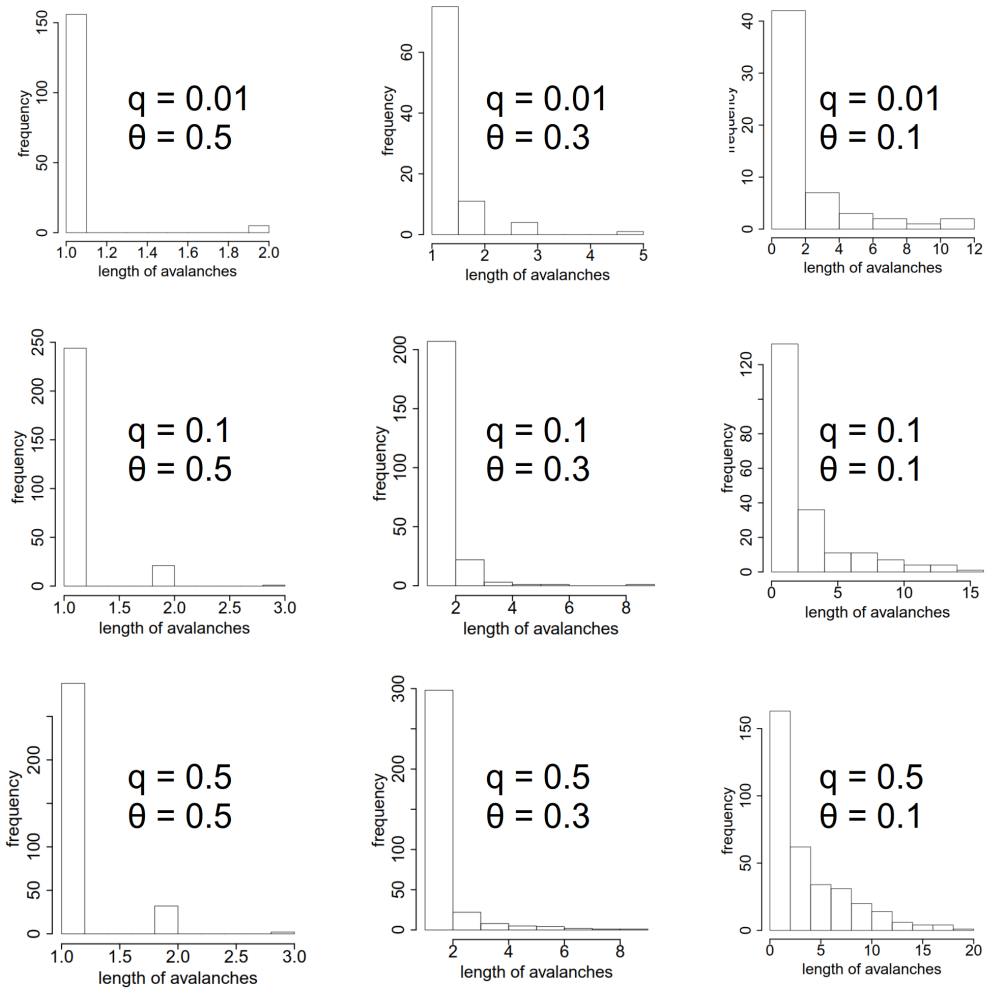

Figure 26: Resilience and connectedness of a 100-step simulation with $\theta = 0.3$, $q = 0.1$. The vertical red lines denote the times of the perturbations. The underlying information network right before (59) and shortly after (61) a classical system breakdown is shown.

this phenomenon. The perturbations at time steps 37, 69, and 74 provoke classical breakdowns of the system, reflected in strong declines in connectedness and contemporaneous increases in resilience. In contrast, the perturbations at time steps 42 and 77 cause increases in connectedness. It is comprehensible that during times of low connectedness, when the number of edges is high and the average edge weight low, random rearrangements can lead to a contraction of the network. From time step 77 to 78, this contraction and the consequent decline in resilience and increase in connectedness is clearly visible in the corresponding networks. From time step 42 to 43, both connectedness and resilience increase.

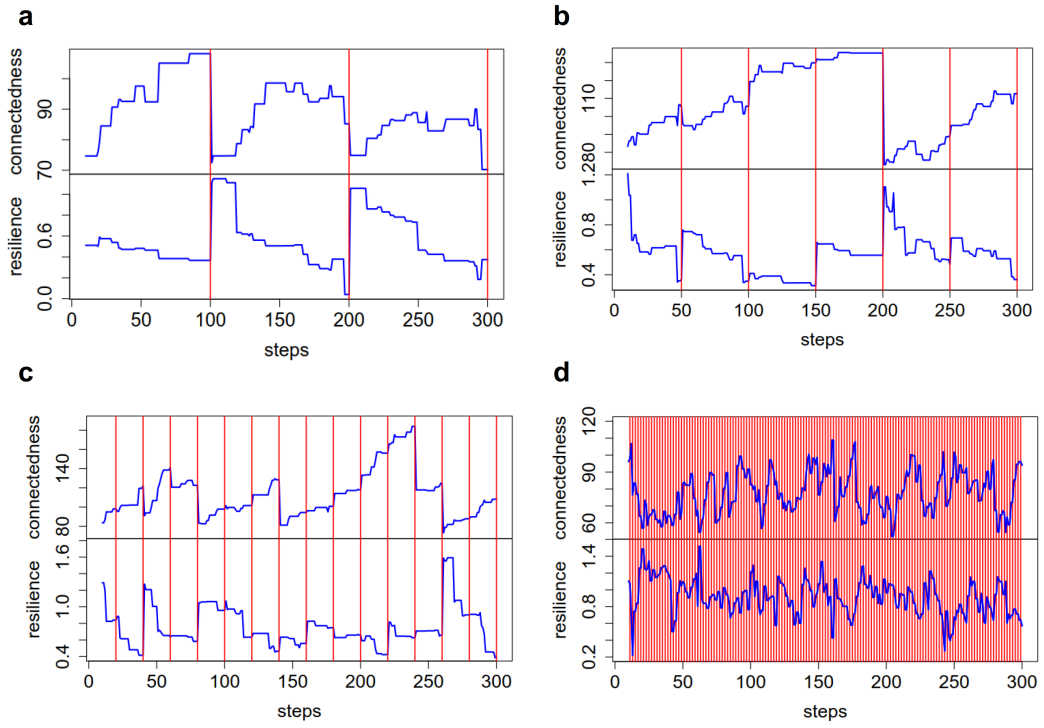

Figure 27: Resilience and connectedness of 300-step simulations with $\theta = 0.3$ and an increasing number of equidistant perturbations, marked by vertical red lines. (a) Perturbation at every 100th step. (b) Perturbation at every 50th step. (c) Perturbation at every 20th step. (d) Perturbation at every second step.

Our second observation concerns the adaptation cascades. We see a power-law behavior of the length (number of mutated edges) and frequency of adaptation cascades (see Figure 29). This phenomenon is called *criticality* and has been detected in many real-world and simulated systems (see for example Bak's sand-pile model [13], Bak and Sneppen's model for Darwinian evolution [71], or Kauffman's NKC model [47]). With decreasing sensitivity threshold θ, the average length of cascades increases, better revealing the power-law in the distribution of lengths.

The results confirm our hypothesis that the interplay of optimization processes and perturbations of the same type can lead to the cyclic behavior of network topology and systemic variables as described in the adaptive cycle metaphor. The frequency, amplitude, and regularity of these cycles is depending on various parameters, among them the perturbation probability q and the sensitivity threshold θ. According to the distribution of the adaptation cascades' lengths, the model generates systems in the state of criticality. We will now approach the model's characteristics mathematically.

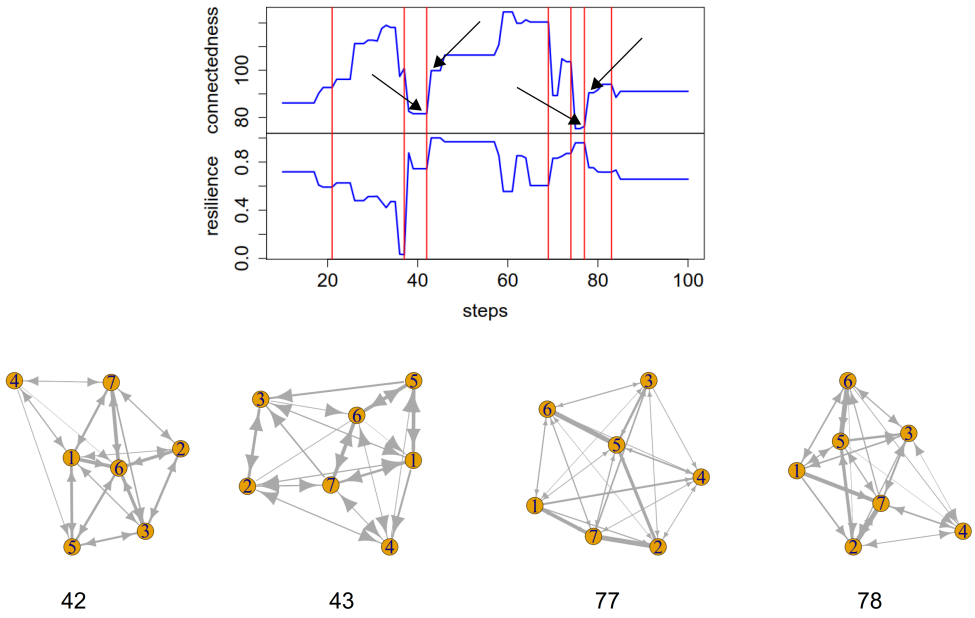

Figure 28: Resilience and connectedness of a 100-step simulation with $\theta = 0.3$, $q = 0.1$. Every perturbation is marked by a vertical red line. The underlying information network before and after perturbations provoking an increase in connectedness is shown.

6.3 Mathematical exploration of the model

The simulation results show that our model indeed generates the network dynamics described in the adaptive cycle metaphor. In this section, we want to underpin this observation mathematically. To this end, we introduce the notion of a *phase change*. In the context of complex systems, a phase change or transition typically includes a sudden change of the system's behavioral identity, i.e. of its defining structures and processes (see e.g. [72]). In the language of the adaptive cycle metaphor, the sudden onset of the Ω-phase, showing in profound structural changes, can be understood as a phase change of the underlying system. Such a phenomenon occurs in our model as well, mainly if a perturbation hits a highly contracted, rigid system, leading to wide-ranging rearrangements and a sudden decrease in connectedness.

Let e be the number of edges being perturbed in the perturbation step of our model. We denote by a phase change the situation of a perturbation hitting a predefined number $c \leq \min(N, e)$ of edges each of which being the only positively-weighted outgoing edge of a node. Of course a phase change is only possible if at least c nodes are assigned non-zero outgoing

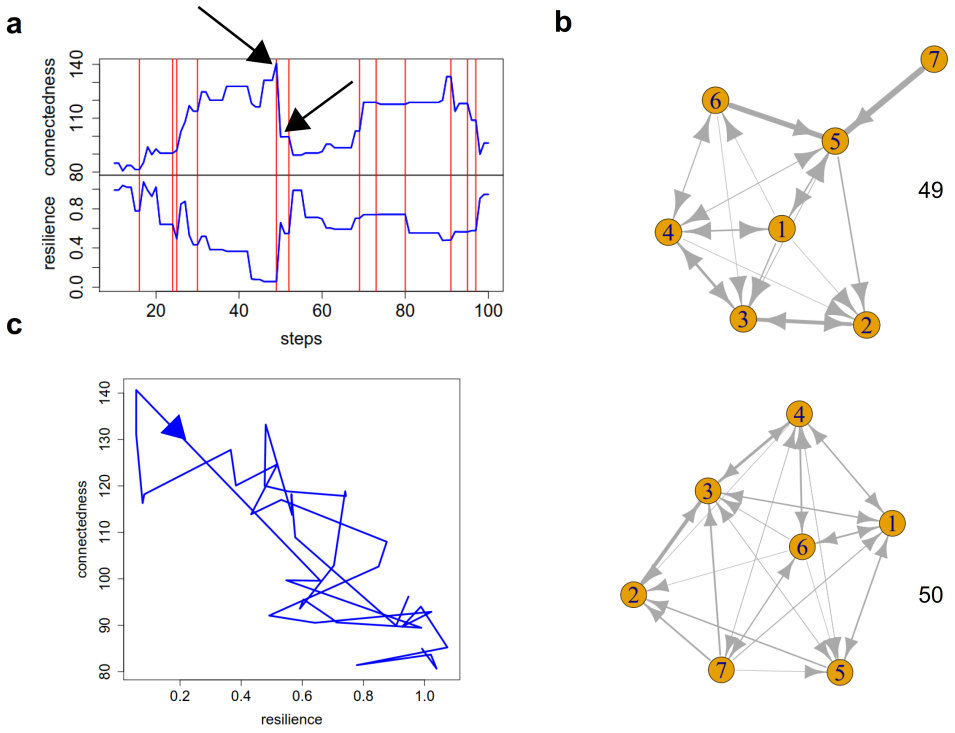

Figure 29: Connectedness and histograms of cascade lengths for 1000-step simulations with $q = 0.1$. (a) $\theta = 0.5$. (b) $\theta = 0.3$. (c) $\theta = 0.1$.

edges in the initial graph. If this is the case, we say that the initial graph *allows* a phase change.

Theorem 2. *If in an infinite realization of the Markov process defined in Section 6.1, $q > 0$ and the initial graph allows a phase change, it happens with probability 1.*

Proof. For fixed N, W, p, q, and θ, our model defines a stationary Markov process on a finite state space of adjacency matrices

$$D = \{0, \ldots, (N-1) \cdot W\}^{N \times N}.$$

Consider an infinite realization $(K_n)_{n \in \mathbb{N}}$ of the process. Recall that the sum over all entries in a row of a matrix K_n represents the total outgoing weight of the respective node, which stays constant throughout the process. Let $r = (r_1, \ldots, r_N)$ be the vector of these row sums. Let $D_r \subset D$ be the set of all adjacency matrices with row sums $(r_1, \ldots, r_N)$. It follows directly from the definitions that finitely repeated perturbation can transfer any state of D_r into any other state of D_r. Since there is a chance of the adaptation step leaving the system unaffected, the Markov process defined by the model is irreducible when being restricted to D_r. In the following, we work with this irreducible Markov process.

If K_n has at most one nonzero entry in each row we say the system is *maximally contracted* at time n. In this case, since a phase change is possible by assumption, there is a positive probability ϵ_1 of a phase change occurring in step n.

Due to the irreducibility and the finite state space of the Markov process, we know that there is a number of steps s such that, irrespective of the current state of the system, the probability of the system reaching a maximally contracted state within the next s steps is bounded from below by some uniform $\epsilon_2 > 0$. We divide the sequence $(K_n)_{n\in\mathbb{N}}$ into successive non-overlapping sub-strings S_i of length $s+1$. By the previous considerations, the probability of the system reaching a maximally contracted state during the first s steps of S_i and going through a phase change in the subsequent step is bounded from below by $\epsilon := \epsilon_1 \cdot \epsilon_2$, independent of the state of the system at the beginning of S_i.

Let A_i denote the event that no phase change happens during S_i, i.e. at none of the time steps $(i-1)\cdot(s+1)+1, \ldots, i\cdot(s+1)$. Then it follows that

$$P\left(A_i \,\middle|\, \bigcap_{j\leq i-1} A_j\right) \leq 1-\epsilon$$

since the condition of $\bigcap_{j\leq i-1} A_j$ only concerns the state of the system prior to S_i. As a consequence, we obtain

$$\begin{aligned} P\left(\bigcap_{j\leq i} A_j\right) &= P\left(A_i \,\middle|\, \bigcap_{j\leq i-1} A_j\right) \cdot P\left(\bigcap_{j\leq i-1} A_j\right) \\ &= \prod_{k=2}^{i} P\left(A_k \,\middle|\, \bigcap_{j\leq k-1} A_j\right) \cdot P(A_1) \\ &\leq (1-\epsilon)^i \underset{i\to\infty}{\to} 0, \end{aligned}$$

which proves the theorem. □

Hence, we have learned that the interplay of adaptation and perturbation indeed almost surely leads to phase changes and thereby to the "contract and spread" pattern described in the adaptive cycle metaphor. However, the theorem gives an existence statement, only. We want to gain insight into how the parameters q and θ affect the frequency of phase changes. To this end, we restrict ourselves to a simplified version of our model, which however still shares its defining characteristics with the original model. The simplified model is identical to the original model except for the following changes.

- There is no cascade effect.
- The adapting node is chosen randomly and not according to its eigenvector centrality.

- An adaptation is carried out *in any case*, independently of the eigenvector centrality of the edge's old and new destination.

In the simplified model, the development of one node's distribution of weight on its outgoing edges is independent of the weight distribution on all other edges. Thus, the development of a single node's weight distribution defines a Markov process. The global behavior of the simplified model is described by these local Markov processes. So in the following, we fix a node and examine the Markov process on the state space of the node's weight distributions. Let $n \coloneqq N - 1$ be the number of possible out-neighbors of the node and $h > 0$ the total weight on its outgoing edges. Then

$$D \coloneqq \left\{ (w_1, \ldots, w_n) \;\middle|\; \sum_{i=1}^{n} w_i = h,\ w_i \in \mathbb{N}_0 \right\}$$

is defined as state space of the Markov process, i.e. all possible integer partitions of the total weight h on the possible n edges.
We assume that one edge is perturbed during perturbation. We define a phase change as the situation in which all outgoing weight of the node is accumulated on a single edge and the edge is perturbed in the perturbation step. Analogous argumentation as in the proof of Theorem 2 yields that in infinite realizations of the Markov process, phase changes happen with probability 1 if the initial graphs allows it.
Fix an order of the elements of D. Let $S,\ M \in \mathbb{R}^{D \times D}$ denote transition probability matrices describing perturbation and adaptation, respectively. Then, D together with the transition probability matrix $S \cdot M$ defines a stationary Markov process. For every two states $d_1, d_2 \in D$, d_2 can arise from d_1 through finitely many perturbation steps. Since there is a chance of the adaptation step not having any effect on the system, it follows that the Markov process is irreducible. In the following, we will determine S and M, consider them as transition matrices of separate Markov processes, and examine their limit distributions.

The perturbation step

For two states $v, w \in D$, we compute the probability that $v = (v_1, \ldots, v_n)$ transitions into $w = (w_1, \ldots, w_n)$ via a perturbation. For $j \in \{1, \ldots, N\}$, consider the jth unit vector e_j. Let $\circ$ denote the Hadamard product, i.e. the component-wise multiplication of two vectors. Set

$$V_j \coloneqq (w - (v - v \circ e_j)). \tag{14}$$

This vector specifies how, in case of a perturbation of edge j, the weight of j has to be distributed among the other positions such that v transitions into w. If any entry of V_j is negative, then a transition from v to w via perturbation of edge j is not possible. Let $V_j(i)$

denote the ith entry of V_j. Clearly, the total weight of vector V_j is the weight of edge j. Let

$$b_j := \sum_{i=1}^{n} V_j(i)$$

denote the weight of edge j. The probability that V_j is the result of distributing b_j weight units randomly on n edges of weight zero is

$$P^S_{V_j} = \left(\frac{1}{n}\right)^{b_j} \cdot \prod_{l=1}^{n-1} \binom{b_j - \sum_{s=1}^{l-1} V_j(s)}{V_j(l)},$$

under the convention that $\binom{a}{b} = 0$ for $b < 0$. To see this, note that there are b_j distinguishable weight units, which get distributed to n possible edges, making for a total of n^{b_j} outcomes. We are interested in those results where $V_j(i)$ units get assigned to the ith edge. In this case, in particular, a subset of $V_j(1)$ many of the weight units is assigned to the first edge and there are $\binom{b_j}{V_j(1)}$ possibilities to choose this subset. Now for each of these possibilities, there are $\binom{b_j - V_j(1)}{V_j(2)}$ many possibilities of which of the remaining $b_j - V_j(1)$ weight units are the ones which get assigned to the second edge. Continuing this process inductively, we obtain the product formula above.
Taking into account that the perturbing edge is chosen randomly among all possible outgoing edges of the node, the probability of a transition from v to w via a perturbation is

$$\begin{aligned} P^S(v \to w) &= \frac{1}{n} \cdot \sum_{j=1}^{n} P^S_{V_j} \\ &= \frac{1}{n} \cdot \sum_{j=1}^{n} \left(\frac{1}{n}\right)^{b_j} \cdot \prod_{l=1}^{n-1} \binom{b_j - \sum_{s=1}^{l-1} V_j(s)}{V_j(l)}. \end{aligned}$$

Just like in the original model, a perturbation is taking place with probability q and if it takes place, the perturbing node is chosen randomly. Hence, the *perturbation matrix* S is defined as

$$S(w,v) = \begin{cases} q \cdot \frac{1}{n+1} \cdot P^S(v \to w) & w \neq v \\ (1-q) + q \cdot \left(\frac{n}{n+1} + \frac{1}{n+1} \cdot P^S(v \to w)\right) & w = v. \end{cases}$$

The perturbation matrix S and the state space D define an irreducible Markov process. Numerical computations indicate that, independently of N and k, the limit distribution of this process is the uniform distribution.

Remark 4. *Considering the possible numbers of non-zero outgoing edges, what does the limit distribution look like? Intuitively, one would say that, if the total outgoing weight h is*

high enough, having x $(0 \leq x \leq n-1)$ outgoing edges of weight zero should be less likely than having $x+1$ outgoing edges of weight zero. The following computation confirms the assumption and yields the required value of h. We have

$$\begin{aligned} |D_x| &= |\{v = (v_1, \ldots, v_n) \in D \,|\{i|v_i = 0\}| = x\}| \\ &= \binom{h-1}{n-1-x} \cdot \binom{n}{x} \end{aligned}$$

To see this, note that for an element of D_x, there are $\binom{n}{x}$ possibilities of which x edges are the ones with zero weight. Then, since at least one weight unit has to be assigned to each of the remaining $n-x$ edges, there are $h-(n-x)$ weight units left to be distributed among $n-x$ edges, for which there are again $\binom{h-1}{n-1-x}$ possibilities. Hence, for $0 \leq x \leq n-2$, we get

$$\begin{aligned} & |D_x| - |D_{x+1}| > 0 \\ \Leftrightarrow & \binom{h-1}{n-1-x} \cdot \binom{n}{x} - \binom{h-1}{n-2-x} \cdot \binom{n}{x+1} > 0 \\ \Leftrightarrow & h > \frac{n^2 - n \cdot x - x - 1}{x+1}. \end{aligned}$$

The term on the right hand side reaches its maximum at $x = 0$, yielding

$$h > n^2 - 1.$$

Hence, under this condition, the most likely number of edges with positive weight is n. This underpins the intuition that the perturbation process is antagonistic to the adaptation process, which we will show to converge to a maximally contracted state.

The adaptation step

Let us now define a second Markov process on D with the transition probabilities describing the adaptation of the simplified model. To this end, consider again two states v, $w \in D$, and the corresponding vector V_j (as defined in Equation (14)). If V_j contains more than one non-zero entry, a transition from v to w by adapting edge j is not possible. If V_j contains exactly one non-zero entry, v transitions to w with a probability of $\frac{1}{n}$ when adapting edge j. Formally, the probability that v transitions into w when edge j is adapted is

$$P^M_{V_j} = \begin{cases} \frac{1}{n}, & |\{i|V_j(i) \neq 0\}| = 1, \\ 0, & \text{else.} \end{cases}$$

Set $g = |\{i|v_i \neq 0\}|$. Taking into account that the adapting edge is chosen randomly

among all outgoing edges of the node, the probability of a transition from v to w via an adaptation is

$$P^M(v \to w) = \frac{1}{g} \cdot \sum_{j|v_j \neq 0} P^M_{V_j}.$$

In the simplified model, the adapting node is chosen randomly. Hence, the *adaptation matrix* is defined as

$$M(w,v) = \begin{cases} \frac{1}{n+1} \cdot P^M(v \to w), & w \neq v, \\ \frac{n}{n+1} + \frac{1}{n+1} \cdot P^M(v \to w), & w = v. \end{cases}$$

The adaptation matrix M together with state space D defines a reducible Markov process. Reducibility is due to the fact that the number of positively-weighted outgoing edges cannot increase throughout the process. In the following, we will show that this Markov process always converges. Consider an event $d = (w_1, \ldots, w_n)$. Assume that

$$|\{i|w_i > 0\}| = j \geq 2.$$

The probability that j reduces to $j-1$ in an adaptation step is $\frac{1}{n+1} \cdot \frac{j-1}{n} > \epsilon$. Hence, the probability that the node has only one positively-weighted edge left after t simulation steps is greater or equal

$$1 - \sum_{x=0}^{j-2} \epsilon^x \cdot (1-\epsilon)^{t-x} \cdot \binom{t}{x}. \tag{15}$$

In the above expression, increasing t by 1 leads to each summand being multiplied by the factor $(1-\epsilon)\frac{t+1}{t+1-x}$. Since x is fixed for each summand, this factor converges to $1-\epsilon$ for large t. Consequently, expression 15 converges to 1 if t goes to infinity.

We will now turn to the influence of different parameters on the expected frequency of phase changes. A phase change is usually a result of a perturbation after a long adaptation without effective perturbation. Thus a value of interest is the expected number of unperturbed adaptations after which all weight of the node is assembled on a single edge. This of course depends on the number of edges of nonzero weight in the initial network. We denote by t_i the expected time, i.e. the number of adaptation steps, until all weight is accumulated on a single edge, starting with positive weight on exactly i outgoing edges for $1 \leq i \leq N-1$. Obviously, $t_1 = 0$. The other values can be determined via the recursive formula

$$t_i = 1 + \left(1 - \frac{N-2}{N \cdot (N-1)}\right) \cdot t_i + \frac{N-2}{N \cdot (N-1)} \cdot t_{i-1}, \; 2 \leq i \leq N-1. \tag{16}$$

In particular, we deduce that

$$k \coloneqq t_{N-1} = \sum_{i=2}^{N-1} \frac{N \cdot (N-1)}{N-i} \tag{17}$$

gives an upper bound for the expected number of adaptation steps, independent of the initial network. For $t \geq 0$, we call a series of t unperturbed steps followed by one perturbation of the node a *perturbation break of length t+1*. Following the observation above, intuitively, there is a strong correlation between the frequency of perturbation breaks of a certain lengths and the frequency of phase changes. Note, however, that the occurrence of a phase change is not necessarily the result of a perturbation break of a certain length. This is due to the possibility that a perturbation does not cause a large spreading of edge weights.

In the above light, the question ensues after how many steps in the model the first perturbation break of length $k+1$ can be expected. We denote by s_* the expected time, i.e. the number of steps, starting at the initial situation $*$ as specified below, until a perturbation break of length k has happened. Possible initial situations for $1 \leq i \leq k$ are

1	the last step was a perturbed step following less than k unperturbed steps
$0, i$	the last step was the ith unperturbed step in a row after a perturbed step
$k, 1$	the last step was a perturbed step following k unperturbed steps

We are interested in $l \coloneqq s_1$. Clearly, $s_{k,1} = 0$. Denote by $q' = \frac{q}{N}$ the probability that the node is perturbed. The s_* are connected via the following recursive formulas for $1 \leq i \leq k-1$.

$$\begin{aligned} s_1 &= 1 + q' \cdot s_1 + (1-q') \cdot s_{0,1} \\ s_{0,i} &= 1 + q' \cdot s_1 + (1-q') \cdot s_{0,i+1} \\ s_{0,k} &= 1 + q' \cdot s_{k,1} + (1-q) \cdot s_{0,k} \end{aligned}$$

A short computation shows that

$$l \coloneqq s_1 = \frac{1}{(1-q')^k \cdot q'}. \tag{18}$$

Example 2. *In a network of* 5 *nodes, we have* $k = 37$ *with* k *defined as above. For a perturbation probability of* $q = 0.01$*, the expectation value of the number of steps after which a perturbation break of length* $k+1$ *has taken place, is bounded from above by* $l = 539$ *steps. For* $q = 0.1$*,* l *decreases to* 106 *steps, for* $q = 0.75$*, it increases to* 2726 *steps.*

Example 2 already indicates that l might be maximal for some intermediate value of q. We will prove this assumption in the following remark.

Remark 5. *Computing the derivative of l (Equation (18)) with respect to q' yields insights into the influence of the perturbation probability on the expected time after which a phase change has happened.*

$$\frac{\mathrm{d}}{\mathrm{d}q'}\frac{1}{(1-q')^k \cdot q'} = \frac{-(1-q')^{k-1} \cdot (1-(k+1)\cdot q')}{(1-q')^{2k} \cdot q'^2}$$
$$\begin{cases} < 0, & \text{if } q' < \frac{1}{1+k}, \\ = 0, & \text{if } q' = \frac{1}{1+k}, \\ > 0, & \text{if } q' > \frac{1}{1+k}. \end{cases}$$

The fact that term $l(q')$ has one local minimum for an intermediate q' depending on k is very intuitive and matches the intuition for the analogous behavior with respect to phase changes. With decreasing q' (and thereby q), the probability of a perturbation triggering a phase change increases. However, perturbations happen so rarely that phase changes are rare as well. On the contrary, if q' is large, perturbations happen very often but the network has not enough time to contract between the perturbations and hence, phase changes are very rare.

Remark 6. *Increasing the probability for an adaptation, e.g. by adapting several nodes in one time step, the convergence speed of the adaptation process increases. An increased convergence speed leads to a decrease in k (Equation (17)) and thereby to a decrease in l (Equation (18)). This matches the intuition that an accelerated concentration process of the edges leads to a higher frequency of phase changes. Both this and the previous remark can be qualitatively transferred to the original model.*

Conclusion

We developed a method to quantify the maturation process of general complex systems on basis of the adaptive cycle metaphor. The abstract nature of the metaphor itself and our two-fold information theoretic approach open up a wide field of application. So far, this field comprises simulated and real-world ecological, microbiological, and economic systems.

Our case studies support the general idea of the adaptive cycle. At the same time, they stress its metaphorical character. Oftentimes, the systemic variables do not exactly follow the idealistic "lying-eight" figure of the adaptive cycle. Deviations from the classical pattern of potential, connectedness, and resilience are often indicators for exceptional interactions between internal and external processes. We cannot confirm all details described in the metaphor. For instance, following our case studies, phases of release and reorganization are not of a generally shorter duration than phases of exploitation and conservation.

Future work on the method lies, inter alia, in improving scalability of the approach. We address this task in a current project, dealing with the mycorrhizal community of drought-stressed beeches and spruces (see [5] for an overview of the experimental background). Depending on the taxonomic level, the system under consideration might consist of a few hundred components. Besides, we are currently studying river systems being exposed to flood events (see [2] for preliminary results). At the moment, this analysis is restricted to a small system during a two month time window but the project is aiming at a local and temporal extension of the analysis to the last decades of Europe-wide river systems.

By means of our agent-based model, we provide another perspective on the adaptive cycle metaphor. It allows us to identify internal and external mechanisms whose interplay causes adaptive cycles in complex systems' development. A detailed statistical exploration of the systems' properties will yield further insights into the interaction of the model's parameters and thereby the cycles' driving forces.

So far, we have used our method to analyze and understand the development of a complex system *retrospectively*. However, the knowledge and experience gained in such a backward analysis can form the basis to predict the system's *future* development. Using these predictions for guiding interventions, our method can serve as a powerful tool for system management.

Our research was driven by the question if the adaptive cycle metaphor can serve both as a conceptional and computational framework to comprehend and analyze change in complex systems development. On basis of our results, we affirm this question. In most cases, we are still far from understanding, not to mention controlling change. However, accepting change as part of existence, being aware of its destructive potential while at the same time embracing its innovative capability, is a first step in the right direction.

References

[1] Adaptive cycle. https://www.resalliance.org/adaptive-cycle. Accessed: 2018-09-24.

[2] Digital earth newsletter september 2020 (1). https://www.digitalearth-hgf.de/documents/1294585/1367265/Newsletter_DE_2020_13.pdf/475f416d-074b-4073-adaf-dee57b11c7e8. Accessed: 2018-09-21.

[3] Eurostat. *Eurostat Database* https://ec.europa.eu/eurostat/data/database. Accessed: 2018-04-23.

[4] Financial assistance to Greece. https://ec.europa.eu/info/business-economy-euro/economic-and-fiscal-policy-coordination/eu-financial-assistance/which-eu-countries-have-received-assistance/financial-assistance-greece_en#esm-stability-support-programme. Accessed: 2018-07-05.

[5] Kroof project. https://www.kroof.wzw.tum.de/ueberblick/. Accessed: 2018-09-21.

[6] Long-term studies of secondary succession and community assembly in the prairie-forest ecotone of eastern Kansas. https://foster.ku.edu/long-term-studies-secondary-succession-and-community-assembly-prairie-forest-ecotone-eastern-kansas#methods. Accessed: 2019-05-19.

[7] Plants database of the united states department of agriculture. https://plants.sc.egov.usda.gov/java/. Accessed: 2019-04-26.

[8] Weather history lawrence. *US climate data* https://www.usclimatedata.com/climate/lawrence/kansas/united-states/usks0319/2019/1. Accessed: 2018-04-25.

[9] World government bonds. https://www.investing.com/rates-bonds/world-government-bonds. Accessed: 2019-04-08.

[10] D.G. et al. Angeler. Quantifying the adaptive cycle. *PLOS ONE*, 10(12):1–17, 12 2016.

[11] P. Bak and K. Chen. Self-organized criticality. *Scientific American*, 264(1):46–53, 1991.

[12] P. Bak and K. Sneppen. Punctuated equilibrium and criticality in a simple model of evolution. phys. rev. lett. 59, 381-384. *Physical review letters*, 71:4083–4086, 01 1994.

[13] P. Bak, C. Tang, and K. Wiesenfeld. Self-organized criticality. *Physical Review A*, 38:364–374, 07 1988.

[14] E. Bauer, J. Zimmermann, F. Baldini, I. Thiele, and C. Kaleta. Bacarena: Individual-based metabolic modeling of heterogeneous microbes in complex communities. *PLoS computational biology*, 13:e1005544, 05 2017.

[15] F. Bauer. Normalized graph laplacians for directed graphs. *Linear Algebra and its Applications*, 436, 07 2011.

[16] N. Becker, J. Kunath, G. Loh, and M. Blaut. Human intestinal microbiota: Characterization of a simplified and stable gnotobiotic rat model. *Gut microbes*, 2:25–33, 11 2010.

[17] C. Beier, A. Lovecraft, and F.S. Chapin III. Growth and collapse of a resource system: An adaptive cycle of change in public lands governance and forest management in alaska. *Ecology and Society*, 14, 12 2009.

[18] C.H. Bennett. *Dissipation, information, computational complexity and the definition of organization*, pages 297–313. 1985.

[19] M. Blaut. *Composition and Function of the Gut Microbiome*, pages 5–30. 07 2018.

[20] T. Bossomaier, L. Barnett, M. Harré, and J. Lizier. *An Introduction to Transfer Entropy*. 01 2016.

[21] A. Broido and A. Clauset. Scale-free networks are rare. *Nature Communications*, 10, 03 2019.

[22] B. Burkhard and K.T. Gee. Establishing the resilience of a coastal-marine social-ecological system to the installation of offshore wind farms. *Ecol. Soc.*, 17(4), 2012.

[23] S. Carpenter, B. Walker, J. Anderies, and N. Abel. From metaphor to measurement: Resilience of what to what? *Ecosystems*, 4:765–781, 12 2001.

[24] K. Christensen, S. Collobiano, M. Hall, and H.J. Jensen. Tangled nature: A model of evolutionary ecology. *Journal of Theoretical Biology*, 216:73–84, 2002.

[25] F. Chung. *Spectral Graph Theory*. CBMS Regional Conference Series in Mathematics Number 92, 1997.

[26] F. Chung. The diameter and laplacian eigenvalues of directed graphs. *Electr. J. Comb.*, 13, 02 2006.

[27] T. M. Cover and J. A. Thomas. *Elements of Information Theory (Wiley Series in Telecommunications and Signal Processing)*. Wiley-Interscience, USA, 2006.

[28] G. Cumming, G. Barnes, S.G. Perz, M. Schmink, K. Sieving, J. Southworth, M. Binford, R. Holt, C. Stickler, and T. Van Holt. An exploratory framework for the empirical measurement of resilience. *Ecosystems*, 8:975–987, 12 2005.

[29] M. De Domenico, A. Solé-Ribalta, S. Gomez, and A. Arenas. Navigability of interconnected networks under random failures. *Proceedings of the National Academy of Sciences of the United States of America*, 111, 05 2014.

[30] G. Dodig Crnkovic. Nature as a network of morphological infocomputational processes for cognitive agents. *The European Physical Journal Special Topics*, 226, 01 2016.

[31] A. Duputié and F. Massol. An empiricist's guide to theoretical predictions on the evolution of dispersal. *Interface Focus*, 3(6):20130028, 2013.

[32] M. Esposito and J. Chatzimarkakis. The european financial crisis - analysis and a novel intervention. Technical report, Harvard University and European Parliament, 2014.

[33] M. Fiedler. Algebraic connectivity of graphs. *Czechoslovak Mathematical Journal*, 23:298–305, 01 1973.

[34] S. Fridriksson. Vascular plants on surtsey 1981-1990. *Surtsey Research*, 10:17–30, 01 1992.

[35] J. Frieden, M. Copelovitch, and S. Walter. The political economy of the euro crisis. *Comparative Political Studies*, 49:1–30, 03 2016.

[36] J. Frieden and S. Walter. Understanding the political economy of the eurozone crisis. *Annual Review of Political Science*, 20(1):371–390, 2017.

[37] E. N. Gilbert. Random graphs. *Ann. Math. Statist.*, 30(4):1141–1144, 12 1959.

[38] J.P. Grime, Hodgson J.G., and R. Hunt. *Comparative plant ecology: a functional approach to common British species*. Springer Science+Business Media Dordrecht, 1988.

[39] L.H. Gunderson and C.S. Holling. *Panarchy: Understanding Transformations in Human and Natural Systems*. Island Press, 2002.

[40] C. Holling. Understanding the complexity of economic, ecological, and social systems. *ECOSYSTEMS*, 4:390–405, 08 2001.

[41] C.S. Holling. Resilience and stability of ecological systems. *Annual Review of Ecology and Systematics*, 4(1):1–23, 1973.

[42] L. Hood and D. Galas. The digital code of dna. *Nature*, 421:444–8, 02 2003.

[43] L. Horstmeyer, T. Pham, J. Korbel, and S. Thurner. Predicting collapse of adaptive networked systems without knowing the network. *Scientific Reports*, 10:1223, 01 2020.

[44] T. Iversen, D. Soskice, and D. Hope. The eurozone and political economic institutions. *Annual Review of Political Science*, 19(1):163–185, 2016.

[45] A. Kaiser and T. Schreiber. Information transfer in continuous processes. *Physica D, v.166, 43-62 (2002)*, 166, 06 2002.

[46] S. Katare and D. West. Optimal complex networks spontaneously emerge when information transfer is maximized at least expense: A design perspective. *Complexity*, 11:26–35, 03 2006.

[47] S.A. Kauffman and S. Johnsen. Coevolution to the edge of chaos: Coupled fitness landscapes, poised states, and coevolutionary avalanches. *Journal of Theoretical Biology*, 149(4):467–505, 04 1991.

[48] A. Kraskov, H. Stögbauer, and P. Grassberger. Estimating mutual information. *Physical Review E*, 69(6), Jun 2004.

[49] J. Lizier. Jidt: An information-theoretic toolkit for studying the dynamics of complex systems. *Frontiers in Robotics and AI*, 1, 08 2014.

[50] J. Lizier, S. Pritam, and M. Prokopenko. Information dynamics in small-world boolean networks. *Artificial life*, 17:293–314, 07 2011.

[51] J. Lizier and M. Prokopenko. Differentiating information transfer and causal effect. *The European Physical Journal B*, 73, 12 2008.

[52] J. Lizier, M. Prokopenko, and A. Zomaya. Information modification and particle collisions in distributed computation. *Chaos (Woodbury, N.Y.)*, 20:037109, 09 2010.

[53] J. T. Lizier, M. Prokopenko, and A. Y. Zomaya. Information modification and particle collisions in distributed computation. *Chaos (Woodbury, N.Y.)*, 20(3):037109, 09 2010.

[54] R. MacArthur. Fluctuations of animal populations and a measure of community stability. *Ecology*, 36(3):533–536, 1955.

[55] B. Magnússon, S. Magnússon, and S. Fridriksson. Developments in plant colonization and succession on surtsey during 1999–2008. *Surtsey Research*, 12:57–76, 01 2009.

[56] S. Magnusdottir, A. Heinken, L. Kutt, D. Ravcheev, E. Bauer, A. Noronha, K. Greenhalgh, C. Jäger, J. Baginska, P. Wilmes, R. Fleming, and I. Thiele. Generation of genome-scale metabolic reconstructions for 773 members of the human gut microbiota. *Nature Biotechnology*, 35, 11 2016.

[57] S. Martin, G. Deffuant, and J. Calabrese. *Defining Resilience Mathematically: From Attractors To Viability*, volume 2011, pages 15–36. 08 2011.

[58] M. Mitchell. Biological computation. *The Computer Journal*, 55, 01 2010.

[59] M. E. J. Newman, S. H. Strogatz, and D. J. Watts. Random graphs with arbitrary degree distributions and their applications. *Physical Review E*, 64(2), 07 2001.

[60] F.J Odling-Smee, K.N. Laland, and M.W. Feldman. Niche construction. *The American Naturalist*, 147(4):641–648, 1996.

[61] E.P. Odum. The strategy of ecosystem development. *Science*, 164:262–270, 1969.

[62] M. Pelling and D. Manuel-Navarrete. From resilience to transformation: the adaptive cycle in two mexican urban centers. *Ecology and Society*, 16, 06 2011.

[63] G. Peterson. Estimating resilience across landscapes. *Conservation Ecology*, 6, 06 2002.

[64] E.R. Pianka. On r- and k-selection. *The American Naturalist*, 104(940):592–597, 1970.

[65] Baldursson S. and A. Ingadóttir, editors. *Nomination of Surtsey for the UNESCO World Heritage List*. Icelandic Institute of Natural History, Reykjavík, Iceland, 2007.

[66] N. Schreiber and H. Schrenk. Qtac (quantifying the adaptive cycle). `https://github.com/hannahschrenk/QtAC`, 2020.

[67] T. Schreiber. Measuring information transfer. *Physical review letters*, 85:461–4, 08 2000.

[68] H. Schrenk. Drivers of the adaptive cycle. preprint, 2020.

[69] H. Schrenk, J. Betel Geijo Fernández, C. Garcia Perez, and W. zu Castell. Information processing in a simulated human intestinal microbiota. preprint, 2020.

[70] H. Schrenk, B. Magnússon, B. Sigurdsson, and W. zu Castell. Systemic analysis of a developing plant community on the island of surtsey. submitted, 2020.

[71] K. Sneppen, P. Bak, H. Flyvbjerg, and M. Jensen. Evolution as a self-organized critical phenomenon. *Proceedings of the National Academy of Sciences of the United States of America*, 92:5209–5213, 06 1995.

[72] R. V. Solé, S. C. Manrubia, B. Luque, J. Delgado, and J. Bascompte. Phase transitions and complex systems: Simple, nonlinear models capture complex systems at the edge of chaos. *Complexity*, 1(4):13–26, 1996.

[73] J.C. Torrico and M.J.J. Janssens. Rapid assessment methods of resilience for natural and agricultural systems. *Anais da Academia Brasileira de Ciencias*, 82 4:1095–1105, 2010.

[74] R. Ulanowicz. *Ascendency: A measure of ecosystem performance*, pages 303–315. 01 2000.

[75] R. Ulanowicz. Information theory in ecology. *Computers & chemistry*, 25:393–9, 08 2001.

[76] R. Ulanowicz, S. Goerner, B. Lietaer, and R. Gomez. Quantifying sustainability: Resilience, efficiency and the return of information theory. *Ecological Complexity*, 6:27–36, 03 2009.

[77] X. Wang, J. Miller, J. Lizier, M. Prokopenko, and L. Rossi. Quantifying and tracing information cascades in swarms. *PloS one*, 7:e40084, 07 2012.

[78] M. Wibral, J. Lizier, S. Vögler, V. Priesemann, and R. Galuske. Local active information storage as a tool to understand distributed neural information processing. *Frontiers in Neuroinformatics*, 8:1, 2014.

[79] J. H. Wilkinson. *The Algebraic Eigenvalue Problem.* Oxford University Press, Inc., USA, 1988.

[80] C. Wu. On bounds of extremal eigenvalues of irreducible and m-reducible matrices. *Linear Algebra and its Applications*, 402:29–45, 06 2005.

[81] C. Wu. On rayleigh–ritz ratios of a generalized laplacian matrix of directed graphs. *Linear Algebra and its Applications*, 402:207–227, 06 2005.

[82] J. Zhu, J. Bellanger, H. Shu, and R. Le Bouquin Jeannès. Contribution to transfer entropy estimation via the k-nearest-neighbors approach. *Entropy*, 17:4173–4201, 06 2015.

[83] W. zu Castell and H. Schrenk. Computing the adaptive cycle. *Scientific Reports*, 2020(10):18175, 10 2020.

Supplementary

A Manual of the R package QtAC

Package 'QtAC'

August 29, 2020

Type Package

Title Quantifying the Adaptive Cycle

Version 0.1.0

Author Nico Schreiber and Hannah Schrenk

Maintainer <hannah-schrenk@arcor.de>

Description
QtAC provides tools to analyze the maturation process of complex systems in the sense of Gunderson's and Holling's adaptive cycle metaphor (see e.g. Holling 2001). Using time series of a system's components' abundance data, the dynamics of information transfer among the components are estimated. On the basis of the resulting information networks, potential, connectedness, and resilience can be computed. The development of these three variables de<U+FB01>nes the system's course through the adaptive cycle. In addition to the functions needed to carry out the just described calculations, the package offers several options to visualize the results. The main function requires a transfer entropy estimator being included in the JIDT toolkit (Lizier 2014). Besides, functions of the packages pracma, rJava, igraph, and rgl are used.

License

Encoding UTF-8

LazyData true

RoxygenNote 7.1.1

R topics documented:

QtAC 2
QtAC.2dmixplot 3
QtAC.2dplot 3
QtAC.3dplot 4
QtAC.maturation 4
QtAC.network 5
QtAC.Signfactor 6
QtAC.TXT.reader 7
QtAC.WriteAdjSgn 7

Index **8**

QtAC *QtAC (Main function)*

Description

This function calculates the transfer entropy between two species each for shifting time windows of fixed length. The output is a list of adjacency matrices and the corresponding significance matrices.

Usage

```
QtAC(
  Data,
  num_timepoints = 5,
  JavaPath,
  num_PermCheck = 1000L,
  k = 1L,
  k_tau = 1L,
  l = 1L,
  l_tau = 1L,
  delay = 1L
)
```

Arguments

Data	data array containing time series of the system's components' abundance data
num_timepoints	length of the time windows of abundance data serving as basis of the transfer entropy calculations
JavaPath	path of the file "infodynamics.jar"
num_PermCheck	number of surrogate samples to bootstrap to generate the distribution in the significance test
k	embedding length of destination past history to consider
k_tau	embedding delay for the destination variable
l	embedding length of source past history to consider
l_tau	embedding delay for the source variable
delay	time lag between last element of source and destination next value

Value

list of two lists (adjacency and corresponding significance matrices)

`QtAC.2dmixplot` *2dmixplot*

Description

This function plots two selected systemic variables w.r.t. each other.

Usage

```
QtAC.2dmixplot(
  Mat,
  prop1,
  prop2,
  Save = FALSE,
  filename = paste("2dmixplot", prop1, prop2, sep = "_")
)
```

Arguments

`Mat`	data frame containing the systemic variables
`prop1`	variable on x-axis ("potential","connectedness","resilience")
`prop2`	variable on y-axis ("potential","connectedness","resilience")
`Save`	If Save = TRUE, the 2D plot will be saved in a PNG file.
`filename`	If Save = TRUE, the network will be saved in a file called filename.

Value

2D plot and, if Save = TRUE, a PNG file containing the plot

`QtAC.2dplot` *2dplot*

Description

This function plots graphs of potential, connectedness and resilience with respect to time.

Usage

```
QtAC.2dplot(
  Mat,
  prop = NULL,
  time_int = NULL,
  Save = FALSE,
  filename = "2dplot"
)
```

Arguments

Mat	dataframe containing the systemic variables
prop	If prop = NULL, the three systemic variables are plotted w.r.t time in one plots each. If prop = "potential", "connectedness", or "resilience", only the selected systemic variable is plotted w.r.t time.
time_int	vector containing start time, end time, and step size to define the xaxis
Save	If Save = TRUE, the 2D plot will be saved in a PNG file.
filename	If Save = TRUE, the network will be saved in a file called filename.

Value

2D plot and, if Save = TRUE, a PNG file containing the plots.

QtAC.3dplot *3dplot*

Description

3D plot of the three systemic variables w.r.t each other.

Usage

```
QtAC.3dplot(Mat, Mat_points = FALSE)
```

Arguments

Mat	data frame containing the three systemic variables
Mat_points	If Mat_points = TRUE, the maturation points are visible.

Value

3D plot

QtAC.maturation *maturation*

Description

This function computes the three systemic variables (potential, connectedness, and resilience) of each adjacency matrix.

Usage

```
QtAC.maturation(result_mtx, res_norm = "continous", res_stand = "maxweight")
```

Arguments

result_mtx	list of adjacency matrices and significance matrices
res_norm	normalization variant of the Laplacian matrices ("continous", "symmetric"). If res_norm = "symmetric", $L_{out} = c{\cdot}D_{out}^{-\frac{1}{2}}\,(D_{out} - A)$ and $L_{in} = c{\cdot}(D_{in} - A)\,D_{in}^{-\frac{1}{2}}$. If res_norm = "symmetric", $L_{out} = c \cdot D_{out}^{-\frac{1}{2}}(D_{out} - A)D_{out}^{-\frac{1}{2}}$ and $L_{in} = c \cdot D_{in}^{-\frac{1}{2}}(D_{in} - A)D_{in}^{-\frac{1}{2}}$.
res_stand	standardization constant c of the Laplacian matrices ("none", "maxweight", "maxweight2", "nodes", "maxweightnodes"). Let N be the number of nodes of the underlying graph and M its maximal edge weight. If res_stand = "none", $c = 1$. If res_stand = "maxweight", $c = \frac{1}{\sqrt{M}}$. If res_stand = "maxweight2", $c = \frac{1}{M}$. If res_stand = "nodes", $c = \frac{\sqrt{N-1}}{N}$. If res_stand = "maxweightnodes", $c = \frac{\sqrt{N-1}}{N{\cdot}\sqrt{M}}$.

Value

dataframe containing the three systemic variables (potential, connectedness, and resilience) of each adjacency matrix

---

`QtAC.network` *network*

Description

This function plots a selected adjacency matrix as network.

Usage

```
QtAC.network(
  result_mtx,
  num_mtx,
  edge_label = FALSE,
  dec = 2,
  layout = "circle",
  edge_width = 3,
  arrow_width = 5,
  col_node = "palegreen3",
  col_edge = "steelblue3",
  vertex_label = "short",
  Save = FALSE,
  filename = "network"
)
```

Arguments

result_mtx	list of adjacency matrices and significance matrices
num_mtx	number of the adjacency matrix you want to plot
edge_label	If edge_label = TRUE, the weight of the edges are plotted next to the edges.
dec	number of decimal digits in the edge labels
layout	layout format ("circle","star","fruchterman.reingold","grid","nicely")

edge_width	muliplicator for the width of the edges
arrow_width	muliplicator for the width of the arrows
col_node	color of the vertices
col_edge	color of the edges
vertex_label	If vertex_label = "short", the first 3 letters of the components' names will be used as vertex labels, if vertex_label = "long", the whole names will be used as vertex labels. Via vertex_label = c(...), customized names can be used as vertex labels.
Save	If Save = TRUE, the network will be saved as a PNG file.
filename	If Save = TRUE, the network will be saved in a file called filename.

Value

network plot and, if Save = TRUE, a PNG file containing the plot

---

`QtAC.Signfactor` *Signfactor*

Description

This function sets all entries in the adjacency matrices to 0 whose p-value is above the predefined significance level.

Usage

```
QtAC.Signfactor(result_mtx, signfac = 0.1)
```

Arguments

result_mtx	list of adjacency and significance matrices
signfac	significance level

Value

list of two lists (adjacency matrix containing only significant transfers and significance matrices)

`QtAC.TXT.reader` *TXT-reader*

Description

This function is used to import the data in R. The data should be in a tab-seperated file with or without column/row names. Columns should contain time points, rows the system's components.

Usage

```
QtAC.TXT.reader(filename, col_names = FALSE, row_names = FALSE)
```

Arguments

`filename`	path of the file you want to import
`col_names`	logical operator. TRUE if the file contains column names, FALSE if it does not
`row_names`	logical operator. TRUE if the file contains row names, FALSE if it does not

Value

data array. If no column or row names were given, column or row names of the form "t_ " and "C_ " respectively are added.

`QtAC.WriteAdjSgn` *WriteAdjSgn*

Description

This function writes a selected adjacency and significance matrix to CSV files.

Usage

```
QtAC.WriteAdjSgn(
  result_mtx,
  num_mtx,
  file_name_adj = "adjacency_matrix",
  file_name_sgn = "significance_matrix"
)
```

Arguments

`result_mtx`	list of adjacency and significance matrices
`num_mtx`	number of the adjacency and significance matrix you want to write to a CSV file
`file_name_adj`	name of the file to which the adjacency matrix is written
`file_name_sgn`	name of the file to which the significance matrix is written

Value

two CSV files, one containing the selected adjacency, one the significance matrix

Index

QtAC, 2
QtAC.2dmixplot, 3
QtAC.2dplot, 3
QtAC.3dplot, 4
QtAC.maturation, 4
QtAC.network, 5
QtAC.Signfactor, 6
QtAC.TXT.reader, 7
QtAC.WriteAdjSgn, 7

B Exemplary series of networks generated on basis of the principle of overexploitation

1

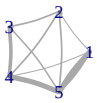

2

3

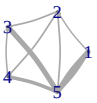

4

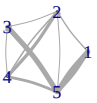

5

6

7

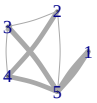

8

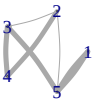

9

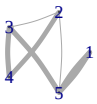

10

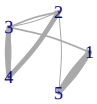

11

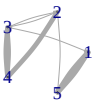

12

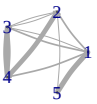

13

14

15

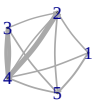

16

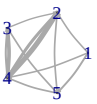

17

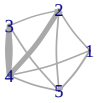

18

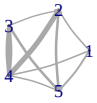

19

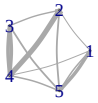

20

21

22

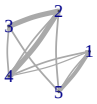

23

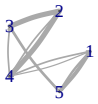

24

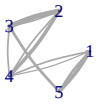

25

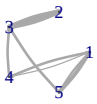

26

27

28

29

30

31

32

33

34

35

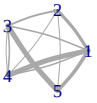

36

37

38

39

40

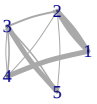

41

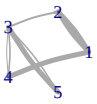

42

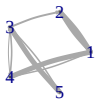

43

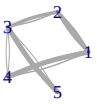

44

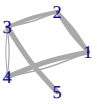

45

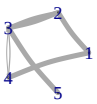

46

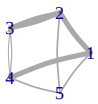

47

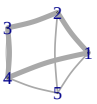

48

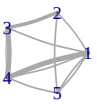

49

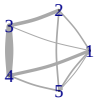

50

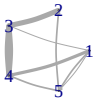

51

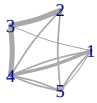

52

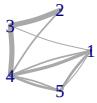

53

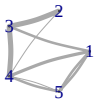

54

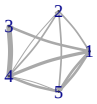

55

56

57

58

59

60

61

62

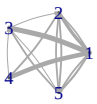

63

64

C Parameters of the Tangled Nature Model simulation

initial population size	$N(0) = 2$
coupling parameters	$\Theta = 0.3$ and $c = 14.3$
reproduction parameter	$\mu = 0.2$
mutation probability	$p_{mut} = 0.001$
annihilation probability	$p_{kill} = 0.02$

Supplementary Table 1: Parameters used in the Tangled Nature Model simulation.

D Species and metadata of the Kansas case study

Species	Growth Habit	Duration	Fire Tolerance	Growth Rate	Drought Tolerance	After Harvest Regrowth Rate	Vegetative Spread Rate
Acalypha,virginica	f	a	none	rapid	medium	slow	none
Achillea,millefolium	f	p	high	moderate	medium	moderate	slow
Agrostis,hyemalis	g	p	high	moderate	low	moderate	moderate
Ambrosia,artemisiifolia	f	a					
Andropogon,virginicus	g	p	high	slow	high	slow	none
Apocynum,cannabinum	f	p	none	moderate	medium	slow	none
Aristida,oligantha	g	a					
Asclepias,syriaca	f	p	burning stimulates				
Asclepias,verticillata	f	p					
Bromus,inermis	g	p	high	moderate	medium	slow	rapid
Chamaecrista,fasciculata	f	a	none	rapid	medium		none
Cirsium,altissimum	f	b					
Conyza,canadensis	f	a,b	low	rapid	low	slow	none
Cornus,drummondi	t,s	p	low	rapid	low		rapid
Cynanchum,laeve	f,v	p					
Desmodium,canadense	f	p	burning stimulates		low		
Erigeron,strigosus	f	a,b,p	low	moderate	medium	slow	none
Eupatorium,altissimum	f	p					
Eupatorium,serotinum	f	p					
Ipomoea,lacunosa	f,v	a					
Lepidium,virginicum	f	a,b,p					
Kummerowia,stipulacea	f	a	medium	rapid	medium	slow	none
Lespedeza,capitata	f	p	high	slow	high	slow	none
Monarda,fistulosa	f,ss	p	none	moderate	no	slow	slow
Oxalis,stricta	f	p			high		
Panicum,capillare	g	a			high		
Poa,pratensis	g	p	high	moderate	low	moderate	rapid
Pycnanthemum,tenuifolium	f	p		high	medium		rapid
Setaria,faberii	g	a					
Setaria,glauca	g	a			medium	moderate	rapid
Solidago,canadensis	f	p	high	rapid	medium	moderate	
Sida,spinosa	f,ss	a,p					
Solanum,carolienense	f,ss	p					
Sorghastrum,nutans	g	p	high	moderate	medium	moderate	moderate
Sporobolus,cryptandrus	g	p	medium	moderate	high	slow	none
Tridens,flavus	g	p	high	moderate	high	rapid	none
Unknown,forb,A							
Vernonia,baldwini	f	p					

Supplementary Table 2: Features of the species occurring in unit 13 of the succession experiment in Kansas [7]. The following abbreviations are used: f - forb/herb, g - graminoid, t - tree, s - shrub, ss - subshrub, v - vine, a - annual, p - perennial, b - biennial.

E System components in the Europe case study

Quantity	**Unit**
gross domestic product	mio €
exports of goods and services	mio €
imports of goods and services	mio €
volume of freight transport	index (2010 = 100)
volume of passenger transport	index (2010 = 100)
greenhouse gas emissions	index (1990 = 100)
pollutant emissions from transport	nitrogen oxides
greenhouse gas emissions intensity of energy consumption	index (2000 = 100)
energy consumption of transport	index (2000 = 100)
gross value added of the agricultural industry	mio €
railway passenger volume	mio
goods transported by railway	thousands of tonnes
motorization rate	cars per 1000 inhabitants
goods transported by road	thousands of tonnes
air transport of passengers	passengers
air transport of goods	tonnes
final consumption expenditure of households	mio €
people at risk of social poverty or exclusion	thousands of people
current account transactions - balance	mio €

Supplementary Table 3: Quantities and the corresponding units used in the Eurostat case study.

F Information networks of the vascular plant system on Surtsey

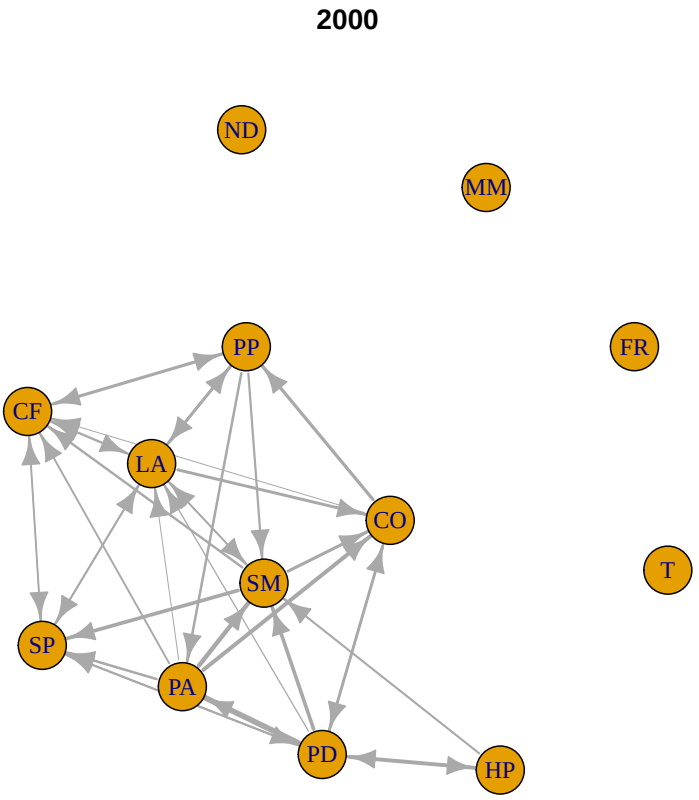

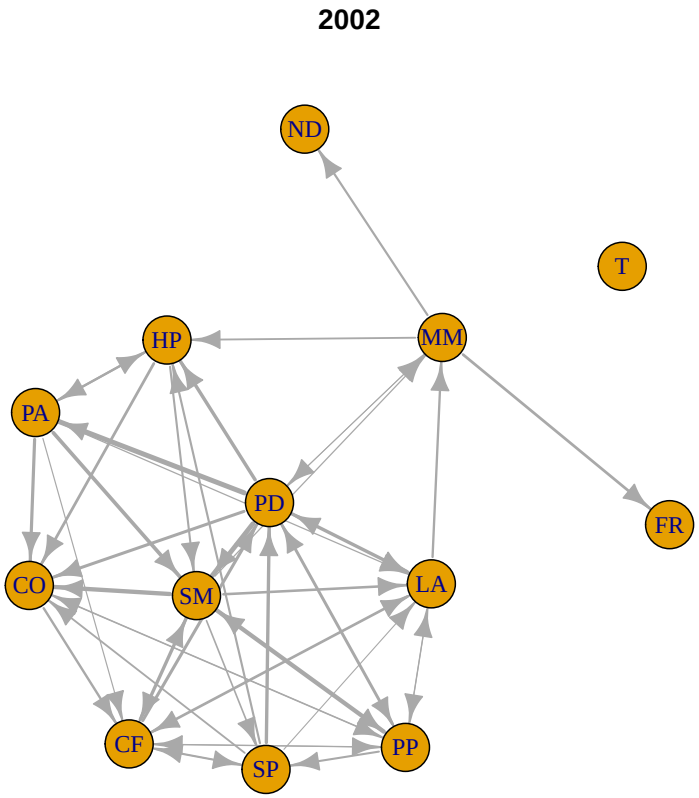
2002
ND
T
HP
MM
PA
PD
FR
CO
SM
LA
CF
PP
SP

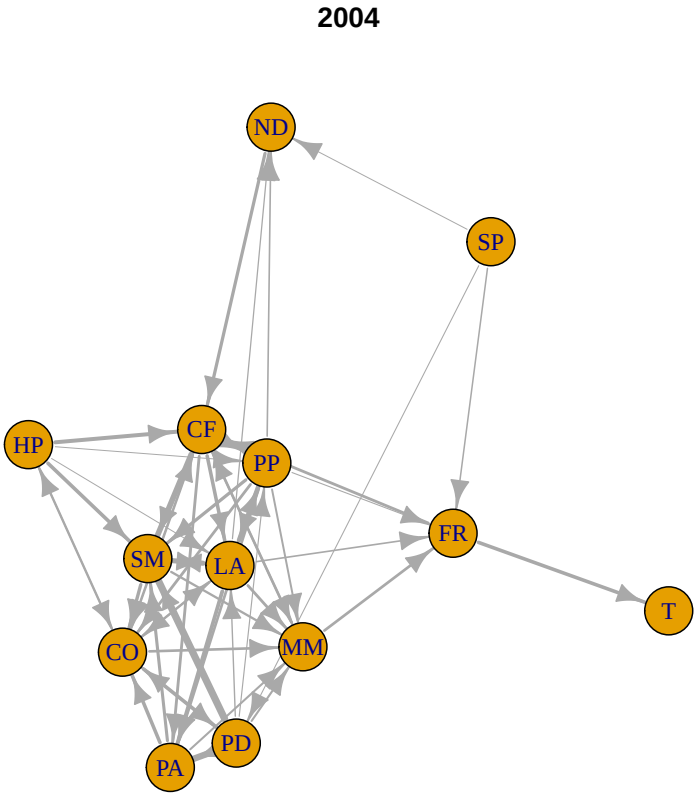
2004
ND
SP
HP
CF
PP
FR
SM
LA
T
CO
MM
PD
PA

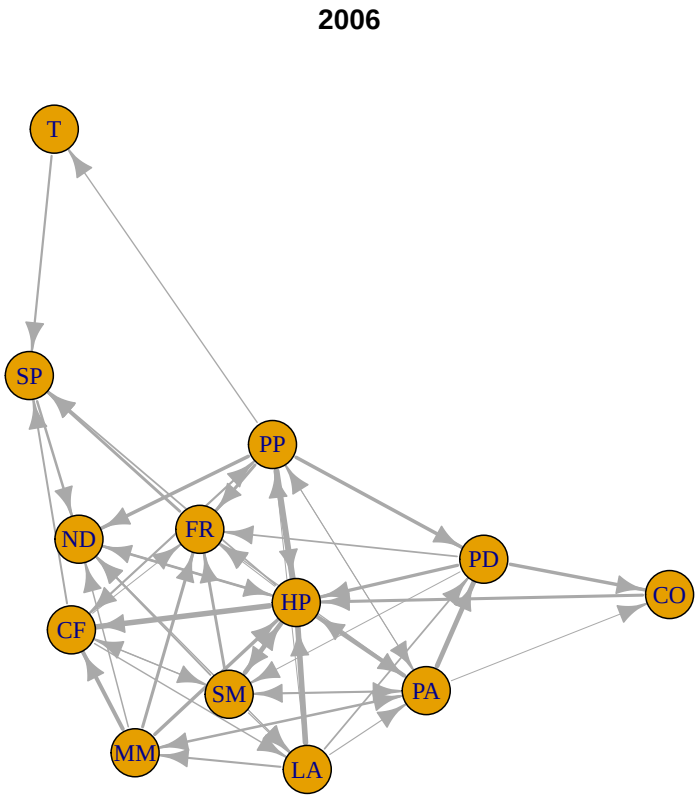
2006
T
SP
PP
ND
FR
PD
CO
HP
CF
SM
PA
MM
LA

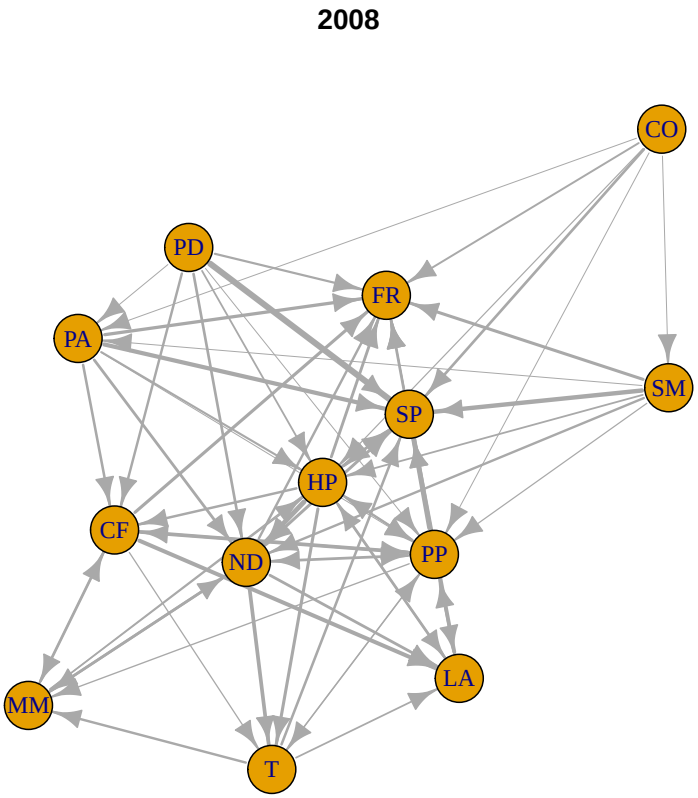
2008
CO
PD
FR
PA
SM
SP
HP
CF
ND
PP
LA
MM
T

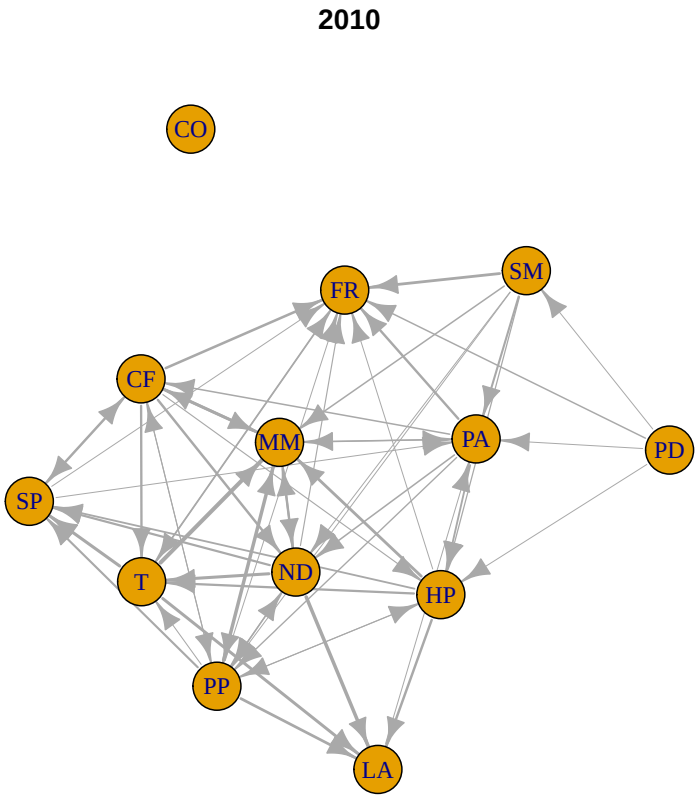
2010
CO
SM
FR
CF
MM
PA
PD
SP
ND
T
HP
PP
LA

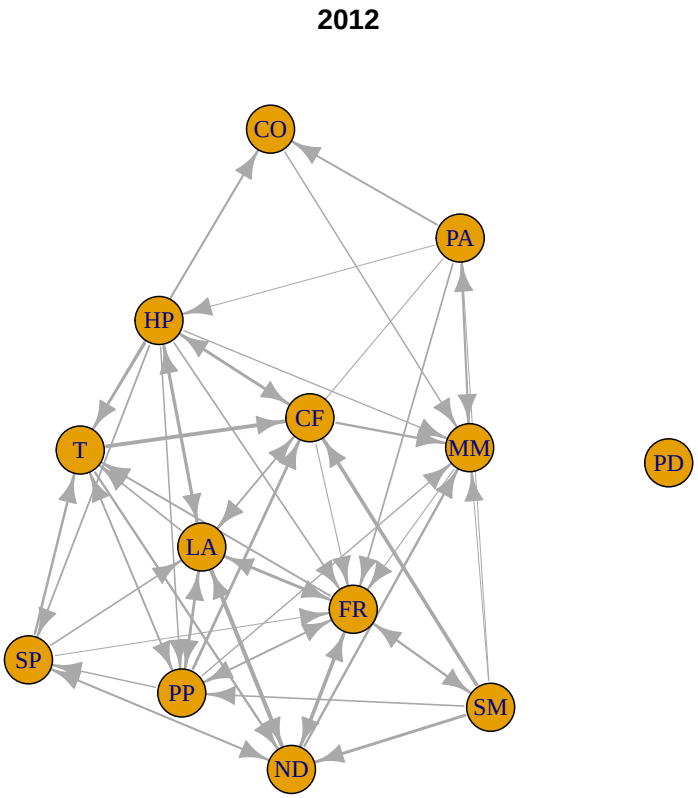
2012
CO
PA
HP
CF
T
MM
PD
LA
FR
SP
PP
SM
ND

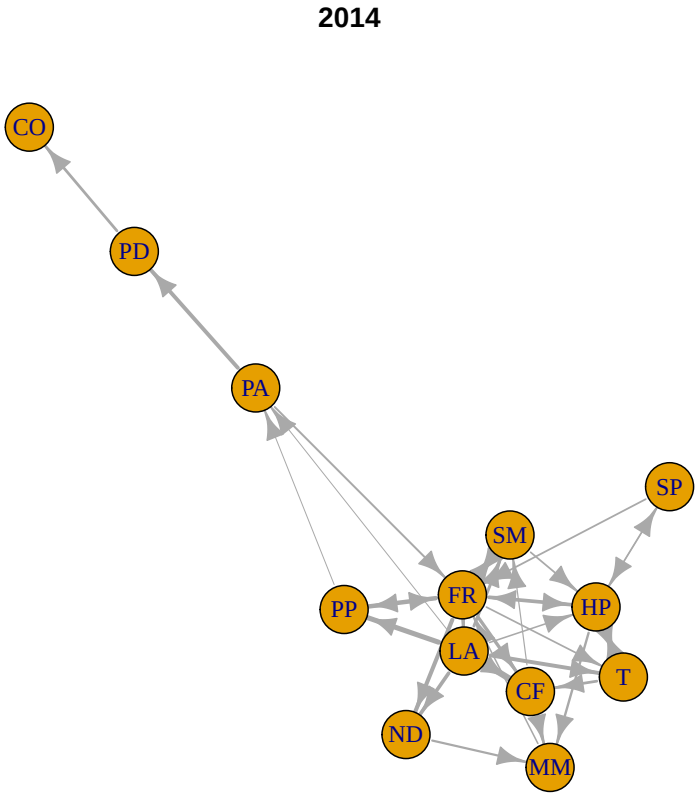
2014
CO
PD
PA
SP
SM
FR
HP
PP
LA
T
CF
ND
MM

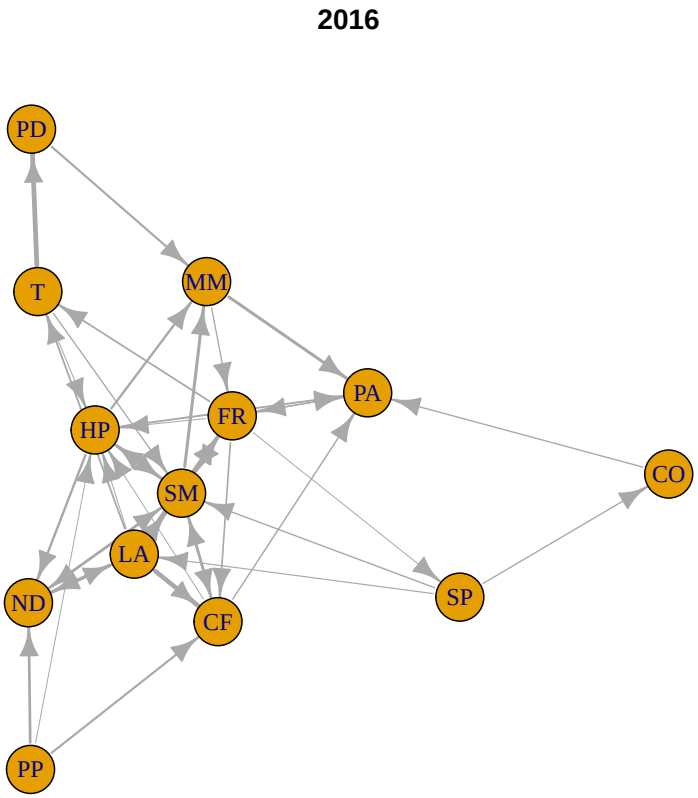
2016
PD
T
MM
PA
HP
FR
CO
SM
LA
ND
SP
CF
PP

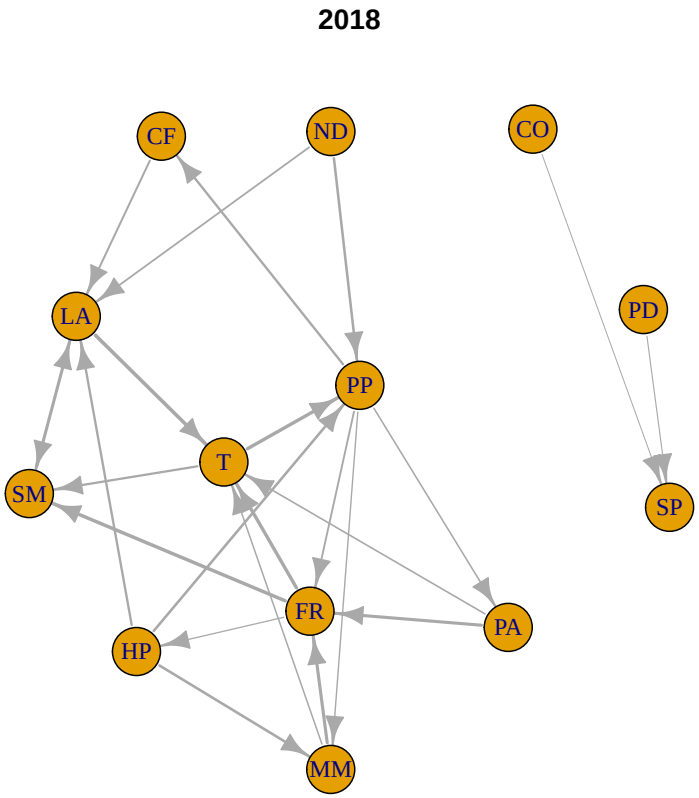
2018
CF
ND
CO
LA
PD
PP
T
SM
SP
FR
PA
HP
MM